Stockholm University

Study of the phase diagram of Z_n symmetric chains

Iman Mahyaeh

Doctoral Thesis in Theoretical Physics at Stockholm University, Sweden 2020

Study of the phase diagram of Z_n symmetric chains

Iman Mahyaeh

Academic dissertation for the Degree of Doctor of Philosophy in Theoretical Physics at Stockholm University to be publicly defended on Tuesday 9 June 2020 at 13.15 in sal FB42, AlbaNova universitetscentrum, Roslagstullsbacken 21.

Abstract

In this thesis we study the phase diagrams of Z_n symmetric chains. We start with investigating the topological phases of the Kitaev chain, a Z_2 symmetric model, with long range couplings and a phase gradient. Then we go beyond the free fermion classification of topological phases and consider the effect of interactions by studying the Kitaev-Hubbard chain, incorporating a density-density interaction. Next we move on to the Z_3 symmetric models and present a frustration free model with an exact three-fold degenerate ground state. In the end we present the phase diagram of a hopping model of Z_3 Fock parafermions, the generalization of polarized Dirac fermions which could host at most two particles per site. The model has a pairwise hopping which is forbidden for fermions. In our studies we use analytical methods like the Lieb-Schultz-Mattis method, bosonization and conformal field theory, as well as numerical ones like exact diagonalization and the density matrix renormalization group.

Stockholm 2020
http://urn.kb.se/resolve?urn=urn:nbn:se:su:diva-180941

ISBN 978-91-7911-164-9
ISBN 978-91-7911-165-6

Department of Physics

Stockholm University, 106 91 Stockholm

STUDY OF THE PHASE DIAGRAM OF Z_N SYMMETRIC CHAINS

Iman Mahyaeh

Stockholm
University

Study of the phase diagram of Z_n symmetric chains

Iman Mahyaeh

ISBN print 978-91-7911-164-9
ISBN PDF 978-91-7911-165-6

Printed in Sweden by Universitetsservice US-AB, Stockholm 2020

To my parents Lida and Hamid
and
my grandparents Fatemeh and Khosrow

Abstract

In this thesis we study the phase diagrams of $\mathbb{Z}_n$ symmetric chains. We start with investigating the topological phases of the Kitaev chain, a $\mathbb{Z}_2$ symmetric model, with long range couplings and a phase gradient. Then we go beyond the free fermion classification of topological phases and consider the effect of interactions by studying the Kitaev-Hubbard chain, incorporating a density-density interaction. Next we move on to the $\mathbb{Z}_3$ symmetric models and present a frustration free model with an exact three-fold degenerate ground state. In the end we present the phase diagram of a hopping model of $\mathbb{Z}_3$ Fock parafermions, the generalization of polarized Dirac fermions which could host at most two particles per site. The model has a pairwise hopping which is forbidden for fermions. In our studies we use analytical methods like the Lieb-Schultz-Mattis method, bosonization and conformal field theory, as well as numerical ones like exact diagonalization and the density matrix renormalization group.

Svensk Sammanfattning

I den här avhandlingen studerar vi fasdiagrammen av kedjor som har $\mathbb{Z}_n$ symmetri. Vi börjar med att undersöka de topologiska faser i Kitaev kedjor (med $\mathbb{Z}_2$ symmetri) som har hoppning över längre avstånd och en fas gradient. Vi fortsätter med system som inte faller i den klassificeringen av topologiska faser i system bestående av fria fermioner, genom att studera effekten av växelverkan mellan fermionerna. Vi gör det genom att studera Kitaev-Hubbard kedjan, som har en täthet-täthet term i hamiltonianen.

Sedan tittar vi på kedjor med $\mathbb{Z}_3$ symmetri, och vi beskriver en kedja som inte har frustration i grundtillståndet, som har en exact trefaldig degeneration. Till slut ger vi fasdiagrammet av en model som beskriver hoppande $\mathbb{Z}_3$ parafermioner. $\mathbb{Z}_3$ parafermioner är en generalisering av (polariserade) Dirac fermioner, i bemärkelsen att det kan finnas maximalt två $\mathbb{Z}_3$ parafermioner på en site, istället av bara en i det fermioniska fallet.

I våra studier använder vi analytiska metoder som Lieb-Schultz-Mattis metoden, bosonisering och konform fältteori, samt numeriska metoder som exakt diagonalisering och täthetsmatris renormaliseringsgruppen.

List of Accompanying Papers and Contribution

Paper I I. Mahyaeh and E. Ardonne,*Zero modes of the Kitaev chain with phase-gradients and longer range couplings*, J. Phys. Commun. **2**, 045010 (2018).

DOI:10.1088/2399-6528/aab7e5.

Paper II I. Mahyaeh and E. Ardonne,*Exact results for a $\mathbb{Z}_3$-clock-type model and some close relatives*, Phys. Rev. B **98**, 245104 (2018).

DOI: 10.1103/PhysRevB.98.245104.

Paper III I. Mahyaeh and E. Ardonne, *Study of the phase diagram of the Kitaev-Hubbard chain*, Phys. Rev. B **101**, 085125 (2020).

DOI:10.1103/PhysRevB.101.085125.

Paper IV I. Mahyaeh, J. Wouters and D. Schuricht, *Phase diagram of the $\mathbb{Z}_3$-Fock parafermion chain with pair hopping*, arXiv:2003.07812.

In all the above mentioned papers, I derived almost all the analytical results and independently checked the other ones. I performed most of the numerical results for paper III. In paper IV, I and Jurriaan Wouters performed two independent numerical simulations. I wrote the first draft of all the papers and actively participated in finalizing the manuscripts.

We have the permissions for reprinting.

Note: chapter 2 and chapter 3 are, in part, based on my licentiate thesis, "Edge modes of $\mathbb{Z}_n$ symmetric chains", (2017) Stockholm University.

Acknowledgements

First and foremost I want to thank my beloved family, *Lida, Hamid, Fatemeh* and *Khosrow*, for their love, care and encouragement. All of my accomplishments, including writing this thesis, were achieved only because of your love, assurance and constant support. This thesis is dedicated to you and my deepest gratitude, thankfulness and appreciation always go to you.

I will be always grateful to my PhD supervisor, *Eddy Ardonne*. With his patience and passion to perform an original research, he taught me a lot, ranging from physics to English. With the freedom that he gave me and his constant support and enthusiasm, I gained and developed valuable skills. Importantly he taught me the importance of numerical analysis and how to perform it.

During my PhD studies I had a very pleasant collaboration with *Dirk Schuricht* and *Jurriaan Wouters*. I enjoyed it a lot indeed. I would also like to thank people at the Institute for Theoretical Physics at Utrecht University for a very nice time that I had there.

I would like to thank my teachers in the physics olympiad committee in Iran, *Mahmud Bahmanabadi, Mohammad Khorrami, Mehdi Saadat, Ahmad Shariati, Ahmad Shirzad, Hossein Mirzaei, Mr. Sharifzadeh, Mr. Rajabi, Mr. Lotfozzaman* and all the people in Young Scholars Club who helped me to start my journey in physics.

I would like to thank *Shahin Rouhani* from whom I learned statistical mechanics. I found a lot of joy and fun in the lovely Ising model during his lectures. *Saman Moghimi* taught me a lot of physics. We always had very nice time with him, back in Sharif University. My first course on solid state physics was taught by *Mohammad Akhavan*. That hard bachelor course was actually the beginning of my journey in the condensed matter physics. *Shahin, Saman and Mohammad* saved me from working on something "not even wrong". Thank you so much.

I worked on my first project in condensed matter physics under the supervision of *Akbar Jafari* in accompany with my dear friend *Mahdi Mashkoori*. That was a fantastic experience.

I have been sharing an office with very nice friends, *Babak Majidzadeh, Christian Spånslätt, Axel Gagge, Carlos Ortega Taberner, Yoran Tournois* and *Kang Yang*. Thanks a lot for all the discussions and the pleasant time we had together.

I would like to thank my dear friends for all of their kindness, help and supports. I have had a very nice time with *Mahdi Mashkoori, Fatemeh Kazemizadeh, Fariborz Parhizgar, Fatemeh Iranmanesh, Amin Ahmadi, Marjan Khamesian* and *Mohammd Pakdaman*.

I had very a delightful and memorable time in Albanova during the past five years. Specially all the lunchtimes. Many thanks go to *Hans Hansson, Anders Karlhede, Supriya Krishnamurthy, Fawad Hassan, Maria Hermanns, Sören Holst, Yaron Kedem, Emma Jakobsson, Vasileios Fragkos, Theresa Leistner, Thomas Kvorning, Jonas Larson, Irina Dumitru, Jonas Kjäll, Krishanu Chowdhury, Sreekant Manikandan, Ole Andersson, Pil Saugmann, Themis Mavrogordatos, Julia Hannukainen, Ahmed Abouelkomsan, Johan Carlström, Marcus Stålhammar, Jan Åman, Emil Bergholtz, Ingemar Bengtsson, Igor Pikovski, Jan Tuziemski, Elisabet Edvardsson, Flore Kunst, Qing-Dong Jiang, Matthew Lawson, Alex Millar, Frank Wilczek, Sara Strandberg, Edwin Langmann* and *Jens Bardarson*.

I would like to specially thank *Supriya Krishnamurthy, Åsa Larson* and *Fredrik Hellberg* for helping me to organize *Fika and News and Views*.

Thank you so much *Per-Erik Tegnér* for all the supports during the past few years.

And many thanks to all the people in the administration at Fysikum.

Contents

Chapter 1

Introduction

Phases of matter and phase transitions

In the field of theoretical condensed matter and statistical physics, a main goal is understanding, determining and classifying different phases of matter and the properties of each phase. One can track this back to the *classical elements*, earth, water, air and fire. With the progress in physics and chemistry the classification of states of matter evolved and changed to the three main categories, namely solid, liquid and gas [§]. Each state has its own properties. For instance, a typical solid can resist external pressure to some extend and for many applied purposes one can assume that a solid has a constant volume. Although the volume of a liquid is fixed and typically has negligible dependency on the pressure, the volume of a gas does depend on the external pressure and temperature. One can also consider other properties like thermal and electrical conductivity. Usually metals are efficient in thermal conduction and gasses are quite poor. For instance the thermal conductivity of air at room temperature and 1 Bar presssure is $\kappa_{air} \approx 3 \times 10^{-2} W/mK$, negligible in comparison with the thermal conductivity of Copper, $\kappa_{Cu} \approx 6 \times 10^{2} W/mK$ [1]. As it is clear, theys are different by four orders of magnitude. The electrical conductivity of these two are also different by many orders of magnitude. The electrical conductivity of air in the earth's atmosphere ranges form $\sigma_{air} \approx 10^{-13} 1/\Omega m$ to $10^{-9} 1/\Omega m$. Copper, however, is a very good conductor with electrical conductivity $\sigma_{Cu} \approx 5 \times 10^{7} 1/\Omega m$ [2].

This variety of properties makes the importance of having a *phase diagram* clear. A phase diagram shows the possible phases of a material, a substance or in theoretical studies a model, as a function of a set of parameters. These parameters could be external parameters like temperature and pressure over which we have control. On the other hand we do not have control over the interaction strength between the constituents of a material, say electrons in a solid. In such a case we consider the interaction as a parameter and study the behaviour of, say, a theoretical model over a range of it. By knowing the exact parameters for a specific material, either from an experiment or an ab-initio numerical study, one can predict the behaviour of the given material. Moreover having a phase diagram at hand, we can contemplate about the possibility of

[§]Some scientists later added plasma as the fourth category.

engineering new phases or desired behaviour by tuning the control parameters appropriately. This can be done in ultra-cold atom setups [3–5].

Defining a phase of matter is rather hard task. An intuitive definition is that all the points which belong to a phase share the same properties. For instance if the parameters of a given system belong to a point in the solid phase of the phase diagram, the system has a rather constant volume but if they lie in the gas phase, one can change its volume by applying appropriate pressure [§]. In quantum systems, as we will discuss in this thesis, one is usually interested in the presence of the gap Δ, the energy difference between the first excited state and the ground state, in the thermodynamic limit. A model with a finite gap is called *gapped* and otherwise the model is *gapless*. If a set of points in the phase diagram belong to the same phase, for all of them the system of interest or the model is either gapped or gapless. Therefore if the gap closes along a manifold in the phase diagram, that manifold *can* in principle separate two different phases [¶]. In general we are also interested in correlation functions (the connected ones where the averages are subtracted) in physical models. For a gapped system these are usually exponentially decaying functions with a correlation length ξ of the order of the inverse gap Δ^{-1} [6]. For gapless systems, however, the correlation functions usually decay as a power law in the absence of any characteristic length scale [7] [‡].

Defining *phase transitions* is simpler than defining phases of matter. Let us continue with the phase diagram of a typical substance as is shown in Fig. 1.1 [8]. There are three regions indicated by solid, gas and liquid in the phase diagram. Nonetheless one may wonder whether they are all different phases?

As we mentioned defining the phase itself is rather a hard task and usually it is done intuitively. To be rigorous and be able to do calculations we can, however, focus on the transitions. About half a century ago this was a major subject in statistical mechanics and condensed matter physics. It turns out that one can pinpoint a phase transition by studying the free energy density $f = F/V$, where V is the volume and F is the free energy of a system at finite temperature [6,8] and the ground state energy density $e_g = E_g/V$ where E_g is the ground state energy of a quantum system at zero temperature [6,9]. *Phase transitions are nailed down and classified (to some extend) by determining the order of the derivative of the free energy density or the ground state energy density with respect to a coupling, either an external one like temperature or a parameter in the model, at which it is not smooth and continuous.*

Consider the phase diagram in Fig. 1.1. For simplicity one may imagine the water as the substance, though note that for water the slope of the line separating solid and liquid is negative. Here the external parameters or the

[§] Note that these are the statements in the thermodynamic limit.

[¶] As we will later discuss there could be just a crossover rather than a phase transition.

[‡] This is guaranteed if the model has conformal symmetry [7].

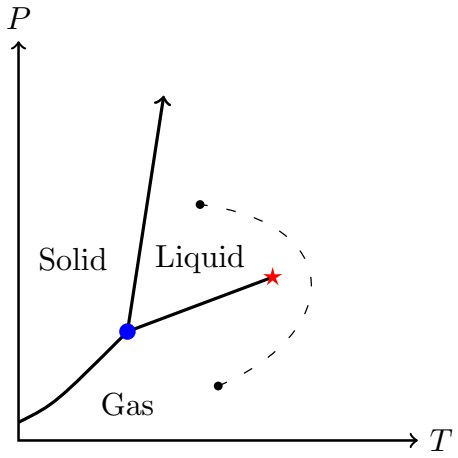

Figure 1.1: Schematic phase diagram of a substance as a function of temperature T and pressure P. The blue circle and the red star indicate the triple point and the critical point respectively.

couplings are the pressure P and the temperature T. The triple point where the three "phases" meet is marked with a blue circle. There are solid black lines separating apparent different phases, namely solid, liquid and gas. Across the solid lines a phase transition occurs. In this case the transition is of *first* order. Recall that a typical substance needs a latent heat to, say, melt or evaporate. Therefore there is a *discontinuity* in the entropy of the system S across the solid lines. Note that at finite temperature, entropy of a system can be calculated by taking a derivative of the free energy with respect to the temperature at constant volume, i.e. $S = -\left(\partial F/\partial T\right)_V$.

In the same way the first order transition in the quantum systems shows itself in the discontinuity of the first derivative of the ground state energy. This is usually the case when a level crossing occurs [8] as it is depicted in Fig. 1.2. In such a case close to the critical coupling λ_c at which the transition occurs, the two lowest eigenstate change their role. For $\lambda < \lambda_c$ the ground state is $|0\rangle$ and for $\lambda > \lambda_c$ the ground state is $|0'\rangle = |1\rangle$. Therefore although the ground state energy is continuous across the transition, its first order derivative with respect to λ at $\lambda = \lambda_c$ has a discontinuity. Such a transition is a first order quantum phase transition at zero temperature and we will see its examples in this thesis.

We now go back to the phase diagram in Fig. 1.1. The line which separates

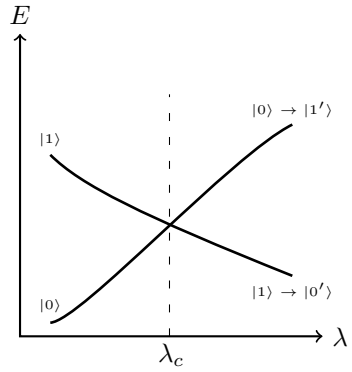

Figure 1.2: Schematic first order quantum phase transition at λ_c. The states $|0\rangle$ and $|1\rangle$ are the ground state and the first excited states for $\lambda < \lambda_c$ respectively. The states $|0'\rangle$ and $|1'\rangle$ are the ground state and the first excited states for $\lambda > \lambda_c$ respectively.

the liquid and solid phases "in principle" [§] continues [8]. Therefore there *is* always a first order transition between the solid phase and the rest of the phase diagram. For the gas and liquid regions, however, this is not the case. There is a critical point, marked with a red star at (T_c, P_c), at which the solid line separating them ends. For a temperature higher than the critical temperature T_c there is no transition between the two "phases". Actually as it is shown in the figure with a dashed line, one can connect any two points in these regions to each other without passing the solid line. Therefore the gas and the liquid are actually the same phase with our definition.

Having a *connected path* between the two points, representing a set of couplings, in the phase diagram is an important argument and will be also used for the quantum systems and later in the case of topological phases as well. Given two points in the phase diagram one asks whether a path between them exists along which the gap does not close? If such a path exists the two points belong to the same phase. If not, for any given path in the phase diagram which connects the two points, there is at least a point where the gap closes. This, however, does *not* imply that the two points belong to two different phases. Gap closing is a necessary condition but not sufficient for a phase transition. Usually when the gap closes a phase transition occurs but there could be a crossover as well. To claim that a phase transition occurs, one should also check it by studying the derivatives of the ground state energy and be sure

[§]This phrase is exactly quoted from Ref. [8].

that there is a discontinuity or divergence at some order [§]. For a crossover, although some behaviours of the system change, but there is no discontinuity or divergence in the derivatives of the ground state energy. We will encounter such a case in chapter 2.

Order parameter and symmetry breaking

The phases in Fig. 1.1 can be distinguished by means of an *order parameter*. The order parameter could be, for instance, a real scalar field or a vector field. A real scalar order parameter divides a phase diagram into two phases. One phase is usually called the *disordered* phase and the other is called the *ordered* phase. In the case of our substance in Fig. 1.1 the order parameter is the deviation from the average density. In the liquid/gas phase we have a uniform density. This is the disordered phase. In the solid phase, however, the atoms reside on the special positions determined by the lattice structure. Therefore there is indeed a deviation from the average density. In a more technical manner we can look at the Fourier transform of the density field. For the liquid/gas phase the main component is the one with zero momentum, the average. In the solid phase, however, we expect non-zero Fourier modes at specific momenta due to the lattice structure. In this sense the solid phase is the *ordered* phase. Therefore there is jump in the order parameter across the solid-liquid/gas phase boundary. The presence of a jump in the order parameter is a typical signature of a first order phase transition.

To shed more light on the names of the phases, ordered and disordered, we consider the Hamiltonian. Assume that we have a set of atoms which have kinetic and potential energy. If we assume that the atoms are simple spheres with no structure the potential energy between two atoms would only depend on their relative distance. In such a case the Hamiltonian describing the system has both translational and rotational symmetries. Although the liquid/gas phase respect these symmetries, the solid phase breaks both. In a solid one can only have translation symmetry if the translation is done by a vector belonging to the lattice. Moreover the system is not symmetric under an arbitrary rotation, though it may still respect a subgroup of the full group, say, SO(3).

The concepts of order parameter and symmetry breaking were among the most important and useful ones in condensed matter physics. They led to a deep understanding of phase transitions in general, and second order transitions in particular. A classic example of such a transition is the magnetic phase transition. Let us study this in some detail.

Consider a cubic lattice with the lattice constant a where on each site a magnetic atom lives. The spin of an atom on site $\vec{r}_i$ will be treated classically

[§]The case of Berezinskii-Kosterlitz-Thouless transition is more involved. Sometimes it is called an infinite order transition.

and is represented by a vector $\vec{s}(\vec{r}_i)$. We are not interested in the details of the spin configuration and do not need to know which spin is in what direction. Therefore we define a *coarse-grained* field $\vec{m}(\vec{r})$, the *magnetization*, and will work with it. To define a continuous and smooth field we consider a cube $\mathcal{C}$ of size l around a point $\vec{r}$ in space. The cube should enclose a considerable number of spins, $l \gg a$, and at the same time must be much smaller than the system size $l \ll L$, since we would need to consider the fluctuations in space. By averaging over the atoms residing in the cube we define the magnetization,

$$\vec{m}(\vec{r}) = \frac{1}{l^3} \sum_{\vec{r}_i \in \mathcal{C}} \vec{s}(\vec{r}_i) \ . \tag{1.1}$$

This field is the order parameter in magnetic systems. At high temperatures and zero external magnetic field there is no magnetization ($\vec{m}(\vec{r}) = \vec{0}$). This is the *paramagnetic* phase. By decreasing the temperature however, in the limit of zero external magnetic field, the system becomes magnetic with non-zero magnetization. This is the *ferromagnetic* phase. In this transition, unlike the first order transition, the order parameter does not jump and it actually increases slowly below a critical temperature T_c which depends on the details of the material. In Fig. 1.3 we present the schematic behaviour of the magnetization across the phase transition [8].

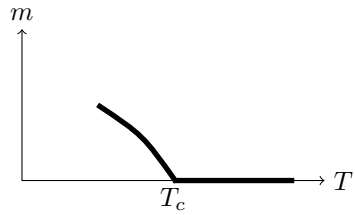

Figure 1.3: Schematic behaviour of magnetization close to the critical temperature.

As it is evident in Fig. 1.3, for temperatures lower than critical temperature the magnetization gradually increases, and one can define the exponent β as,

$$m(T) \sim (T_c - T)^{\beta} \ . \tag{1.2}$$

This is one of the *critical exponents* which characterize a critical point. Two other exponents can be defined using the divergence of the correlation length ξ and specific heat C close to the transition,

$$\xi \sim |T - T_c|^{-\nu} \ , \tag{1.3}$$

$$C \sim |T - T_c|^{-\alpha} \ . \tag{1.4}$$

One, however, does not need to know all the exponents since having two critical exponents and the space dimension d, fixes all the other exponents [8, 10]. For example we have,

$$\nu = \frac{2-\alpha}{d} \ . \tag{1.5}$$

The theoretical framework for critical phenomena was developed by Landau and Ginzburg [8, 10]. The main idea, in a nutshell, is as follows. To calculate the partition function $\mathcal{Z}$ one needs to know the Boltzmann weight of each configuration. As we said we rather work with a smooth field, say $\vec{m}(\vec{r})$, and need a Boltzmann weight for a given configuration of fields. In principle one can start from the microscopic model, and derive the corresponding weight, which is a complicated task. Instead one can take the phenomenological approach [8,10].

We first note that we are looking for a functional $\mathcal{H}$, the celebrated Landau-Ginzburg (LG) *effective* Hamiltonian, with which one can calculate the weight,

$$\mathcal{Z} = \int \mathcal{D}\vec{m}(\vec{r}) e^{-\mathcal{H}[\vec{m}(\vec{r})]} \ . \tag{1.6}$$

The integral is a functional integral over all the realizations of the vector field $\vec{m}(\vec{r})$ and we absorbed the $\beta = 1/k_B T$ in $\mathcal{H}$ where k_B is the Boltzmann constant. Second we assume that the effective interaction between the fields are also local and the functional $\mathcal{H}$ does only depend on the order parameter, its derivatives and the external local magnetic field. In addition since we are interested in the physics at the vicinity of the transition, we will expand the LG Hamiltonian in a power series of the order parameter and its derivatives.

The very crucial piece of the recipe is respecting the symmetries. In the case of spins, we know that the interaction between the two spins does only depend on their relative orientation and by rotating the full system (both spins simultaneously) nothing changes. Hence we put the same constraint on the LG Hamiltonian and demand that it should be invariant under rotation, i.e. for an arbitrary rotation $\mathcal{R}$ we should have $\mathcal{H}[\mathcal{R}\vec{m}(\vec{r})] = \mathcal{H}[\vec{m}(\vec{r})]$.

Putting this together, one can write the LG Hamiltonian,

$$\mathcal{H}[\vec{m}(\vec{r})] = \int d^d\vec{r} \left[\frac{K}{2} (\nabla \vec{m})^2 + \frac{t}{2} m^2 + \frac{u}{4} m^4 - \vec{h}(\vec{r}).\vec{m}(\vec{r}) + \cdots \right] \ . \tag{1.7}$$

The first term, the natural generalization of the simple harmonic oscillator potential energy, tries to reduce the fluctuations and is minimized by a constant order parameter. The coupling K is usually called the stiffness. The quadratic term, $m^2 = \vec{m}(\vec{r}).\vec{m}(\vec{r})$, is the lowest order term in the field respecting the desired rotational symmetry. The next order is m^4 and, of course, one can add higher order terms but there is no need to do so [8, 10]. The term $-\vec{h}(\vec{r}).\vec{m}(\vec{r})$ represents the effect of an external magnetic field. The other two real couplings are t and u. The coupling $t \sim T - T_c$ controls the phase transition. As

we mentioned there is no need to consider higher order terms (in the "Taylor expansion") and it suffices to keep what we already have in Eq. 1.7. Since the integral in the partition function should be well-defined and we do not expect large magnetization to have a considerable probability, in the case of Eq. 1.7 we should only consider $u > 0$. This concludes our brief discussion about the LG effective Hamiltonian [§].

We can now explain the concept of symmetry breaking. Consider the case with no external magnetic field, i.e. $\vec{h}(\vec{r}) = \vec{0}$. We constructed the LG Hamiltonian such that it has rotational symmetry. For $t > 0$, $T > T_c$, the lowest energy is obtained by the configuration $\vec{m}(\vec{r}) = \vec{0}$. This is the paramagnetic phase where the system has no magnetization and its configuration does also respect rotational symmetry. Below the critical temperature $t < 0$, the mean-field solution $\vec{m}(\vec{r}) = m\hat{m}$, which has no fluctuation in space, is,

$$m = \left(-\frac{t}{u}\right)^{\frac{1}{2}} , \qquad t < 0 . \tag{1.8}$$

Note that by minimizing the LG Hamiltonian we can only get the magnitude of the magnetization and have *no* information about its direction $\hat{m}$. The magnetization in fact could be in any direction and there is no preference for one [¶]. No matter which direction the magnetization has, this configuration of magnetization represents the ferromagnetic phase and *breaks* the rotational symmetry of the underlying LG Hamiltonian. This is the *spontaneous symmetry breaking* (SSB) mechanism which can be used to distinguish different phases and describes many phase transitions.

A set of critical exponents defines a *universality class*, describes a critical point and the behaviour of a given model across the transition. It turned out that the phase transition in many materials and models fall in to the same universality class, although the underlying microscopic details are quite different [11]. It is also worth to mention that from Eq. 1.8 we can read the mean-field prediction for one of the exponents, $\beta_{MF} = 1/2$. This is, however, different from many experimental results [8,10] and to get the correct exponent one needs to, of course, not only consider the fluctuations around the mean-field solution but also use the techniques like renormalization group and the so-called $\epsilon-$expansion [8,10]. These methods are very well established but will not be treated in this thesis.

Spontaneous symmetry breaking was (and still is) a quite powerful and fruitful framework to understand phases and phase transitions. Among the well-known examples in condensed matter we can mention the superconductiv-

[§] In Ref. [8] and in the literature in general this is also called Landau-Ginzburg free energy. However, since it appears in the Boltzmann weight of a given configuration, we prefer to call it an *effective* Hamiltonian. In any case the concept is much more important than the name.

[¶] In practice, however, any small external magnetic fixes the direction.

ity phenomena where below the transition temperature the global U(1) symmetry is broken down to the $\mathbb{Z}_2$ symmetry. The global U(1) symmetry represents the conservation of total number of electrons. In a superconductor, however, the parity of the number of electrons is conserved and there is a possibility for an electron pair annihilation or creation. It is also worthwhile to mention that applications of the SSB mechanism were not restricted to condensed matter systems and statistical physics models. The celebrated Higgs mechanism (in high-energy physics) with which elementary particles acquire mass uses the same framework [12].

The Berezinskii-Kosterlitz-Thouless transition

Symmetry breaking and the presence of an ordered phase is not always possible. For instance the Peierls argument shows that in one dimension there is no ordered phase at *finite temperature* [8]. To see this consider the Ising model on an open chain of size L. A classical spin $s_i = \pm 1$ lives on each site and the energy of a spin configuration $\underline{s} = (s_1, s_2, \cdots)$ is,

$$E[\underline{s}] = -\sum_{\langle ij \rangle} J s_i s_j \ . \tag{1.9}$$

The coupling J is a positive real number with the dimension of energy. At zero temperature ($T = 0$) the two configurations with the lowest possible energy are $(+1, +1, \cdots, +1)$ and $(-1, -1, \cdots, -1)$. These are clearly ordered. So an ordered phase *exists* at zero temperature. At finite temperature we need to consider the other states as well. The lowest possible "excitions" are domain walls, like

$$(+1, +1, \cdots, +1, \underbrace{+1}_{\mathrm{i^{th}site}}, \underbrace{-1}_{\mathrm{i+1^{th}site}}, -1, \cdots, -1, -1) \ . \tag{1.10}$$

Although the excitation energy of such a domain wall is finite, $+2J$, it can happen on any bond on the chain for which there are $L - 1$ choices. Therefore the presence of such a domain wall changes the free energy as follows,

$$\Delta F = 2J - k_B T \ln(L - 1) \ . \tag{1.11}$$

As it is evident due to the entropy contribution, presence of the domain walls are favourable in the thermodynamic limit and hence the order will be destroyed at any finite temperature. We note that the Ising model in two dimensions, however, has a phase transition at finite temperature and the ordered phase does also exist at finite temperature [10, 13].

There is an analogous situation for models with a continuous symmetry. A model with a continuous symmetry has massless Goldstone modes as excitations in its ordered phase [10,12]. The Mermin-Wagner theorem states that the

presence of Goldstone modes destroy the order and prevents the SSB in models with a continuous symmetry at finite temperature in dimensions $d \leq 2$ [10, 14]. Note that the theorem requires a continuous symmetry. Hence the phase transition in the Ising model in two dimensions which is a $\mathbb{Z}_2$ symmetry breaking transition does *not* violate this theorem.

Having all these concepts and consistent framework, studies on the classical XY model [§] came as a surprise. Let us first define the classical XY model and explain its peculiar behaviour. Consider a two dimensional square lattice. A two dimensional unit vector $\hat{s}_i$ (a "spin") lives on each site. The vectors lie in the lattice plane, say the xy-plane. The angle between the vector and, say, the $x-$axis is θ_i. For a given configuration of vectors $\underline{\hat{s}} = (\hat{s}_1, \hat{s}_2, \cdots)$ the energy is,

$$E[\underline{\hat{s}}] = \sum_{\langle ij \rangle} -J \hat{s}_i . \hat{s}_j = \sum_{\langle ij \rangle} -J \cos(\theta_i - \theta_j) \ . \tag{1.12}$$

As before J is a positive real coupling constant and the sum is over nearest neighbours.

As it is clear this model has a continuous symmetry, namely the global rotation around the $z-$axis which leaves all the angle differences invariant. Since the model is defined on a two dimensional lattice, the Mermin-Wagner theorem dictates that there is no ordered phase in the model. On the other hand the high temperature expansion of the model, done by Stanley and Kaplan [15], showed a divergence in the susceptibility at some finite temperature. This was a clear signature of a phase transition and yet an ordered phase at low temperature was not an option.

To distinguish between the two phases let us consider the two-point spin-spin correlation function. At high temperature $T \gg J/k_B$ one gets,

$$\langle \hat{s}(\vec{0}) . \hat{s}(\vec{r}) \rangle \approx e^{-r/\xi}, \qquad \xi = \frac{1}{\ln(2k_B T/J)} \ , \tag{1.13}$$

as the dominant term [10]. The $\langle \mathcal{O} \rangle$ denotes the thermal ensemble average. The exponential decay with a correlation function which decreases as the temperature increases is a signature of a disordered phase. This is also intuitive.

At low temperature the two-point spin-spin correlation function behaves differently,

$$\langle \hat{s}(\vec{0}) . \hat{s}(\vec{r}) \rangle \approx \left(\frac{a}{r} \right)^{\frac{k_B T}{2\pi J}} \ , \tag{1.14}$$

where a is the short distance cutoff. This is not a constant function but it is not decaying exponentially fast either. More importantly it can also be shown that the interaction among Goldstone modes does not change the presence of the power law decay [10]. Therefore there are clearly two *distinct* phases separated

[§] In the next chapters we will study the *quantum* XY model in one dimension.

by a *phase transition*. Note that the Mermin-Wagner theorem states that there is no ordered phase at low temperature, but it does not say anything about the presence of *another* type of phase.

Unravelling the nature of the low temperature phase and the phase transition was done by an important observation by Berezinskii [16] and Kosterlitz and Thouless [17]. The crucial point is that all the "spin" configurations are not *topologically* equivalent. To understand this, consider the situation where $\nabla\theta$ represents a *vortex* and is given by (in the continuum limit) [10],

$$\nabla\theta(x,y) = \frac{n}{r^2}(-y,x) \ , \tag{1.15}$$

where $n \in \mathbb{Z}$ and $r = \sqrt{x^2+y^2}$. The $n = 0$ case has no *topological defect*. The cases with $n \neq 0$ are rather different. For these cases for a closed loop enclosing the origin $\mathcal{C}$, no matter what the shape of the loop is, we have,

$$\oint_{\mathcal{C}} \nabla\theta.d\vec{\ell} = 2\pi n \ , \tag{1.16}$$

and otherwise the integral gives zero. A configuration with such a defect *can not* be continuously deformed to the case without any defect (regardless of the energy cost). Even it is not possible to continuously deform configurations with different topological number n. This is simply due to the fact that n is an integer and a continuous deformation can not change it [§].

The responsible constituents for the transition are actually these vortices. To see the role of the vortices it suffices for our purpose to study the free energy of a single vortex ($n = 1$) of size a within a system of linear size L in the continuum limit [10],

$$U_1 \approx \frac{J}{2}\int_a^L d^2r\,(\nabla\theta)^2 = \pi J \ln\left(\frac{L}{a}\right) \ , \tag{1.17}$$

$$S_1 \approx k_B \ln\left(\frac{L}{a}\right)^2 \ , \tag{1.18}$$

$$F_1 = U_1 - TS_1 \approx (\pi J - 2k_BT)\ln\left(\frac{L}{a}\right) \ . \tag{1.19}$$

This clearly shows a transition at $T_c = \pi J/2k_B$. At high temperature $T > \pi J/2k_B$ the presence of vortices will lower the free energy. In low temperatures, however, their presence increases the free energy and hence they are absent. In addition it can be shown that a dipole, a bound configuration of a vortex, say $n = +1$, and an anti-vortex, say $n = -1$, has finite energy and can be present at any temperature. This indicates that the transition is driven by the

[§]I do accept that this is not a proof, but I think it is sufficiently rigorous and intuitive for physicists.

vortices. At low temperature the model is described by a gas of dipoles without any free vortices and in the high temperature it consists of free vortices. This is the Berezinskii-Kosterlitz-Thouless (BKT) transition. We note that across the BKT transition, although there are divergences in different quantities, the energy and its derivatives are smooth and continuous. In this sense this transition is sometimes called an infinite order transition. As a consequence probing this transition numerically is a quite hard task.

Topological phases at zero temperature

Later deviations from the SSB scheme were found in quantum systems (setups): the integer and fractional quantum Hall effects [18,19], topological insulators [20–23] and topological superconductors [24,25], to name a few. Based on these experimental and theoretical studies, and many others, concepts of *topological phases and phase transitions* of quantum systems emerged. Such phases occur at zero temperature where any phase transition is driven by quantum fluctuations.

In a very general classification topological phases can be divided into two groups. The gapped topological phases and the gapless ones. Although the gapless phases have a quite rich and intriguing physics, here we will only focus on the gapped topological phases. The gapped topological phases can further be divided into two rich groups. There are the so-called *intrinsically topologically ordered phases* and the *symmetry protected topological* (SPT) phases.

In systems and models with an *intrinsic topological order*, the main role is usually played by a strong interaction. The well-known examples of such systems are fractional quantum Hall effect and the Toric code model [26]. Distinguishing features of these systems are the presence of fractional excitations and *anyonic* statistics [27]. We will show an example of anyons, namely *semions*, in the Toric code model.

The very existence of SPT phases, however, does depend on a specific symmetry or a set of symmetries. In an SPT scheme, we have the *trivial phase* where the ground state is a simple product state. For example in a system of $S = 1/2$ spins such a state (a reference state) is, say, all spins in the $+z$-direction $(|\uparrow\rangle^{\otimes L}$ where L is the total number of spins). For a fermionic system the trivial state could be filling all the states or leaving them all to be empty. Hamiltonians with the trivial state as their ground state belong to the trivial phase.

In addition we need to provide a rather rigorous definition for *being in the same phase*. To do so given the Hamiltonians $\mathcal{H}_i$ and $\mathcal{H}_f$ one asks whether it is possible to connect them *adiabatically*? To assert that it *is* possible to do so, one needs to find a one parameter family of Hamiltonians $\mathcal{H}(s)$ for $s \in [0, 1]$ such that,

1) We have $\mathcal{H}(0) = \mathcal{H}_i$ and $\mathcal{H}(1) = \mathcal{H}_f$.

2) The Hamiltonian $\mathcal{H}(s)$ is gapped all along the path.

3) The Hamiltonian $\mathcal{H}(s)$ respects the desired symmetries all along the path.

If such a family of Hamiltonians exists, the given Hamiltonians and their ground sates belong to the same phase. Hence if one can *not* connect a given Hamiltonian $\mathcal{H}_T$ to a Hamiltonian with the reference state as its ground state, the Hamiltonian $\mathcal{H}_T$ and its ground state belong to a *topological phase*. Since along the above mentioned path one needs to respect a specific set of symmetries, these phases are called symmetry protected topological phases and, of course, can be adiabatically connected to the trivial phase by breaking at least one of the protecting symmetries.

We will name a few properties which usually distinguish topological phases. We note that a topological phase can only have some of these properties. As we mentioned earlier intrinsic topological phases hosts fractional excitations in their bulk. To the best of our knowledge, however, so far no fractional excitations were found in the bulk of an SPT phase. Another important feature of a topological phase is the dependency of the ground state degeneracy on the topology of manifold on which the model is defined. As we show below, the Toric code on a torus with genus g has 2^{2g} degenerate ground states. The so-called *localized gapless edge modes* are another property of topological phases. These appear on the boundary between a topological phase and a trivial phase. We will see examples of them in chapter 2, chapter 3 and chapter 5. In addition these phases have quantized transport properties. For instance in the integer and fractional quantum Hall effects where electrons interact in an effectively two-dimensional system and a strong external magnetic field is also applied, plateaus in the conductance (σ) were found upon increasing the magnetic field [18, 19]. The conductance on these plateaus is quantized as,

$$\sigma = \nu \frac{e^2}{h} \ , \tag{1.20}$$

where e is electron charge, h is the Planck constant and ν takes the integer or fractional values. Aspects of entanglement, like the degeneracy in the entanglement Hamiltonian, also play crucial roles in detecting topological phases.

In what follows we first present the Toric code and discuss its properties. This is an exactly solvable model where we can see, for instance, fractional statistics of excitations. After that we discuss the classification of non-interacting fermionic systems which includes the systems like integer quantum Hall effect, quantum spin Hall effect and the Kitaev chain, to name a few.

The Toric code

An exactly solvable model of spins which shows some of the above mentioned properties was introduced and solved by Kitaev [26]. Since the features like the dependency of the ground state degeneracy on the manifold on which the model lives and anyonic excitations can be rather easily seen in this model, it is quite fruitful if we briefly discuss it.

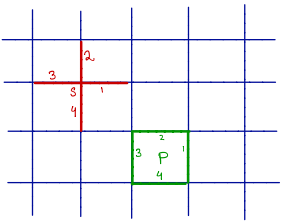

Figure 1.4: Star and plaquette operators in the Toric code.

The model is defined on a square lattice. A spin$-\frac{1}{2}$ lives on each edge and the Hamiltonian reads,

$$H = -J_e \sum_s A_s - J_m \sum_p B_p \ , \tag{1.21}$$

in which J_e and J_m are positive couplings. The first sum is over all the stars, the second sum is over all the plaquettes (see Fig. 1.4) and the operators are defined as follows,

$$A_s = \prod_{j \in s} \sigma_j^z, \qquad B_p = \prod_{j \in p} \sigma_j^x \ . \tag{1.22}$$

This model is exactly solvable since all the star and plaquette operators commute with each other. Moreover note that,

$$A_s^2 = B_p^2 = \mathbf{1} \ , \tag{1.23}$$

where $\mathbf{1}$ is the identity operator. This means that the ground state of the model is an eigenstate of all the star and plaquette operators with the eigenvalue $+1$. A state where all the spins are aligned in $+z$-direction, $|\uparrow\uparrow\cdots\rangle$ (usually called the reference state), does the job for the star operators. But it is not the only state with such a property and any state where two or four edges of each star are flipped is also acceptable. These states can actually be constructed by applying plaquette operators and to get the ground sate it suffices to sum them all,

$$|GS\rangle = \prod_p (\mathbf{1} + B_p) \, |\uparrow\uparrow\cdots\rangle \ . \tag{1.24}$$

It is straight forward to show that $A_s |GS\rangle = B_p |GS\rangle = |GS\rangle$ for all s and p. Moreover one can be convinced that the down spins form a set of closed loops in the states which appear in Eq. 1.24. As example in Fig. 1.5 we show the following two terms,

$$B_{p_1} B_{p_2} B_{p_3} |\uparrow\uparrow \cdots\rangle \ ,$$
$$B_{p_1} B_{p_2} B_{p_3} B_{p_4} B_{p_5} |\uparrow\uparrow \cdots\rangle \ .$$

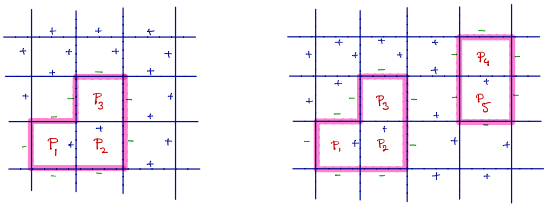

Figure 1.5: Examples of closed loops of down spins which appear in Eq. 1.24.

One may now wonder does the state in Eq. 1.24 include all the possible loops? The answer to this question depends on the manifold on which we want to study the model on. On a plane the answer is yes. Since any loop on a plane (without a defect) is *contractible* to a *point*, a finite number of plaquette operators is sufficient to form any desired loop. Therefore, owing to the product in Eq. 1.24, we get all the possible loops on an plane.

What about other manifolds? To be specific let us consider periodic boundary conditions and study the model on a torus with genus $g = 1$. In this case we can see that Eq. 1.24 does not include the *non-contractible* loops of a torus. There are two of them on a torus with genus $g = 1$. One of the non-contractible loops and the corresponding configuration are depicted in Fig. 1.6.

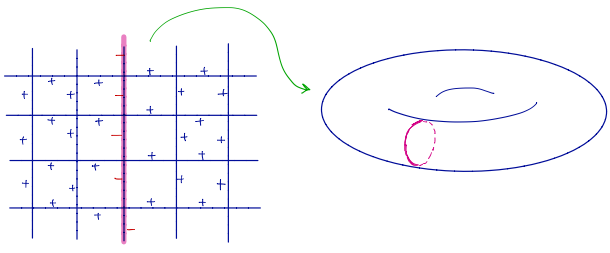

Figure 1.6: A configuration of flipped spins along a non-contractible loop of a torus.

To appreciate the importance of the non-contractible loops on a torus [§] and understand the degeneracy of the ground state we need to consider the constraints and the excitations. On a torus with N vertices there are, of course, N star and N plaquette operators with the following two constraints due to the periodic boundary conditions,

$$\prod_s A_s = \prod_p B_p = \mathbf{1} \ . \tag{1.25}$$

The number of edges, where the spins live on, is $2N$. Therefore the Hilbert space is 2^{2N} dimensional. Although all the star and plaquette operators do commute with the Hamiltonian and with each other, due to the above mentioned constraints there are only $2N-2$ independent of them to label the states, and hence we need two more operators with which one can label the full many-body spectrum without any ambiguity. These two operators are not local, and need to be defined along the non-contractible loops of the torus. To further motivate them (and although it may sound counter intuitive) let us study the excitations and introduce the other two operators using them.

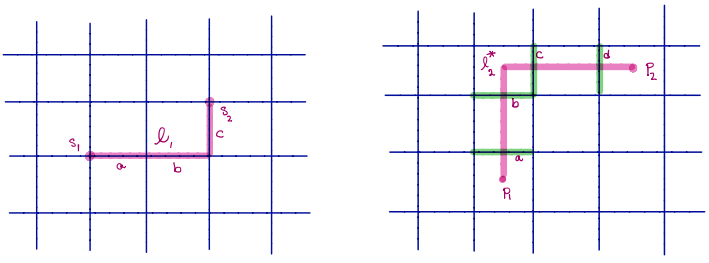

(a) (b)

Figure 1.7: (a) Electric and (b) magnetic excitations of the toric code.

There are two types of excitations in the Toric code. On can either make an excitation in the star operators, the so-called electric charges (Fig. 1.7a), or in the plaquette operators, the so-called magnetic charges (Fig. 1.7b). For the path in Fig. 1.7a we define the operator which flips the spins,

$$W^e_{l_1} = \prod_{j \in l_1} \sigma^x_j = \sigma^x_a \sigma^x_b \sigma^x_c \ . \tag{1.26}$$

The operator $W^e_{l_1}$ commutes with all star and plaquette operators except A_{s_1} and A_{s_2}, with which it anticommutes. Therefore by defining an excited state

[§] From now on we will only consider the case $g = 1$ and just mention the result for $g > 1$ in the end.

as,

$$|s_1, s_2\rangle = W^e_{l_1} |GS\rangle \ , \tag{1.27}$$

we have,

$$A_{s_1} |s_1, s_2\rangle = - |s_1, s_2\rangle \ , \qquad A_{s_2} |s_1, s_2\rangle = - |s_1, s_2\rangle \ , \tag{1.28}$$

which results in ,

$$H |s_1, s_2\rangle = (E_{GS} + 4J_e) |s_1, s_2\rangle \ , \tag{1.29}$$

where E_{GS} is the ground state energy. An intriguing feature of these excitations is that their energy does *not* depend on the length of its string, namely l_1. Hence these excitations, if exists, can freely move without costing any energy. In addition they always appear in pairs.

The so-called magnetic excitations can also be defined as it is shown in Fig. 1.7b,

$$W^m_{l^*_2} = \prod_{j \in l^*_2} \sigma^z_j = \sigma^z_a \sigma^z_b \sigma^z_c \sigma^z_d \ . \tag{1.30}$$

With the same type of reasoning as presented above, one can show that the state,

$$|p_1, p_2\rangle = W^m_{l^*_2} |GS\rangle \ , \tag{1.31}$$

is an excited state with energy $E_{GS} + 4J_m$.

To study the degeneracy in the ground state, without losing generality, we continue with the electric charges. The string operator W^e_l flips all the spins on the path l. For an open path, as discussed above, this results in an excited state. One can, however, study the closed ones as well. In such a case the two ends *fuse* and one get a closed loop of flipped spins. The energy of such a state is the ground sate energy. The important question is about the path l: Is it possible to contract it to a point or is it one of the non-contractible loops of the the torus (see Fig. 1.8)? In the former case, the state has been already considered in the ground state wavefunction in Eq. 1.24. In the later case, however, we end up at *another* ground state.

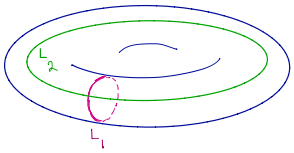

Figure 1.8: Two non-contractible loops of a torus.

In fact the other two operators with which we can close the set of operators needed for labeling the full many-body Hilbert space are $W^e_{L_1}$ and $W^e_{L_2}$ which should be defined along the two non-contractible loops of a torus (see Fig. 1.8).

These two operators commute with all star and plaquette operators and hence the Hamiltonian. These two are *nonlocal* operators and since they also commute with each other, their eigenvalues, (± 1), can *distinguish* different ground states. The four ground states can be written as follows,

$$|w_1, w_2\rangle = \left(\mathbf{1} + w_1 W^e_{L_1}\right)\left(\mathbf{1} + w_1 W^e_{L_2}\right)|GS\rangle \ , \tag{1.32}$$

and we have,

$$W^e_{L_i}\,|w_1, w_2\rangle = w_i\,|w_1, w_2\rangle \ . \tag{1.33}$$

One can also show that the degeneracy of the model on a torus with genus g is 2^{2g} where $2g$ is the number of non-contractible loops.

Before closing this section we mention the statistics among the excitations. Since electric charges are always formed by applying σ^x operators along some paths, they behave like bosons and by exchanging them nothing happens. The same is true for magnetic ones. Therefore these are bosons among themselves. However, the mutual statistics between an electric charge and a magnetic charge is more involved. As it is depicted in Fig. 1.9 by taking an electric charge, going around a magnetic charge and arriving the initial position, the two stings attached to the charges cross. Due to this the wavefunction picks up a *minus sign*. This is usually called the *semionic* statistics and it shows that in two dimensional systems, statistics beyond bosonic and fermionic is possible. Remind that this behaviour is quite different from fermionic and bosonic ones where under double exchange of particles nothing happens to the wavefuncion [§].

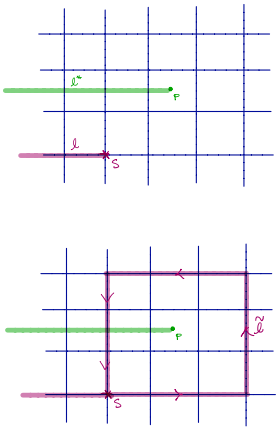

Figure 1.9: Braiding (two exchanges) an electric charge around a magnetic one.

[§]Note that we do not consider the dynamical phase. We are only interested in the mutual statistics

Topological phases of non-interacting fermions

In this section we will discuss the classification of topological phases of non-interacting fermions. This will include phenomena and models like the integer quantum Hall effect, the quantum spin Hall effect, the Kitaev chain any many more. These are the non-interacting SPT phases and the resulting classification is known as the *Altland-Zirnbauer* table [28].

Consider a second quantized Hamiltonian as follows,

$$\hat{H} = \sum_{\alpha\beta} \Psi^\dagger_\alpha H_{\alpha\beta} \Psi_\beta = \Psi^\dagger H \Psi \ , \tag{1.34}$$

where $\Psi = (\Psi_1, \Psi_2, \cdots)^T$ is a column vector of annihilation operators on different sites, and in case it is needed one can also include the spin index as $\Psi = (\Psi_{1\uparrow}, \Psi_{1\downarrow}, \Psi_{2\uparrow}, \Psi_{2\downarrow}, \cdots)^T$. The matrix H with the entries $H_{\alpha\beta}$ is called the *first quantized* or *single-particle* Hamiltonian [29]. In the presence of superconductivity paring one needs to use the Bogoliubov–de–Gennes (BdG) form,

$$\hat{H} = \frac{1}{2} \sum_{\alpha\beta} \Psi^\dagger_\alpha H_{\alpha\beta} \Psi_\beta = \frac{1}{2} \Psi^\dagger H \Psi \ , \tag{1.35}$$

where $\Psi = \left(\Psi_1, \Psi_2, \cdots, \Psi^\dagger_1, \Psi^\dagger_2, \cdots\right)^T$ is a column vector of annihilation operators on different sites followed by the creation operators.

We assume that all the unitary symmetries of the first quantized Hamiltonian have been already used and they are block-diagonalized using all the generators of the unitary symmetries. Therefore the above mentioned Hamiltonian needs to be treated as it is one of the blocks of the Hamiltonian [29]. In such a case we are only left with the *anti-unitary* symmetries (and their combination) and should study them. Hence three symmetries which should be considered and play the crucial role in this classification are the *time-reversal symmetry*, the *particle-hole symmetry* and the *chiral symmetry* (*sublattice symmetry*) [29–32]. We introduce and summarize their properties in what follows:

- *Time-reversal symmetry*: The first quantized Hamiltonian is time-reversal symmetric if an *anti-unitary* operator $\mathbf{T}$ exists such that,

  $$\mathbf{T} H \mathbf{T}^{-1} = H \ . \tag{1.36}$$

  The operator $\mathbf{T}$ can also be written as,

  $$\mathbf{T} = U_T K \ , \tag{1.37}$$

  in which U_T is a unitary matrix and K is the complex conjugate operator. Using the Schur's Lemma one can show that there are two possibilities

for $\mathbf{T}^2$ [§],

$$\mathbf{T}^2 = \pm\mathbf{1} \ . \tag{1.38}$$

- *Particle-hole symmetry*: The first quantized Hamiltonian is particle-hole symmetric if an *anti-unitary* operator $\mathbf{P}$ exists such that,

$$\mathbf{P}H\mathbf{P}^{-1} = -H \ . \tag{1.39}$$

The operator $\mathbf{P}$ can also be written as,

$$\mathbf{P} = U_P K \ , \tag{1.40}$$

in which U_P is a unitary matrix and K is the complex conjugation operator. Like what we had for the time-reversal operator, there are two possibilities for the particle-hole operator,

$$\mathbf{P}^2 = \pm\mathbf{1} \ . \tag{1.41}$$

- *Chiral symmetry*: The first quantized Hamiltonian has the chiral symmetry if a *unitary* operator $\mathbf{C}$ exists such that,

$$\mathbf{C}H\mathbf{C}^{-1} = -H \ . \tag{1.42}$$

If the operators $\mathbf{T}$ and $\mathbf{P}$ exist, the operator $\mathbf{C}$ can be written as,

$$\mathbf{C} = \mathbf{T}\mathbf{P} = U_T U_P^* \ . \tag{1.43}$$

We can always choose the unitary matrices such that [29],

$$\mathbf{C}^2 = \mathbf{1} \ . \tag{1.44}$$

In Table. 1.1 we present all the possible classes based on the above mentioned symmetries. There are eight classes where at least either time-reversal or particle hole symmetry exists. In these eight classes the presence or absence of the chiral symmetry can be concluded from the other two. In the Table. 1.1 we present all of these eight cases. In addition using $\pm\mathbf{1}$ we show the squared of the time-reversal or particle-hole symmetry operator if they exist. The squared of the chiral symmetry, as discussed above, is always $+\mathbf{1}$, and hence its presence (absence) is shown by $\mathbf{1}$ (0).

If neither time-reversal symmetry nor particle-hole symmetry exists, still the chiral (sublattice) symmetry can exist. This gives two more classes, namely the Cartan classes **A** and **AIII**.

[§]One may recall this is also the case for the time-reversal operator for spins. For integer spins we have $\mathbf{T}^2 = +\mathbf{1}$ while for half-integers we have $\mathbf{T}^2 = -\mathbf{1}$.

	Symmetries			d		
Cartan label	**T**	**P**	**C**	1	2	3
A	0	0	0	0	$\mathbb{Z}$	0
AIII	0	0	**1**	$\mathbb{Z}$	0	$\mathbb{Z}$
AI	$+\mathbf{1}$	0	0	0	0	0
BDI	$+\mathbf{1}$	$+\mathbf{1}$	**1**	$\mathbb{Z}$	0	0
D	0	$+\mathbf{1}$	0	$\mathbb{Z}_2$	$\mathbb{Z}$	0
DIII	$-\mathbf{1}$	$+\mathbf{1}$	**1**	$\mathbb{Z}_2$	$\mathbb{Z}_2$	$\mathbb{Z}$
AII	$-\mathbf{1}$	0	0	0	$\mathbb{Z}_2$	$\mathbb{Z}_2$
CII	$-\mathbf{1}$	$-\mathbf{1}$	**1**	$2\mathbb{Z}$	0	$\mathbb{Z}_2$
C	0	$-\mathbf{1}$	0	0	$2\mathbb{Z}$	0
CI	$+\mathbf{1}$	$-\mathbf{1}$	**1**	0	0	$2\mathbb{Z}$

Table 1.1: The Altland-Zirnbauer table for the classification of free fermionic Hamiltonians. The label is named after Élie Cartan who studied symmetric spaces [28, 29]. The entry $\pm\mathbf{1}$ shows the squared of the operator. The entry $\mathbf{1}/0$ shows whether a symmetry exists/does not exist. The spatial dimension is represented by d.

For each class depending on the spatial dimension d we have 0 or a group. If all the phases of a given Hamiltonian belong to the same phase, the trivial phase, we have 0. Therefore in such a case there is no topological phase at all. However, if we have a group, say $\mathbb{Z}$, elements of the group distinguish different phases. The identity element represent the trivial phase and the other ones represent the topological ones.

For example the integer quantum Hall effect is a two-dimensional setup which belongs to the class **A** (no symmetry). Therefore different phases are classified with the group $\mathbb{Z}$. This integer is exactly the one that we had in quantized conductance. Physically the conductance and this integer are related to the Chern invariant of the occupied bands in the system [33].

In chapter 2 we will discuss the Kitaev chain [25] and its generalization with phase-gradients and longer range couplings. The Kitaev chain with real couplings belongs to the class **BDI**. The topological phases of this class in one dimension are classified with the group $\mathbb{Z}$ which represents the number of Majorana zero modes on the edges. Upon breaking the time-reversal symmetry the class changes to **D** where in one dimension we have the $\mathbb{Z}_2$ classification.

Therefore given a Hamiltonian and a spatial dimension one can figure it out which group distinguishes different phases. In the case of interacting fermions, however, there is no full classification yet. We will comment on this in chapter 3 and chapter 6.

Summary and the outline of the thesis

In summary we briefly discussed the meaning of a phase and phase transitions. We presented the spontaneous symmetry breaking scheme which was a tremendously powerful method in classifying phase transitions. We then showed that the phase transition of the classical XY model can not be described by the SSB scheme. Then we continued with the topological phases at zero temperature, discussed their properties and presented the classification of the non-interacting fermionic Hamiltonians.

In chapter 2 we will be discussing generalizations of the Kitaev chain and specifically focus on the Majorana zero modes in the topological phases. In chapter 3 we discuss $\mathbb{Z}_n$ frustration free models. We present some introductory material on Bosonization and matrix product sates in chapter 4 and chapter 5 respectively. These will be extensively used in our study on the Kitaev-Hubbard chain in chapter 6 and hopping models of Fock parafermions in chapter 7.

Chapter 2

The Kitaev chain with phase-gradients and longer range couplings

Introduction

The classical Ising model, which is quite simple to state, turned out to be one of the most fruitful models in theoretical physics. The model is defined as follows. Consider a lattice (or graph) with $\mathcal{N}$ sites (or nodes). A classical spin $s_i = \pm 1$ lives on each site. For a given configuration of spins $\underline{s} = (s_1, s_2, \cdots)$, the energy is defined as follows,

$$E[\underline{s}] = -\sum_{\langle ij \rangle} J s_i s_j \ , \tag{2.1}$$

where J is the interaction strength and one needs to sum over all the nearest neighbour pairs, i.e. bonds or edges of the graph. In statistical mechanics the main goal is the calculation of the partition function for arbitrary temperature and study the phase diagram of the model.

The classical Ising model has been exactly solved on a chain (one dimension) [8], the two dimensional square lattice [10, 13] and the hexagonal lattice [34]. The mean field solution is valid in $d > 4$ dimensions [8]. The model does not show any phase transition in one dimension. In two dimensions, however, it has two phases. For low temperatures it has an ordered phase in which the net magnetization $\sum_i s_i/\mathcal{N}$ is non-zero in the thermodynamic limit. For high temperatures the model is in a disordered phase where the spins are randomly oriented with no net magnetization. The critical temperature T_c separates the ordered and the disordered phases [13],

$$T_c = \frac{2J}{k_B \ln(1+\sqrt{2})} \ , \tag{2.2}$$

where k_B is the Boltzmann constant.

To study the phase transition and the behavior of the model close to the critical point one can use the classical to quantum map as discussed by Fradkin and Susskind [6, 35]. One can show that by taking an appropriate limit properties of the classical Ising model can be inferred from the the transverse

field Ising model (TFIM) [6, 35],

$$H_{\mathrm{TFIM}} = -J_x \sum_{j=1}^{L-1} \sigma_j^x \sigma_{j+1}^x - h \sum_{j=1}^{L} \sigma_j^z \ , \tag{2.3}$$

in which σ_j^α are Pauli matrices, J_x, and h are real coupling constants and L is number of sites. One can calculate J_x and h in terms of the energy unit J, the temperature T, the classical system's size and the lattice spacing of the classical model. We do not need the exact relation in what follows. Note that the classical model has been defined in two spatial dimensions and through the map we get a $(1+1)$-dimensional quantum model.

To make the connection between these two models more clear, we present a short "dictionary". The ground state energy of the TFIM is the free energy of the classical Ising model. Therefore divergences in the derivatives of the free energy will be also seen in the derivatives of the ground state energy of the quantum model (see chapter 1). This means that the quantum model also has different phases. In addition the gap and the ground state expectation values of operators in the TFIM correspond to the correlation length and the ensemble averages in the classical model [6, 35].

One can solve the TFIM exactly [36] by mapping it to a free fermionic model using the Jordan-Wigner (JW) transformation [37]. As one expects the TFIM has also two phases, namely an ordered phase for $|h| < |J_x|$ and a disordered phase for $|h| > |J_x|$. The model has a $\mathbb{Z}_2$ symmetry which simply means that the Hamiltonian is invariant under flipping all the spins. In the disordered phase $\langle \sigma_i^x \rangle = 0$ the ground state is unique and respects the symmetry. In the ordered phase $\langle \sigma_i^x \rangle \neq 0$, however, the $\mathbb{Z}_2$ symmetry is broken and the ground states are not invariant under the generator of the $\mathbb{Z}_2$ symmetry.

As we mentioned the exact solution was done by mapping the model to free fermions. This map has always been thought of as a trick to solve the model. Nevertheless one can ask, as Kitaev did [25], about the meaning of the two phases in the fermionic incarnation. Put it another way, what would have been the phases of the fermionic model, had the fermions been the constituents of a physical system?

Kitaev showed that the fermionic incarnation of the model, nowadays known as the Kitaev chain, does have two phases indeed. Although these two phases can not be distinguished by a local order parameter, as it can be done for the ordered phase and the disordered phase of the TFIM, they can be differentiated by a *topological invariant* ν (see chapter 1). The ordered phase of the TFIM corresponds to the topological phase of the fermions with $\nu = 1$ and the disordered phase corresponds to the trivial phase of the Kitaev chain with $\nu = 0$.

One can, of course, wonder about the physical meaning of the topological invariant. Is it just a number distinguishing the two phases of the fermionic

model or does it have a meaning? Kitaev showed that the topological invariant (the non-trivial topology of the bulk) represents itself in terms of the zero energy edge modes of an open chain [25]. Hence the topological invariant is interpreted as follows. The model in the trivial phase with $\nu = 0$ has no zero mode for an open chain. In the topological phase with $\nu = 1$, however, the model hosts one Majorana zero mode (MZM) on each edge of an open chain [25]. The crucial point is that the number of MZMs per edge is the same as the topological invariant. In addition note that a Majorana fermion is "half" of a fermion, in the sense that one needs two Majorana fermions to form one Dirac fermion. Therefore in the topological phase of the Kitaev chain on an open chain with $\nu = 1$, the model has one *non-local* fermionic state with support on the two edges. This non-locality makes the zero mode quite robust and resilient against local perturbations and disorder.

Following the presence of the zero mode we can contrast the bosonic and the fermionic incarnation of the model. The TFIM in the ordered phase has two degenerate ground states no matter the model lives on an open or a closed chain. The Kitaev chain, however, responds to the manifold on which it lives on. Although it has a unique ground state on a ring [38], on an open chain it has a unique ground state in the trivial phase and doubly degenerate one in the topological phase [25]. Therefore independent of the manifold, the model has a unique ground state in the trivial phase. But the degeneracy of the ground state in the topological phase does depend on the manifold. Actually the presence of the non-local fermionic mode in the topological phase of the model on an open chain results in the two-fold degeneracy of the model in such a case.

In this chapter we briefly review our results in paper I. We present the exact solution for the full many-body spectrum of the Kitaev chain. Then we study the effect of longer range hopping and pairing as well as the phase-gradient on the Kitaev chain. Throughout this chapter we will specifically focus on the MZMs wavefunctions.

The Kitaev chain and its symmetries

To motivate the Kitaev Hamiltonian, show its relations with spin models and for our interests in the next chapters we consider a more general model rather than the TFIM. Let us consider the XY model in a longitudinal magnetic field,

$$H = -\sum_{j=1}^{L-1} \left(J_x \sigma_j^x \sigma_{j+1}^x + J_y \sigma_j^y \sigma_{j+1}^y \right) - h \sum_{j=1}^{L} \sigma_j^z \ , \tag{2.4}$$

in which $\sigma_j^\alpha (\alpha = x, y, z)$ are the Pauli matrices, J_x, J_y and h are some real coupling constants and L is the system size. Note that the Hamiltonian is defined on an open chain.

To solve the model and introduce the Kitaev model, we use the JW transformation [37],

$$\sigma_j^x = \left[\prod_{k=1}^{j-1}(1-2n_k)\right](c_j + c_j^\dagger) \ , \tag{2.5}$$

$$\sigma_j^y = \left[\prod_{k=1}^{j-1}(1-2n_k)\right]\frac{(c_j - c_j^\dagger)}{i} \ , \tag{2.6}$$

$$\sigma_j^z = 1 - 2n_j \ , \tag{2.7}$$

in which c_j is a spinless fermion annihilation operator acting on site j and it satisfies the usual fermionic algebra,

$$\{c_i, c_j\} = 0 \ , \tag{2.8}$$

$$\{c_i, c_j^\dagger\} = \delta_{ij} \ . \tag{2.9}$$

The operator $n_j = c_j^\dagger c_j$ is the number operator. Performing the transformation, we map the model to a free fermionic model,

$$H_{\mathrm{KC}} = \frac{1}{2}\sum_{j=1}^{L-1}(c_j^\dagger c_{j+1} + \Delta c_j^\dagger c_{j+1}^\dagger + \mathrm{h.c.}) - \mu\sum_{j=1}^{L}(c_j^\dagger c_j - \frac{1}{2}) \ , \tag{2.10}$$

in which we defined the pairing $\Delta = 2(J_y - J_x)$, the chemical potential $\mu = -2h$ and set $J_x + J_y = -1/2$. As it is evident in the fermionic language the model is solvable since it is quadratic.

Due to the importance of the symmetries of the model and the resulting simplifications in studying the phase diagram, we first discuss the symmetries of the model. We start with the particle-hole symmetry which states that H and $-H$ have the same spectrum. Consider $-H$,

$$-H = \sum_{j=1}^{L-1}\left(J_x\sigma_j^x\sigma_{j+1}^x + J_y\sigma_j^y\sigma_{j+1}^y\right) + h\sum_{j=1}^{L}\sigma_j^z \ . \tag{2.11}$$

The spectrum of a Hamiltonian does only depend on the algebra of the operators in it. Hence one can consider another representation of the SU(2) algebra,

$$\begin{aligned} &\sigma_j^x \to (-1)^j\sigma_j^x \ , \\ &\sigma_j^y \to -(-1)^j\sigma_j^y \ , \\ &\sigma_j^z \to -\sigma_j^z \ . \end{aligned} \tag{2.12}$$

Using the new representation we would retrieve H. Therefore the full many-body spectrum of H and $-H$ are the same, though the eigenstates change. In the fermionic picture this is called the particle-hole symmetry.

Another symmetry of the model is the $\mathbb{Z}_2$ symmetry which will be extensively used. One can define the parity operator as,

$$\begin{aligned} P &= \prod_{k=1}^{L} \sigma_k^z \\ &= \prod_{k=1}^{L} (1 - 2n_k) \\ &= (-1)^{\sum_{k=1}^{L} n_k} \ , \end{aligned} \tag{2.13}$$

which has two eigenvalues, ± 1, since $P^2 = \mathbf{1}$ (the identity operator). The parity commutes with the Hamiltonian, $[H, P] = 0$, and hence can be used to label the eigenstates. The states with $P = +1$ form the even sector and those with $P = -1$ form the odd sector. This is the so-called $\mathbb{Z}_2$ symmetry.

We also note that the Hamiltonian in Eq. 2.10 is time-reversal symmetric. In this case the time-reversal $\mathbf{T}$ is simply the complex conjugation K. Due to the pairing term the model is also particle-hole symmetric. If we write the Hamiltonian like what we have in Eq. 1.35 one can see that the particle-hole operator is $\mathbf{P} = (\sigma^x \otimes \mathbf{1}_{L\times L})\, K$. Since we have $\mathbf{T}^2 = \mathbf{P}^2 = \mathbf{1}$, the model belongs to the class **BDI** (see chapter 1).

The spectrum of the Kitaev chain

Although the Kitaev chain has been extensively studied in the past two decades, to the best of our knowledge, the exact spectrum and eigenstates of the model for an open chain were not investigated in full generality. In this section we present all the eigenvalues and wavefunctions of the Kitaev chain for arbitrary pairing and chemical potential using the Lieb-Schultz-Mattis (LSM) method [39]. Since we will later consider the cases where the couplings are not real we consider the most general case of a quadratic Hamiltonian and pay special attention to the possible zero mode solutions.

Consider the following quadratic model,

$$H = \sum_{i,j=1}^{L} c_i^\dagger A_{ij} c_j + \frac{1}{2}(c_i^\dagger B_{ij} c_j^\dagger + \text{h.c.}) \ , \tag{2.14}$$

where i labels the sites, A is a hermitian matrix, B is an antisymmetric matrix and L is the number of sites. We consider a *Bogoliubov-like* transformation in

the real space which diagonalizes the Hamiltonian,

$$\eta_\alpha = \sum_{i=1}^{L} (g_{\alpha,i} c_i + h_{\alpha,i} c_i^\dagger) \ , \tag{2.15}$$

$$H = \sum_{\alpha=1}^{L} \Lambda_\alpha \eta_\alpha^\dagger \eta_\alpha \ , \ \Lambda_\alpha > 0 \ , \tag{2.16}$$

in which α labels the eigenstates and $g_{\alpha,i}$ and $h_{\alpha,i}$ are two functions that need to be found. We note that the transformation is canonical and the η_α operators do also satisfy the fermionic algebra. One can use use the equation of motion $[H, \eta_\alpha] = -\Lambda_\alpha \eta_\alpha$ to find equations governing $g_{\alpha,i}$ and $h_{\alpha,i}$,

$$h_{\alpha,i} B_{ij}^* - g_{\alpha,i} A_{ij} = -\Lambda_\alpha g_{\alpha,j} \ , \tag{2.17}$$

$$h_{\alpha,i} A_{ij}^* - g_{\alpha,i} B_{ij} = -\Lambda_\alpha h_{\alpha,j} \ . \tag{2.18}$$

To further simplify we need to assume that the matrix elements of A and B are real numbers. This is our case of interest for the Kitaev chain. Assuming this, we define new functions,

$$\phi_{\alpha,i} = g_{\alpha,i} + h_{\alpha,i} \ , \tag{2.19}$$

$$\psi_{\alpha,i} = g_{\alpha,i} - h_{\alpha,i} \ , \tag{2.20}$$

which are a set of row vectors, $\phi_\alpha = (\phi_{\alpha,1}, \ldots, \phi_{\alpha,L})$ and $\psi_\alpha = (\psi_{\alpha,1}, \ldots, \psi_{\alpha,L})$. From Eqs. 2.17 and 2.18 we get,

$$\phi_\alpha (A - B) = \Lambda_\alpha \psi_\alpha \ , \tag{2.21}$$

$$\psi_\alpha (A + B) = \Lambda_\alpha \phi_\alpha \ . \tag{2.22}$$

Combining these two we get,

$$\phi_\alpha (A - B)(A + B) = \Lambda_\alpha^2 \phi_\alpha \ , \tag{2.23}$$

$$\psi_\alpha (A + B)(A - B) = \Lambda_\alpha^2 \psi_\alpha \ . \tag{2.24}$$

Therefore to get the full spectrum of a quadratic model one needs to solve these two equations. We will solve them for the open Kitaev chain.

Before going through the details of the Kitaev chain, due to our interest in the MZMs solutions of the models with the complex A and B matrices we simplify the Eq. 2.17 and 2.18 for a MZM solution with the label α^*. To get a real solution (see below), a Majorana mode, we set $h_{\alpha^*,i} = g_{\alpha^*,i}^*$,

$$\mathrm{Re}[g(A - B)] = 0 \ , \tag{2.25}$$

$$\mathrm{Im}[g(A + B)] = 0 \ . \tag{2.26}$$

These equations will be valuable when we add a phase-gradient to the pairing term of the Kitaev chain.

We also remind the reader of Majorana fermions. With a given set of creation and annihilation operators $(c_j, c_j^\dagger)$ we can form two *real* fermions,

$$\begin{aligned} \gamma_{A,j} &= c_j^\dagger + c_j \ , \\ \gamma_{B,j} &= i(c_j^\dagger - c_j) \ , \end{aligned} \tag{2.27}$$

which satisfy,

$$\{\gamma_{r,i}, \gamma_{r',j}\} = 2\delta_{rr'}\delta_{ij} \ . \tag{2.28}$$

For convenience and the future reference we rewrite the MZM operators, η_{α^*}, in terms of Majorana fermions,

$$\eta_{\alpha^*} = \sum_{j=1}^{L} (\mathrm{Re}[g_{\alpha^*,i}]\gamma_{A,j} - \mathrm{Im}[g_{\alpha^*,i}]\gamma_{B,j}) \ . \tag{2.29}$$

We now move on to the Kitaev model. We first solve the model in Eq. 2.10 on a ring. Consider the following Hamiltonian,

$$\begin{aligned} H_{\mathrm{PBC}} &= H_{\mathrm{KC}} + H_{\mathrm{N}} \ , \\ H_{\mathrm{N}} &= \frac{1}{2}(c_N^\dagger c_1 + \Delta c_N^\dagger c_1^\dagger + \mathrm{h.c.}) \ . \end{aligned} \tag{2.30}$$

We read the matrices A and B and plug them in Eq. 2.23,

$$\begin{aligned} &(1-\Delta^2)\phi_{\alpha,j-2} - 4\mu\phi_{\alpha,j-1} + [4\mu^2 + 2(1+\Delta^2)]\phi_{\alpha,j} \\ &+(1-\Delta^2)\phi_{\alpha,j+2} - 4\mu\phi_{\alpha,j+1} = 4\Lambda_\alpha^2\phi_{\alpha,j} \ . \end{aligned} \tag{2.31}$$

Since we know the momentum k is a good quantum number, we consider a plane wave ansatz $\phi_j \sim e^{ikj}$ and get the dispersion relation,

$$\Lambda_k^2 = (\mu - \cos k)^2 + \Delta^2 \sin^2 k \ , k = \frac{2\pi m}{L} \ , m \in \{0, \cdots, L-1\} \ . \tag{2.32}$$

Writing Eq. 2.23 for the Kitaev Hamiltonian with an open boundary condition (OBC) gives Eq. 2.31 for $3 \leq j \leq L-2$. We would, however, get different equations for the boundary sites $j = 1, 2$ and $j = L-1, L$. Since we are still dealing with a linear recursion relation we consider a power law ansatz $\phi_{\alpha,j} \sim x_\alpha^j$ for a state with label α. Moreover since the bulk equation remains the same, we use *the functional form of the dispersion relation* for the eigenvalues, though now is parametrized by α,

$$\Lambda_\alpha^2 = (\mu - \cos\alpha)^2 + \Delta^2 \sin^2\alpha \ . \tag{2.33}$$

Due to the order of the recursion relation we get four independent solutions, $x_\alpha = e^{\pm i\alpha}$ and $x_\beta = e^{\pm i\beta}$, where,

$$\cos\alpha + \cos\beta = \frac{2\mu}{1-\Delta^2} \ . \tag{2.34}$$

As described in detail in paper I, by considering a linear combination of the four solutions and the boundary conditions one gets ϕ_α,

$$\begin{aligned}\phi_{\alpha,j} = A_1\Big\{ &\sin[(L+1)\beta]\sin(j\alpha) - \sin[(L+1)\alpha]\sin(j\beta)\Big\} \\ &+ A_2\Big\{ \sin[(L+1)\beta]\sin[(L+1-j)\alpha] \\ &- \sin[(L+1)\alpha]\sin[(L+1-j)\beta]\Big\} \ ,\end{aligned} \tag{2.35}$$

and a transcendental equation for α,

$$\begin{aligned}&\sin^2\alpha + \sin^2\beta + \frac{1}{\Delta^2}(\cos\beta - \cos\alpha)^2 \\ &- 2\frac{\sin\alpha\sin\beta}{\sin[(L+1)\alpha]\sin[(L+1)\beta]} \times \{1 - \cos[(L+1)\alpha]\cos[(L+1)\beta]\} = 0 \ .\end{aligned} \tag{2.36}$$

By solving Eqs. 2.34 and 2.36 simultaneously, one gets all the possible values of α. This can be done numerically as we show in the paper. We are, however, interested in the phase diagram in the thermodynamic limit and these equations can be simplified in this limit. Specifically these can be solved for a MZM solution which is present in the topological phase.

Before going through the results we mention that the signs of μ and Δ do not affect the phase diagram. The insignificance of the chemical potential's sign can be easier seen in the spin incarnation, Eq. 2.4. To flip the sign of a given field h, one needs to perform an on-site rotation like, $\sigma^{x,z} \to -\sigma^{x,z}$. For the sign of Δ it is easier to consider the Kitaev Hamiltonian. For $\Delta < 0$ we can perform a gauge transformation on fermionic operators as $c_j \to e^{i\pi/2}c_j$ which keeps the hopping and chemical potential terms intact and flips the sign of the pairing term. Hence we assume that the chemical potential and the pairing term are both positive, $\mu, \Delta > 0$.

It can be checked that for large chemical potential ($\mu \gg 1$) Eqs. 2.34 and 2.36 give a set of L distinct real solutions, $0 < \alpha_0, \cdots, \alpha_{L-1} < \pi$. By decreasing the chemical potential the smallest label will be lost for $\mu < 1 + \mathcal{O}(1/L)$ and one only gets $L-1$ real solutions. This means that in the thermodynamic limit for $\mu < \mu_c = 1$ one solution to the Eqs. 2.34 and 2.36 does not lie on the real axis and becomes imaginary. This imaginary solution represents a MZM.

To find the imaginary solutions for α we need to consider three different cases:

1) For $\Delta < 1$ and $\sqrt{1-\Delta^2} < \mu < 1$ we have,

$$\begin{aligned} \alpha^* &= i(\frac{1}{\xi_1} + \frac{1}{\xi_2}) \ , & \beta^* &= i(\frac{1}{\xi_1} - \frac{1}{\xi_2}) \ , \\ \cosh\frac{1}{\xi_1} &= \frac{1}{\sqrt{1-\Delta^2}} \ , & \cosh\frac{1}{\xi_2} &= \frac{\mu}{\sqrt{1-\Delta^2}} \ , \end{aligned} \tag{2.37}$$

for which one can check that $\Lambda_{\alpha^*} = 0$. For this solution the MZM on the left edge takes the following form,

$$\phi_{\alpha^*,j} = Ce^{-j/\xi_1} \sinh\left(\frac{j}{\xi_2}\right) \ , \tag{2.38}$$

with the normalization factor C. Since $\xi_1 < \xi_2$ this is localized on the left edge. One can also calculate $\psi_{\alpha^*,j}$ which would be localized on the right edge.

2) For $\Delta < 1$ and $\mu < \sqrt{1-\Delta^2}$ we have,

$$\begin{aligned} \alpha^* &= q + i\frac{1}{\xi} \ , & \beta^* &= q - i\frac{1}{\xi} \ , \\ \cos q &= \frac{\mu}{\sqrt{1-\Delta^2}} \ , & \cosh\frac{1}{\xi} &= \frac{1}{\sqrt{1-\Delta^2}} \ , \end{aligned} \tag{2.39}$$

which gives the left MZM as follows,

$$\phi_{\alpha^*,j} = Ce^{-j/\xi} \sin(nj) \ . \tag{2.40}$$

In this case the correlation length ξ does only depend on the pairing Δ and the chemical potential affects the oscillatory behaviour of the wave-function.

3) For $\Delta > 1$ we have,

$$\begin{aligned} \alpha^* &= i(\frac{1}{\xi_1} - \frac{1}{\xi_2}) & \beta^* &= \pi + i(\frac{1}{\xi_1} + \frac{1}{\xi_2}) \ , \\ \sinh\frac{1}{\xi_1} &= \frac{1}{\sqrt{\Delta^2-1}} \ , & \sinh\frac{1}{\xi_2} &= \frac{\mu}{\sqrt{\Delta^2-1}} \ . \end{aligned} \tag{2.41}$$

The left MZM reads,

$$\phi_{\alpha^*,j} = Ce^{-j/\xi_1} \times \begin{cases} \cosh(j/\xi_2) & \text{if } j \text{ is odd} \ , \\ \sinh(j/\xi_2) & \text{if } j \text{ is even} \ . \end{cases} \tag{2.42}$$

Being in the topological phase, $\mu < 1$, results in $\xi_1 < \xi_2$ which guarantees the localization of ϕ_{α^*} on the left edge.

In any of the above mentioned cases the model hosts two localized MZMs, ϕ_{α^*} on the left edge and ψ_{α^*} on the right edge. By fusing these two MZMs we form *the zero energy fermionic state* which can be filled or left to be empty. Note that there is no concept of filling for Majorana fermions and we need to make Dirac fermions out of them to be able to talk about the filling.

Since filling an empty fermionic state changes the parity of a given many-body state, the presence of a zero energy fermionic state results in a full doubly degenerate many-body spectrum and pair up the even and the odd sectors. For a finite system, but large in comparison with the correlation length, the edge modes has an exponentially small energy in the system size, $\Lambda_{\alpha^*} \sim \exp(-L/\xi)$ and hence the degeneracy is not exact.

The effect of next nearest neighbour terms and phase-gradient in the pairing term

So far we have studied the Kitaev chain with real couplings. The model was time-reversal symmetric and belonged to the class **BDI**. Adding phase-gradient changes the model drastically since it breaks the time-reversal symmetry and changes the class to which the model belongs to the class **D** of non-interacting fermions. In the class **D** the possible phases are distinguished by the group $\mathbb{Z}_2$ [30–32]. This means that the topological invariant can only take two values, $\nu = 0$ and $\nu = 1$. The $\nu = 0$ phase is the trivial phase without any edge mode and the $\nu = 1$ phase is the topological phase with one MZM on each edge.

Sticlet et al. [40], however, found a model (see below) in the class **D** which can host two MZMs on *one* edge in a certain regime of parameters and no zero mode on the other edge. Put in another way they found a regime of parameters where there is a *localized Dirac fermion* on one edge. This is, of course, not a topological phase and required fine tuning of the parameters. But since the observation by Sticlet et al. was done using the numerical analysis, we were motivated to use the LSM method and investigate the model analytically. In what follows we present the model studied in Ref. [40], present its phase diagram and MZMs' wavefunctions when they are present. We will also study the phase transition between different phases.

Consider the following model,

$$H = \frac{t}{2}\sum_{j=1}^{L-1}(c_j^\dagger c_{j+1} + e^{ij\nabla\theta}c_j^\dagger c_{j+1}^\dagger + \text{h.c.}) + \frac{\lambda}{2}\sum_{j=1}^{L-2}(c_j^\dagger c_{j+2} + e^{ij\nabla\theta}c_j^\dagger c_{j+2}^\dagger + \text{h.c.}) - \mu\sum_{j=1}^{L}(c_j^\dagger c_j - \frac{1}{2}) \ , \tag{2.43}$$

where the hopping and pairing terms for the nearest and next nearest neighbours are t and λ respectively. The phase gradient is $\nabla\theta$ per site and is constant.

To write the Hamiltonian in Eq. 2.43 within the LSM form in Eq. 2.14 we perform a gauge transformation $c_j \to e^{ij\nabla\theta/2}c_j$ and get,

$$\begin{aligned} H = &\frac{t}{2}\sum_{j=1}^{L-1}(e^{i\frac{\nabla\theta}{2}}c_j^\dagger c_{j+1} + e^{-i\frac{\nabla\theta}{2}}c_j^\dagger c_{j+1}^\dagger + \text{h.c.}) \\ &+ \frac{\lambda}{2}\sum_{j=1}^{L-2}(e^{i\nabla\theta}c_j^\dagger c_{j+2} + e^{-i\nabla\theta}c_j^\dagger c_{j+2}^\dagger + \text{h.c.}) \\ &- \mu\sum_{j=1}^{L}(c_j^\dagger c_j - \frac{1}{2}) \ . \end{aligned} \tag{2.44}$$

The phase diagram of this model can be obtained by either studying the model on a ring and performing the Fourier transformation or finding the MZMs solutions on an open chain. We will follow the later approach and then comment on the former one which also gives the same phase diagram, as it should.

We need to solve Eqs. 2.25 and 2.26 for which we plug in $g_j = \frac{1}{2}(\phi_j + i\tilde{\psi}_j)$. For the "bulk" equations we get,

$$-\mu\tilde{\psi}_j + t\cos(\frac{\nabla\theta}{2})\tilde{\psi}_{j-1} + \lambda\cos(\nabla\theta)\tilde{\psi}_{j-2} = 0 \ , \tag{2.45}$$

$$\begin{aligned} &-\mu\phi_j + t\cos(\frac{\nabla\theta}{2})\phi_{j+1} + \lambda\cos(\nabla\theta)\phi_{j+2} = \\ &t\sin(\frac{\nabla\theta}{2})\Big(\tilde{\psi}_{j-1} - \tilde{\psi}_{j+1}\Big) + \lambda\sin(\nabla\theta)\Big(\tilde{\psi}_{j-2} - \tilde{\psi}_{j+2}\Big) \ . \end{aligned} \tag{2.46}$$

The general solution to these equations are,

$$\begin{aligned} &\tilde{\psi}_j = R_+x_+^{L-j+1} + R_-x_-^{L-j+1}, \\ &\phi_n = L_+x_+^j + L_-x_-^j + S_+x_+^{L-j+1} + S_-x_-^{L-j+1}, \\ &S_\pm = \kappa_\pm R_\pm \ , \end{aligned} \tag{2.47}$$

where,

$$x_\pm = \frac{-t\cos(\frac{\nabla\theta}{2}) \pm \sqrt{t^2\cos^2(\frac{\nabla\theta}{2}) + 4\lambda\mu\cos(\nabla\theta)}}{2\lambda\cos(\nabla\theta)} \ , \tag{2.48}$$

$$\kappa_\pm = -\tan(\nabla\theta) + \frac{t\sin(\frac{\nabla\theta}{2})}{\cos(\nabla\theta)\Big[\mu + \lambda\cos(\nabla\theta)\Big]}x_\pm \ . \tag{2.49}$$

The constants $R_\pm$ and $L_\pm$ will be determined using the boundary equations,

$$-\mu\tilde{\psi}_1 = 0 \ , \tag{2.50}$$

$$t\cos(\frac{\nabla\theta}{2})\tilde{\psi}_1 - \mu\tilde{\psi}_2 = 0 \ , \tag{2.51}$$

and

$$-\mu\phi_{L-1} + t\cos(\frac{\nabla\theta}{2})\phi_L = t\sin(\frac{\nabla\theta}{2})(\tilde{\psi}_{L-2} - \tilde{\psi}_L) + \lambda\sin(\nabla\theta)\tilde{\psi}_{L-3} \ , \quad (2.52)$$

$$-\mu\phi_L = t\sin(\frac{\nabla\theta}{2})\tilde{\psi}_{L-1} + \lambda\sin(\nabla\theta)\tilde{\psi}_{L-2} \ . \quad (2.53)$$

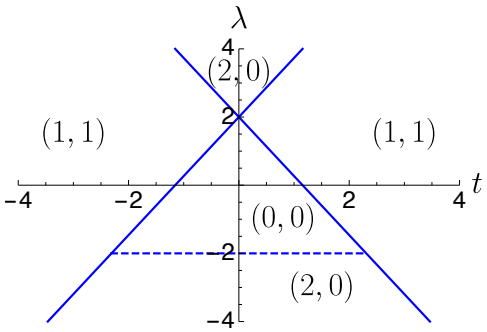

Figure 2.1: The Phase diagram for the model in Eq. 2.44 for $\mu = 1$ and $\nabla\theta = \pi/3$. The pairs (l, r) represent the number of MZMs on each edge. The solid blue lines show phase transitions and the dashed blue line represents the crossover. Note that the points $|\lambda| = 2$ and $t = 0$ do also represent phase transitions. Taken from paper I.

In Fig. 2.1 we present the phase diagram of the model for $\mu = 1$ and $\nabla\theta = \pi/3$. We now look at different cases as follows.

1) For $|x_\pm| > 1$ there is no MZM. This corresponds to the triangle in the middle of Fig. 2.1.

2) For $|x_+| < 1$ and $|x_-| > 1$ we have one MZM on each edge with the following wavefunctions,

$$\tilde{\psi}_j = R_+ x_+^{L-j+1} \ , \quad (2.54)$$

$$\phi_j = L_+ x_+^j + S_+ x_+^{L-j+1} + \tilde{L}_-(\frac{1}{x_-})^{L-j+1} \ , \quad (2.55)$$

where

$$S_+ = \kappa_+ R_+ \ , \quad (2.56)$$

$$\tilde{L}_- = -R_+ \frac{t\sin(\nabla\theta/2)}{\cos(\nabla\theta)(\mu + \lambda\cos(\nabla\theta))} \ . \quad (2.57)$$

This case is rather different from what we have seen so far, since ϕ localizes on both edges rather than just on the left one. This follows from Eqs. 2.46

and 2.45 which couple ϕ and $\tilde{\psi}$. A similar analysis can be done for the case where $|x_+| > 1$ and $|x_-| < 1$. This phase where the model has one localized MZM on each edge is the topological phase, indicated by $(1,1)$ in Fig. 2.1.

3) For $|x_\pm| < 1$ one gets no solutions on the right edge, i.e. $\tilde{\psi} = 0$. For ϕ, however, we get,

$$\phi_j = L_+ x_+^j + L_- x_-^j \ , \tag{2.58}$$

which shows that two MZMs live on the left edge. This corresponds to the Sticlet et al. observation and we indicated it by $(2,0)$ in Fig. 2.1.

Using the above mentioned conditions, we plotted the phase diagram. The solid lines in Fig. 2.1 correspond to $\lambda = \mu/\cos(\nabla\theta) \pm t\cos(\nabla\theta/2)/\cos(\nabla\theta)$. These two lines separate the topological phase from the trivial ones. The dashed line $\lambda = -\mu/\cos(\nabla\theta)$ represents the boundary between the two "different" trivial phases, the one with a localized fermionic mode on the left edge and the one with no zero mode at all.

We also calculated the bulk gap by solving the model on a ring. It turned out that the gap closes along all the lines (solid and dashed) in Fig. 2.1. Gap closing is a necessary condition for a phase transition, but it is not a sufficient one. Therefore the very fact that the gap closes along the solid lines agrees with our conclusion that the region indicated by $(1,1)$ is a topological phase, separated by a phase transition from the trivial ones.

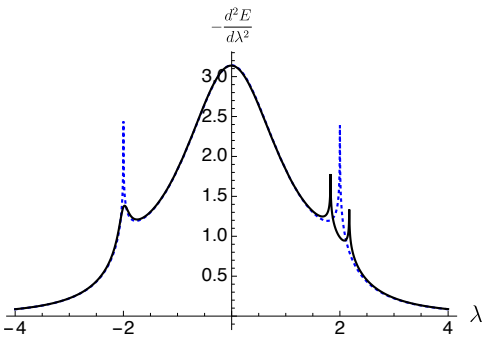

Figure 2.2: The second order derivative of the ground state energy for $\mu = 1$ and $\nabla\theta = \pi/3$ is plotted for $t = 0$ (the blue dashed line) and $t = 0.1$ (the solid black line). Taken from paper I.

Gap closing along the dashed line may lead one to conclude that there is a phase transition between the two trivial regions marked by $(0,0)$ and $(2,0)$. But this is *not* the case. A quantum phase transition reveals itself in a discontinuity or a divergence in the derivatives of the ground state energy. So we calculated

the ground state energy E and its first and second derivatives for fixed values of t across the lines numerically. In Fig. 2.2 we present the result for $t = 0$ and $t = 0.1$ with $\mu = 1$ and $\nabla\theta = \pi/3$. Therefore one can compare with Fig. 2.1.

Note that for $t = 0$ we have two decoupled chains and one needs to study the model separately, as we did in the paper. One can show that for $t = 0$ for $|\lambda > \mu/\cos(\nabla\theta)|$ (in this case $\lambda > 2$) the model is in the topological phase and for $|\lambda < \mu/\cos(\nabla\theta)|$ is in the trivial phase. This shows itself in the two sharp peaks in $-d^2E/d\lambda^2$, indicated by the dashed blue line in Fig. 2.2. For $t = 0.1$, however, $-d^2E/d\lambda^2$ has two sharp peaks close to $\lambda = +2$ and just a bump at $\lambda = -2$. The two sharp peaks correspond to the entering and leaving the topological phase. The bump at $\lambda = -2$ reveals the fact that there is no phase transition between the regions labeled by $(2, 0)$ and $(0, 0)$ and they do belong to the same phase, namely the trivial phase ($\nu = 0$). There is simply a crossover between these two regions [§].

In summary we showed that by using the LSM method one can get the phase diagram of one-dimensional quadratic fermionic models with open boundary conditions. In such a case the model hosts localized zero modes on its edges in a topological phase. The wavefunction of zero modes and hence the localization length of them can be calculated exactly. In addition we showed that although the bulk gap closes across a transition between different phases, gap closing does *not* guarantee the very existence of different phases. It could simply pin a crossover. Studying the ground state energy and its derivatives could, of course, be helpful in distinguishing the phase transitions from the crossovers.

[§]We would like to thank the anonymous referee for her/his suggestion to check the energy derivatives.

Chapter 3

A frustration free $\mathbb{Z}_3$ symmetric model

Introduction

In the previous chapter we studied the Kitaev chain and some its variations. We showed how the Kitaev chain is related to the celebrated Ising model. As we discussed the Kitaev/Ising chain has a $\mathbb{Z}_2$ symmetry, namely the parity of total number of fermions (Eq. 2.13). Hence it is natural to ask whether models with $\mathbb{Z}_n$ symmetry have the same features as we discussed in chapter 2: Do $\mathbb{Z}_n$ symmetric models support zero modes on their edges? Do they have *topological phases*? Is there any classification scheme?

To investigate these questions, we will study the $\mathbb{Z}_3$ symmetric generalization of the TFIM. This is the so-called three-state quantum Potts model, also known as the (chiral) clock model [41]. To define the model consider a chain of size L. On each site there is a "spin" with the local Hilbert space spanned by an orthonormal basis $\{|n\rangle\}$ with $n = 0, 1, 2$. The Hamiltonian reads,

$$H = -J \sum_{j=1}^{L-1} \left(e^{i\theta} X_j^\dagger X_{j+1} + \text{h.c.} \right) - f \sum_{j=1}^{L} \left(e^{i\phi} Z_j^\dagger + \text{h.c.} \right) \ , \tag{3.1}$$

where the Pauli matrices σ^x and σ^z are generalized to X and Z respectively,

$$X = \begin{pmatrix} 0 & 1 & 0 \\ 0 & 0 & 1 \\ 1 & 0 & 0 \end{pmatrix} \ , \qquad Z = \begin{pmatrix} 1 & 0 & 0 \\ 0 & \omega & 0 \\ 0 & 0 & \bar{\omega} \end{pmatrix} \ , \tag{3.2}$$

with $\omega = \exp(i2\pi/3)$. In above we wrote the operators in the $\{|n\rangle\}$ basis, i.e. the eigenvectors of the Z operator with the eigenvalues ω^n. The X operator acts as a *shift* operator in the $\{|n\rangle\}$ basis. The anticommutation relation among Pauli matrices changes to,

$$XZ = \omega ZX \ . \tag{3.3}$$

The parity symmetry in the TFIM also leverages to the $\mathbb{Z}_3$ symmetry,

$$P = \prod_{j=1}^{L} Z_j \ , \qquad P^3 = \mathbf{1} \ , \qquad [H, P] = 0 \ . \tag{3.4}$$

Unlike the TFIM this model can not be solved exactly except for special cases or relations between the couplings. For example for the case of $\theta = \phi = 0$ we can see that in the limiting case of $f = 0$ the model has three ordered ground states and for the case of $J = 0$ has a paramagnet (disordered) ground state. One can use a duality map [42] and show that $f = J$ is the transition point. It is well-known indeed that the for $\theta = \phi = 0$ and $f = J$ the model is integrable and can be described by a conformal field theory (CFT) with the central charge $c = 4/5$ [7].

The phase diagram of this model has been recently investigated using density matrix renormalization group (DMRG) and consists of three phases: an ordered phase, a disordered phase and an incommensurate (IC) phase [42]. The ordered phase and the disordered phase are gapped. The IC phase, however, is gapless with central charge $c = 1$.

In chapter 2 we showed that by using a JW transformation the ordered phase of the TFIM transforms to the topological phase of the fermions, where the model hosts MZMs on the edges of an open chain. Motivated by this, Fendley used the Fradkin-Kadanoff transformation [43] to study the model in the *parafermionic* incarnation [41]. The Fradkin-Kadanoff transformation, which is used to define parafermions, is,

$$\eta_{2j-1} = \left(\prod_{k=1}^{j} Z_k\right) X_j \ , \qquad \eta_{2j} = \omega \left(\prod_{k=1}^{j} Z_k\right) X_j Z_j \ , \tag{3.5}$$

and the set of parafermions $\{\eta_k\}$ satisfy the following algebra,

$$\eta_k^3 = \mathbf{1} \ , \qquad \eta_k^2 = \eta_k^\dagger \ , \qquad \eta_j \eta_k = \omega^{\mathrm{sgn}(k-j)} \eta_k \eta_j \ . \tag{3.6}$$

Applying this transformation to the model in Eq. 3.1 for $f = 0$ we get,

$$H = -J \sum_{j=1}^{L-1} \left(e^{i\theta} \bar{\omega} \eta_{2j}^\dagger \eta_{2j+1} + \mathrm{h.c.} \right) \ . \tag{3.7}$$

It is clear that the very first and last parafermions, η_1 and η_{2L}, do not appear in the Hamiltonian. Importantly they are conserved quantities,

$$[\eta_1, H] = [\eta_{2L}, H] = 0 \ . \tag{3.8}$$

So at this point the model supports *parafermionic edge zero modes*. Since each original degree of freedom, "spin" or clock variable, gives two parafermions, using the two free edge parafermions one can build a non-local state by using the inverse of the Fradkin-Kadanoff transformation. This non-local clock variable would also have three states and gives rise to the three-fold degeneracy of the full many-body Hamiltonian.

Whether the parafemerionic edge zero modes are present for finite f is a under debate [41, 44, 45]. One should notice that being in the ordered phase of clock variables corresponds to the topological phase of the parafermions. Although this topological phase has a three-fold degenerate ground state, presence of the parafermionic edge modes would guarantee the degeneracy in the full many-body spectrum upto exponentially small corrections in the system size.

Since many of the previous results were obtained using a kind of perturbative calculation or numerics, we aimed for exact results. One way to have exact results is looking for frustration free models, where one can obtain the exact form of the ground state. To do so, we first briefly review the Peschel-Emery line, a frustration free model for an interacting Ising model. After that we present the generalization of it to the three-state clock variables. In the paper II one can find more details.

The Peschel-Emery line

In what follows we define the Hamiltonians on bonds between the sites,

$$H = \sum_{j=1}^{\tilde{L}} h_{j,j+1} \ , \tag{3.9}$$

where $h_{j,j+1}$ is a two-body Hamiltonian defined on a link between the sites j and $j+1$. The upper limit in the sum for a system of size L could be $\tilde{L} = L-1$ for an open chain or $\tilde{L} = L$ for a closed one.

Consider the following two-body Hamiltonian for the interacting Ising model,

$$h_{j,j+1} = -\sigma_j^x \sigma_{j+1}^x + \frac{h}{2}(\sigma_j^z + \sigma_{j+1}^z) + U\sigma_j^z \sigma_{j+1}^z \ , \tag{3.10}$$

in which U is a new coupling constant. The phase diagram of this model will be discussed in detail in chapter 6. For the moment it is sufficient to know that this model is not integrable [46], hence the presence of a MZM is not guaranteed.

To construct the Hamiltonian along the Peschel-Emmery (PE) line, a frustration free model, we start with $h = U = 0$. We know that $|{\rightarrow}\rangle^{\otimes L}$ and $|{\leftarrow}\rangle^{\otimes L}$ are eigenstates at this point. We now show that it is possible to tune the two couplings h and U such that for finite values of them the ground states of the model are still product states [47, 48].

We recall that the parity,

$$P = \prod_{k=1}^{L} \sigma_k^z \ , \tag{3.11}$$

is a good quantum number. In the even sector ($P = +1$) of the two-body Hamiltonian we have,

$$h^e_{j,j+1} = \begin{array}{c} \begin{array}{cc} |\uparrow\uparrow\rangle & |\downarrow\downarrow\rangle \end{array} \\ \begin{pmatrix} U+h & -1 \\ -1 & U-h \end{pmatrix} \end{array} , \tag{3.12}$$

with the lowest eigenestate,

$$\epsilon_e = U - \sqrt{1+h^2} \ , \qquad |\psi_e\rangle \sim |\uparrow\uparrow\rangle + \left(h + \sqrt{1+h^2}\right) |\downarrow\downarrow\rangle \ . \tag{3.13}$$

In the odd sector ($P = -1$) of the two-body Hamiltonian we have,

$$h^o_{j,j+1} = \begin{array}{c} \begin{array}{cc} |\uparrow\downarrow\rangle & |\downarrow\uparrow\rangle \end{array} \\ \begin{pmatrix} -U & -1 \\ -1 & -U \end{pmatrix} \end{array} , \tag{3.14}$$

with the lowest eigenestate,

$$\epsilon_o = -U - 1 \ , \qquad |\psi_o\rangle \sim |\uparrow\downarrow\rangle + |\downarrow\uparrow\rangle \ . \tag{3.15}$$

To find a frustration free Hamiltonian with a product state as the ground state we demand, first the two lowest eigenvalues in the even and odd sectors to be equal,

$$\epsilon_e = \epsilon_o \Rightarrow \ 2U + 1 = \sqrt{1+h^2} \ , \tag{3.16}$$

and second, a linear superposition of the two lowest eigenstates exists such that it takes the product state form,

$$|\psi_e\rangle + x|\psi_o\rangle = (|\uparrow\rangle + \alpha|\downarrow\rangle) \otimes (|\uparrow\rangle + \alpha|\downarrow\rangle) \ , \tag{3.17}$$

in which x and α are unknown.

It can be shown that these two requirement are fulfilled by,

$$U = \frac{1}{2}\left[\cosh(l) - 1\right], \qquad h = \sinh(l) \ , \tag{3.18}$$

$$\alpha = e^{l/2}, \quad l \geq 0 \ , \tag{3.19}$$

where l parametrizes the line. Therefore there is a line of frustration free Hamiltonians [§], known as the Peschel-Emery (PE) line [47]. Along this line the ground state is two-fold degenerate with a product state form,

$$|\psi^+(l)\rangle = (|\uparrow\rangle + \alpha|\downarrow\rangle)^{\otimes L}, \quad |\psi^-(l)\rangle = (|\uparrow\rangle - \alpha|\downarrow\rangle)^{\otimes L} \ , \tag{3.20}$$

[§] Adding the term $J_y \sigma^y_j \sigma^y_{j+1}$ to Eq. 3.10 will yield a surface. It can be derived by the same type of calculations [48].

Since we are interested in the eigenstates with a well-defined parity, we make the parity eigenstates out of these product states which are simply the *cat states*,

$$|P = \pm 1(l)\rangle = |\psi^+(l)\rangle \pm |\psi^-(l)\rangle \ . \tag{3.21}$$

These states have a definite fermionic parity. This can be seen by employing the JW transformation on the product states [48],

$$\begin{aligned}
|\psi^\pm\rangle &= (|\uparrow\rangle \pm \alpha|\downarrow\rangle)^{\otimes L} \\
&= \left[\mathbf{1} \pm \alpha\sigma_1^-\right]\left[\mathbf{1} \pm \alpha\sigma_1^z\sigma_2^-\right]\ldots \\
&\left[\mathbf{1} \pm \alpha\left(\prod_{i_{L-1}=1}^{L-2}\sigma_{i_{L-1}}^z\right)\sigma_{L-1}^-\right]\left[\mathbf{1} \pm \alpha\left(\prod_{i_L=1}^{L-1}\sigma_{i_L}^z\right)\sigma_L^-\right]|\uparrow\rangle^{\otimes L} \\
&= (1 \pm \alpha c_1^\dagger)(1 \pm \alpha c_2^\dagger)\ldots(1 \pm \alpha c_{L-1}^\dagger)(1 \pm \alpha c_L^\dagger)|0\rangle^{\otimes L} \\
&= e^{\pm\alpha c_1^\dagger}e^{\pm\alpha c_2^\dagger}\ldots e^{\pm\alpha c_{L-1}^\dagger}e^{\pm\alpha c_L^\dagger}|0\rangle^{\otimes L} \ ,
\end{aligned} \tag{3.22}$$

in which $\sigma^- = (\sigma^x - i\sigma^y)/2$. Now it is evident that $|P = +1(l)\rangle$ has even number of fermions and $|P = -1(l)\rangle$ has odd number of them, just like what we had in the TFIM. In addition these states have high entanglement entropy (see chapter 5). There is also a path (in the space of coupling constants) which smoothly connects the PE line to the topological phase of the Kitaev chain (the free model) without closing the gap. Putting all these together we conclude that the PE line in the fermionic incarnation belongs to the topological phase of interacting fermions.

Strong and weak zero modes

In chapter 2 we discussed the presence of MZMs in the topological phase of the Kitaev chain. We showed that in the topological phase the model has a non-local Dirac mode which can be constructed from the two MZMs living on the two edges of an open chain.

It can be shown that for a system with a finite size L, the zero mode f_0 has an exponentially small energy in the system size, i.e. $\varepsilon_0 \sim \exp(-L/\xi)$ where ξ is the correlation length [39, 41]. As a result the model has not only a degenerate ground state, but all the states are doubly degenerate upto an exponentially small correction in the system size. Put in another way, for each state in the even or odd sector there is partner in the opposite sector with the same energy [§]. The only difference between the two partners is that in one the zero mode is left to be empty and in the other is filled.

[§] We do not keep repeating *upto an exponentially small corrections in the system size.* The reader should have this in mind.

Acting by a MZM on a given state in the many-body spectrum of the Kitaev chain maps it to its partner in the opposite sector. Fendley found the same type of operator for the XYZ model [49] and dubbed it *strong zero mode*. A strong zero mode, Ψ has the following properties,

(1) $[H, \Psi] = \mathcal{O}\left(e^{-L/\xi}\right)$ in the the thermodynamic limit with $\xi > 0$.

(2) Given the parity operator (the generator of a discrete symmetry) P where $[H, P] = 0$ and $P^n = \mathbf{1}$ for a positive integer n, we have $[P, \Psi] \neq 0$.

(3) The operator should be normalizable, i.e. $\Psi^n = \mathbf{1}$.

(4) $\Psi^\dagger = \Psi^{n-1}$.

Finding such an operator is a hard task and to the best of our knowledge the only interacting model for which such an operator was found is the XYZ model. The current understanding is that the strong zero mode can only exist in integrable models, although there is no proof for it. In chapter 6 we discuss the presence of the strong zero mode in a non-integrable model. Using an analytical argument and numerical analysis, we rule out the presence of a strong zero mode in a vast part of the phase digram.

One can, however, relax the first requirement of the strong zero mode and instead ask for an operator which only maps the ground states with different parities to each other. Such an operator is called a *weak zero mode* and should still satisfy the other requirements. Finding a weak zero mode could be an easier task, since it only deals with the ground states and in the case of frustration free models one may hope to write them down exactly.

For the PE line the weak zero modes which live on the edges can be written explicitly [48],

$$W_L = \mathcal{N} \sum_{n=1}^{L} q^{n-1} \gamma_{A,n} \ , \tag{3.23}$$

$$W_R = \mathcal{N} \sum_{n=1}^{L} q^{L-n} \gamma_{B,n} \ , \tag{3.24}$$

$$q = \frac{1-\alpha^2}{1+\alpha^2} \ , \qquad \mathcal{N} = \sqrt{\frac{1-q^{2L}}{1-q^2}} \ . \tag{3.25}$$

These operators are localized on the edges and satisfy the requirements (2) - (4). It can also be checked that they map the two ground states with opposite parities to each other.

A frustration free $\mathbb{Z}_3$ symmetric model

In this section we present a frustration free model analogue to the PE line. The goal is to modify the quantum Potts model such that its ground state is a product state and three-fold degenerate. Having Eq. 3.9 in mind, we will start with,

$$h_{j,j+1} = -X_j^\dagger X_{j+1} + \text{h.c.} \,, \tag{3.26}$$

with the three-fold degenerate ground state,

$$|G_0\rangle = (|0\rangle + |1\rangle + |2\rangle)^{\otimes L} \,, \tag{3.27}$$

$$|G_1\rangle = (|0\rangle + \omega|1\rangle + \bar{\omega}|2\rangle)^{\otimes L} \,, \tag{3.28}$$

$$|G_2\rangle = (|0\rangle + \bar{\omega}|1\rangle + \omega|2\rangle)^{\otimes L} \,. \tag{3.29}$$

Recall that the generator of the $\mathbb{Z}_3$ symmetry is $P = \prod_{j=1}^{L} Z_j$. Since $P^3 = \mathbf{1}$, its eigenvalues can be written as $P = \omega^Q$ with $Q = 0, 1, 2$. We want to write a Hamiltonian with the $\mathbb{Z}_3$ symmetry. By analogy to the $\mathbb{Z}_2$ case in Eq. 3.10 we will add an "external magnetic field", just like what we have in the quantum Potts Hamiltonian, and two other terms which are the natural generalizations of $\sigma_j^z \sigma_{j+1}^z$,

$$\begin{aligned} h_{j,j+1}^{Z_3}(r) = &- X_j^\dagger X_{j+1} - f(r)(Z_j + Z_{j+1}) \\ &- g_1(r) Z_j Z_{j+1} - g_2(r) Z_j Z_{j+1}^\dagger + \text{h.c.} \,. \end{aligned} \tag{3.30}$$

This Hamiltonian respects the $\mathbb{Z}_3$ symmetry. By calculating the ground state energy in the three sectors of the two-body Hamiltonian and setting them to be equal and, demanding a product state as a ground state, we found the following line parametrized by $r > 0$,

$$f(r) = (1 + 2r)(1 - r^3)/(9r^2) \,, \tag{3.31}$$

$$g_1(r) = -2(1 - r)^2(1 + r + r^2)/(9r^2) \,, \tag{3.32}$$

$$g_2(r) = (1 - r)^2(1 - 2r - 2r^2)/(9r^2) \,. \tag{3.33}$$

The model has a three-fold degenerate ground state along this line,

$$|G_0(r)\rangle = (|0\rangle + r|1\rangle + r|2\rangle)^{\otimes L} \,, \tag{3.34}$$

$$|G_1(r)\rangle = (|0\rangle + r\omega|1\rangle + r\bar{\omega}|2\rangle)^{\otimes L} \,, \tag{3.35}$$

$$|G_2(r)\rangle = (|0\rangle + r\bar{\omega}|1\rangle + r\omega|2\rangle)^{\otimes L} \,. \tag{3.36}$$

The energy per bond is $\epsilon_b(r) = -2(1 + r + r^2)^2/(9r^2)$. We can also write down the ground states with a definite eigenvalue for the $\mathbb{Z}_3$ symmetry generator,

$$|Q = 0\rangle = \mathcal{N}_1 \left(|G_0(r)\rangle + |G_1(r)\rangle + |G_2(r)\rangle\right) \,, \tag{3.37}$$

$$|Q = 1\rangle = \mathcal{N}_\omega \left(|G_0(r)\rangle + \bar{\omega}|G_1(r)\rangle + \omega|G_2(r)\rangle\right) \,, \tag{3.38}$$

$$|Q = 2\rangle = \mathcal{N}_{\bar{\omega}} \left(|G_0(r)\rangle + \omega|G_1(r)\rangle + \bar{\omega}|G_2(r)\rangle\right) \,, \tag{3.39}$$

with

$$\mathcal{N}_1 = \left[3(1+2r^2)^L + 6(1-r^2)^L\right]^{-\frac{1}{2}} , \tag{3.40}$$

$$\mathcal{N}_{\omega,\bar{\omega}} = \left[3(1+2r^2)^L - 3(1-r^2)^L\right]^{-\frac{1}{2}} . \tag{3.41}$$

Using the operators,

$$\Sigma^0 = \frac{X}{3}\left(\mathbf{1} + Z + Z^\dagger\right) , \tag{3.42}$$

$$\Sigma^1 = \frac{X}{3}\left(\mathbf{1} + \bar{\omega}Z + \omega Z^\dagger\right) , \tag{3.43}$$

$$\Sigma^2 = \frac{X}{3}\left(\mathbf{1} + \omega Z + \bar{\omega} Z^\dagger\right) , \tag{3.44}$$

we define,

$$A_{Z_3}(r) = \frac{1}{r}\Sigma_1^1 + \Sigma_1^2 + r\Sigma_1^0 , \tag{3.45}$$

$$B_{Z_3}(r) = \bar{\omega} P \left(\frac{1}{r}\Sigma_L^1 + \Sigma_L^2 + r\Sigma_L^0\right) . \tag{3.46}$$

They act as follows on the ground states,

$$A_{Z_3}|0\rangle = \frac{\mathcal{N}_1}{\mathcal{N}_{\bar{\omega}}}|2\rangle \ , \ A_{Z_3}|1\rangle = \frac{\mathcal{N}_\omega}{\mathcal{N}_1}|0\rangle \ , \ A_{Z_3}|2\rangle = |1\rangle \ , \tag{3.47}$$

$$B_{Z_3}|0\rangle = \omega\frac{\mathcal{N}_1}{\mathcal{N}_{\bar{\omega}}}|2\rangle , \ B_{Z_3}|1\rangle = \bar{\omega}\frac{\mathcal{N}_\omega}{\mathcal{N}_1}|0\rangle , \ B_{Z_3}|2\rangle = |1\rangle \ , \tag{3.48}$$

where $|n\rangle$ stands for the many-body parity eigenstate $|Q = n\rangle$.

In the parafermionic representation the operators A_{Z_3} and B_{Z_3} are localized on the left edge and the right edge respectively. They also have the requirements (2) and (3) of a weak zero mode as we discussed in section 3.3. But they do not satisfy the requirement (4) for finite system sizes, i.e. $A_{Z_3}^\dagger \neq A_{Z_3}^2$ and $B_{Z_3}^\dagger \neq B_{Z_3}^2$. Nevertheless in the thermodynamic limit, $L \to \infty$, we have $\mathcal{N}_1/\mathcal{N}_\omega \to 1$. Therefore in the thermodynamic limit we have weak parafermionic zero modes.

Iemini et al. [50] studied a different generalization of the quantum Potts Hamiltonian. They also found a line in the topological phase of parafermions along which the ground state is three-fold degenerate and can be written exactly. Having these two separate lines with common features suggests that there is a manifold in the coupling constants' space (the space of all models) where the model is gapped, the ground state is three-fold degenerate and belongs to the topological phase of parafermions.

These are the very first steps towards analytical studies of parafermions and their possible phases and, hopefully will be enriched by experimental efforts in the near future. In paper II we also discuss the spin-S generalization of the PE line and present a few excited states in all of these models.

Chapter 4

A short introduction to Bosonization

Introduction

In chapter 2 we presented the Jordan-Wigner (JW) transformation, Eq. 2.5, which transforms bosons and fermions in one-dimension to each other. Although bosons from different sites commute with each other, a string operator can transform this algebra to the anticommutation relation which is needed for fermions. As we showed the JW transformation is useful to solve some spin models exactly. In such cases JW helps to transform the model of interest to a free fermionic model which can be easily solved. On the other hand for a typical bosonic model or an interacting fermionic model a JW transformation does not help.

In this chapter we will briefly review Bosonization, another technique essentially doing the same job. It is actually a kind of JW transformation for relativistic Dirac fermions in one dimension and makes it possible to write the low-energy Hamiltonian in terms of a set of bosonic fields. This approach, as will be shown in a set of examples, can be applied not only to free fermionic models but also to models with local interactions. We will show that calculating the correlation functions and the renormalization group (RG) flow of coupling constants in the bosonic theory are quite straightforward and handy, facilitating the exploration of the low-energy physics of different interacting models. Although bosonization is more complicated, but it is more powerful in studying the one-dimensional models indeed.

This chapter is devoted to the bosonization technique which will be used in chapter 6 and chapter 7. We will mainly follow the book by Shankar [6] for this brief review. The other noteworthy and classic references to the subject are the book by Giamarchi [51], the review by von Delft and Schoeller [52] and the lecture notes by Sénéchal [53].

We will start by introducing Massless fermions and scalar fields in one dimension. By calculating special two-point correlation functions in each theory we introduce the bosonization dictionary. After that we apply this technique to the Kitaev-Hubbard chain which will be used in chapter 6 and then, following Shankar, to the XXZ chain to introduce the Luttinger parameter, K, setting the scene for chapter 7. In the end the RG flow, a powerful approach to determine the phase diagram, will be also discussed in a nutshell.

Massless Dirac fermion in one dimension

Consider the following Hamiltonian which is the Kinetic term for a one dimensional fermionic quantum field [§],

$$H = \int \psi^\dagger(x)\sigma^z(-i\partial_x)\psi(x)dx \ , \tag{4.1}$$

where ψ has upper and lower components, the so-called right and left movers,

$$\psi(x) = \begin{pmatrix} \psi_+(x) \\ \psi_-(x) \end{pmatrix} \ . \tag{4.2}$$

These fields obey the fermionic anticommutation algebra,

$$\left\{\psi_s^\dagger(x), \psi_{s'}(y)\right\} = \delta_{ss'}\delta(x-y) \ , \tag{4.3}$$

and the other anticommutators vanish.

The model in Eq. 4.1 can be solved by Fourier transformation,

$$\psi_\pm(x) = \int_{-\infty}^{\infty} \frac{dp}{2\pi}\psi_\pm(p)e^{ipx}e^{-\frac{1}{2}\alpha|p|} \ , \tag{4.4}$$

$$\psi_\pm(p) = \int_{-\infty}^{\infty} \psi_\pm(x)e^{-ipx}dx \ , \tag{4.5}$$

in which α is the convergence factor and in the end we will take the limit $\alpha \to 0$. The Fourier modes also obey the fermionic algebra,

$$\left\{\psi_s^\dagger(p), \psi_{s'}(q)\right\} = \delta_{ss'}2\pi\delta(p-q) \ , \tag{4.6}$$

and the other anticommutators vanish. Rewriting the Hamiltonian in terms of the Fourier modes we get,

$$H = \int \frac{dp}{2\pi}\psi_+^\dagger(p)\ p\ \psi_+(p) + \int \frac{dp}{2\pi}\psi_-^\dagger(p)\ \ (-p)\ \ \psi_-(p) \ . \tag{4.7}$$

Therefore the right and the left movers have a *relativistic* dispersion relation,

$$\varepsilon(p) = \pm p \ . \tag{4.8}$$

We can conclude that at zero temperature the ground state is a "Dirac sea" where all the right movers with negative momentum, $p < 0$, and all the left movers with positive momentum, $p > 0$, are filled. This will actually result in some infinities, like the local particle density in Eq. 4.42, and will be taken care

[§] As Shankar mentioned from the very beginning we will work in the thermodynamic limit and drop the terms $\mathcal{O}\left(\frac{1}{L}\right)$, where L is the system size.

of using normal ordering. We can now calculate different correlation functions. Let us first consider a right movers' two-point correlation function,

$$\begin{aligned}\langle \psi_+(x)\psi_+^\dagger(0)\rangle &= \int \frac{dp}{2\pi} e^{ipx} e^{-\frac{1}{2}\alpha|p|}\ \frac{dq}{2\pi} e^{-\frac{1}{2}\alpha|q|}\ \langle \psi_+(p)\psi_+^\dagger(q)\rangle \\ &= \int \frac{dp}{2\pi} e^{ipx} e^{-\frac{1}{2}\alpha|p|}\ \frac{dq}{2\pi} e^{-\frac{1}{2}\alpha|q|}\ 2\pi\delta(p-q)\ \Theta(q)\ , \end{aligned} \tag{4.9}$$

where Θ is the Heaviside step function. In the last line we used both the fermionic algebra and the fact that $\psi_+^\dagger(q)$ can only create a new fermion with a positive momentum since all the right movers with negative momentum have been already filled. Doing the rest of the calculation for the right movers and the same type of calculation for the left movers is rather straightforward and yields,

$$\langle \psi_+(x)\psi_+^\dagger(0)\rangle = \frac{i}{2\pi}\frac{1}{x+i\alpha}\ , \tag{4.10}$$

$$\langle \psi_-(x)\psi_-^\dagger(0)\rangle = \frac{-i}{2\pi}\frac{1}{x-i\alpha}\ . \tag{4.11}$$

These two-point correlation functions will guide us to establish the bosonization dictionary and will be used in the following calculations, for example in writing the density operator in terms of the bosonic fields.

Massless scalar field

Let us study a massless scalar field in one dimension with the following Hamiltonian,

$$H_B = \frac{1}{2}\int \left(\Pi^2 + (\partial_x\phi)^2\right) dx\ , \tag{4.12}$$

where ϕ and Π are conjugate fields,

$$[\phi(x), \Pi(y)] = i\delta(x-y)\ . \tag{4.13}$$

We can use the Fourier modes $\phi(p)$ with the bosonic algebra,

$$\left[\phi(p), \phi^\dagger(q)\right] = 2\pi\delta(p-q)\ , \tag{4.14}$$

to expand the operators,

$$\phi(x) = \int \frac{dp}{2\pi\sqrt{2|p|}} \left[\phi(p)e^{ipx} + \phi^\dagger(p)e^{-ipx}\right] e^{-\frac{1}{2}\alpha|p|}\ , \tag{4.15}$$

$$\Pi(x) = \int \frac{dp\sqrt{|p|}}{2\pi\sqrt{2}} \left[-i\phi(p)e^{ipx} + i\phi^\dagger(p)e^{-ipx}\right] e^{-\frac{1}{2}\alpha|p|}\ . \tag{4.16}$$

One can check that,

$$[\phi(x), \Pi(y)] = \frac{i}{\pi}\frac{\alpha}{\alpha^2 + (x-y)^2} \underset{\alpha\to 0}{=} i\delta(x-y) \ , \tag{4.17}$$

and the Hamiltonian reads,

$$: H_B : = \int \frac{dp}{2\pi}\phi^\dagger(p)\phi(p)|p| \ , \tag{4.18}$$

where $: \mathcal{O} :$ means normal ordering, i.e. putting all the annihilation operators to the right.

We now define the right and left movers for the scalar field,

$$\begin{aligned}\phi_\pm(x) &= \frac{1}{2}\left[\phi(x) \mp \int_{-\infty}^{x} \Pi(x')dx'\right] \\ &= \pm\int_0^{\pm\infty} \frac{dp}{2\pi\sqrt{2|p|}}\left[\phi(p)e^{ipx} + \phi^\dagger(p)e^{-ipx}\right] e^{-\frac{1}{2}\alpha|p|} \ ,\end{aligned} \tag{4.19}$$

which satisfy the following algebra [§],

$$[\phi_+(x), \phi_+(y)] = [\phi_-(x), \phi_-(y)] = \pm\frac{i}{4}\mathrm{sgn}(x-y) \ , \tag{4.20}$$

$$[\phi_+(x), \phi_-(y)] = \frac{i}{4} \ . \tag{4.21}$$

It is clear that

$$\phi(x) = \phi_+(x) + \phi_-(x) \ . \tag{4.22}$$

It would be fruitful to calculate the following correlation function,

$$\begin{aligned}\langle\phi_+(x)\phi_+(0)\rangle &= \int_0^\infty \frac{dp}{2\pi}\int_0^\infty \frac{dq}{2\pi}\frac{1}{2\sqrt{|pq|}}e^{ipx-\frac{\alpha}{2}(|p|+|q|)}\langle\phi(p)\phi^\dagger(q)\rangle \\ &= \int_0^\infty \frac{dp}{2\pi}\int_0^\infty \frac{dq}{2\pi}\frac{1}{2\sqrt{pq}}e^{ipx-\frac{\alpha}{2}(p+q)}2\pi\delta(p-q) \\ &= \int_0^\infty \frac{dp}{2\pi}\frac{1}{2p}e^{-(\alpha-ix)p} \ .\end{aligned} \tag{4.23}$$

To continue, we need to calculate the following integral,

$$f(\beta) = \int_0^\infty dp\frac{1}{p}e^{-\beta p} \ . \tag{4.24}$$

[§] As Shankar noted, in the "more careful treatment" the left and the right movers commute and the current commutation is for consistency in the thermodynamic limit.

It is easy to show that,

$$\frac{df}{d\beta} = -\frac{1}{\beta} \ , \tag{4.25}$$

and conclude that [§],

$$f(\beta) = -\ln(\beta) + f(1) \ . \tag{4.26}$$

As a result we have,

$$\langle \phi_+(x)\phi_+(0)\rangle = \frac{1}{4\pi}\left[-\ln(\alpha - ix) + f(1)\right] \ , \tag{4.27}$$

$$G_+(x) = \langle \phi_+(x)\phi_+(0) - \phi_+^2(0)\rangle = \frac{1}{4\pi}\ln\frac{\alpha}{\alpha - ix} \ . \tag{4.28}$$

Using the same set of calculations one can show that,

$$G_-(x) = \langle \phi_-(x)\phi_-(0) - \phi_-^2(0)\rangle = \frac{1}{4\pi}\ln\frac{\alpha}{\alpha + ix} \ , \tag{4.29}$$

$$G(x) = \langle \phi(x)\phi(0) - \phi^2(0)\rangle = \frac{1}{4\pi}\ln\frac{\alpha^2}{\alpha^2 + x^2} \ . \tag{4.30}$$

The Bosonization dictionary

To establish the connection between fermions and bosons, we start by studying the following correlation function,

$$G_{+\beta}(x) = \langle e^{i\beta\phi_+(x)} e^{-i\beta\phi_+(0)}\rangle \ . \tag{4.31}$$

To proceed we need to know that,

$$e^A e^B =: e^{A+B} : e^{\langle AB + \frac{A^2+B^2}{2}\rangle} \ , \tag{4.32}$$

$$\langle : e^{\mathcal{O}} :\rangle = 1 \ , \tag{4.33}$$

if $[A,[A,B]] = [B,[A,B]] = 0$. Using these we can simplify Eq. 4.31,

$$\begin{aligned} G_{+\beta}(x) &= \langle : e^{i\beta(\phi_+(x) - \phi_+(0))} :\rangle e^{\beta^2\langle \phi_+(x)\phi_+(0) - \frac{\phi_+^2(x) + \phi_+^2(0)}{2}\rangle} \\ &= \left(\frac{\alpha}{\alpha - ix}\right)^{\frac{\beta^2}{4\pi}} \ . \end{aligned} \tag{4.34}$$

We can also calculate the same correlation function for $\phi_-(x)$,

$$\begin{aligned} G_{-\beta}(x) &= \langle e^{i\beta\phi_-(x)} e^{-i\beta\phi_-(0)}\rangle \\ &= \left(\frac{\alpha}{\alpha + ix}\right)^{\frac{\beta^2}{4\pi}} \ . \end{aligned} \tag{4.35}$$

[§]The constant $f(1)$ is related to the Gamma function through $f(1) = \Gamma(0)$ and is not well-defined. Since it will be canceled out, we will ignore this issue.

These results and what we had for the fermion correlation functions in Eq. 4.10, suggest that we can do the following replacement *to calculate the correlation functions*,

$$\psi_{\pm}(x) = \frac{1}{\sqrt{2\pi\alpha}} e^{\pm i\sqrt{4\pi}\phi_{\pm}(x)} \ . \tag{4.36}$$

It is really crucial to keep in mind that this is *not* an operator identity and it is only valid for calculating the correlation functions of a fermionic model using a free massless scalar field.

For future calculations it would be handy to define the dual field θ,

$$\theta(x) = \phi_{-}(x) - \phi_{+}(x) \ . \tag{4.37}$$

It can also be written as,

$$\theta(x) = \int_{-\infty}^{x} \Pi(x')dx' \ , \tag{4.38}$$

which means that

$$\Pi(x) = \frac{d\theta}{dx} \ . \tag{4.39}$$

Finally for later applications it is helpful to know the following correlation function as well,

$$\langle e^{i\beta\phi(x)} e^{-i\beta'\phi(0)} \rangle = \langle e^{i\beta\theta(x)} e^{-i\beta'\theta(0)} \rangle = \delta_{\beta,\beta'} \left(\frac{\alpha^2}{\alpha^2 + x^2} \right)^{\frac{\beta^2}{4\pi}} \ . \tag{4.40}$$

The presence of the Kronecker delta is due to the invariance of the Hamiltonian, Eq. 4.18, with respect to a constant shift in ϕ or θ. This is the so-called neutrality condition.

Applications

In this section we will first calculate the fermion density operator in terms of the bosonic fields as an example of using the bosonization dictionary. After that we will present a detailed derivation of the bosonized Hamiltonian for the XY model in a longitudinal field. This was used in paper III to study the phase diagram of the Kitaev-Hubbard (KH) model in the attractive regime. We then present the bosonized Hamiltonian of the XXZ spin chain where we introduce the Luttinger parameter K. These two bosonized Hamiltonians contain a term like $\cos(\beta\phi)$ or $\cos(\beta\theta)$. Hence to conclude this chapter we study the RG flow for the coupling constant of such terms. This was used in the study of the KH model.

The fermion density operator

The fermion density operator is

$$\begin{aligned} j_0 &= \psi^\dagger \psi \\ &= \psi_+^\dagger \psi_+ + \psi_-^\dagger \psi_- \ . \end{aligned} \tag{4.41}$$

We will rewrite the first term using Eq. 4.36 and the "point splitting" trick,

$$\begin{aligned} \psi_+^\dagger(x)\psi_+(x) &= \lim_{\ell\to 0} \psi_+^\dagger(x+\ell)\psi_+(x) \\ &= \lim_{\ell\to 0} \frac{1}{2\pi\alpha} e^{-i\sqrt{4\pi}\phi_+(x+\ell)} e^{i\sqrt{4\pi}\phi_+(x)} \\ &= \lim_{\ell\to 0} \frac{1}{2\pi\alpha} e^{4\pi G_+(\ell)} : e^{-i\sqrt{4\pi}\phi_+(x+\ell)+i\sqrt{4\pi}\phi_+(x)} : \\ &= \lim_{\ell\to 0} \frac{1}{2\pi\alpha} \frac{\alpha}{\alpha - i\ell} : e^{-i\sqrt{4\pi}\ell\partial_x\phi_+ + \mathcal{O}(\ell^2)} : \\ &= \lim_{\ell\to 0} \frac{i}{2\pi(\ell + i\alpha)} \ : 1 - i\sqrt{4\pi}\ell\partial_x\phi_+ + \mathcal{O}(\ell^2) \ : \end{aligned}$$

Note that α is a regularizing length scale and is much smaller than *any* other length scale, even ℓ. As a result we can neglect α in the denominator,

$$\begin{aligned} \psi_+^\dagger(x)\psi_+(x) &= \lim_{\ell\to 0} \left[\frac{i}{2\pi\ell} + \frac{1}{\sqrt{\pi}} \frac{\partial\phi_+}{\partial x} + \mathcal{O}(\ell) \right] \\ &= \lim_{\ell\to 0} \left(\frac{i}{2\pi\ell} \right) + \frac{1}{\sqrt{\pi}} \frac{\partial\phi_+}{\partial x} \ . \end{aligned} \tag{4.42}$$

In above the first term represents the Dirac sea in the ground state. Since we are interested in excitations on top of the Dirac sea we do the normal ordering and drop the first term, hence we are left with only the second one. Doing the same calculation for the left movers follows the same path and gives the final result for the density operator as follows,

$$: \psi^\dagger(x)\psi(x) : = \frac{1}{\sqrt{\pi}} \frac{\partial\phi}{\partial x} \ . \tag{4.43}$$

The XY model in a longitudinal field

As we will later see in chapter 6 the Kitaev-Hubbard model can be mapped to the XY model in a longitudinal field with the following Hamiltonian,

$$\begin{aligned} H &= -\sum_j J\sigma_j^x\sigma_{j+1}^x - h\sigma_j^z + U\sigma_j^z\sigma_{j+1}^z \\ &= -\sum_j J\sigma_j^y\sigma_{j+1}^y - h\sigma_j^x + U\sigma_j^x\sigma_{j+1}^x \ , \end{aligned} \tag{4.44}$$

where the first two terms in the first line are the bosonic incarnation of the Kitaev model, namely the TFIM (see chapter 2), and the last term represents a density-density interaction between fermions, i.e. the Hubbard term. Moving to the second line we used the fact that the physical properties of the model only depend on the algebra among the operators, and hence made an on-site rotation on all the lattice sites, $x \to y \to z \to x$. Without loss of generality we assume that $J > 0$.

Here we will show how the bosonization technique can be applied to this lattice model and derive the continuum field theory which describes the low energy physics of it. Then by applying the RG techniques to the field theory one finds the phase boundary between the trivial phase and the topological phase of the KH model for attractive interactions, i.e. $U < 0$. This was done in paper III .

In the first step we need to find the gapless points of the model for some specific coupling constants to construct the massless Dirac fermion Hamiltonian and its operators $\psi_\pm$. It is well-known that the XY model, Eq. 4.44 with $h = 0$, has two gapless points, namely $U = \pm J$ [7]. Since we are interested in attractive interactions we choose $U = -J$ and expand the Hamiltonian around it,

$$H = \sum_j -J\left(\sigma_j^x\sigma_{j+1}^x + \sigma_j^y\sigma_{j+1}^y\right) + \delta U\sigma_j^x\sigma_{j+1}^x - h\sigma_j^x \ , \tag{4.45}$$

where

$$\delta U = U + J \ . \tag{4.46}$$

We now use the following convention for the JW transformation (different from Eq. 2.5) [37],

$$\begin{aligned} \sigma_j^z &= 2\psi_j^\dagger\psi_j - 1 \ , \\ \sigma_j^+ &= \left(e^{i\pi\sum_{k<j}\psi_j^\dagger\psi_j}\right)\psi_j^\dagger \ , \end{aligned} \tag{4.47}$$

in which ψ_j are spinless fermions,

$$\{\psi_j, \psi_k\} = 0 \ , \tag{4.48}$$

$$\left\{\psi_j, \psi_k^\dagger\right\} = \delta_{jk} \ . \tag{4.49}$$

We also use the raising and lowering operators,

$$\sigma^\pm = \frac{1}{2}\left(\sigma^x \pm i\sigma^y\right) \ . \tag{4.50}$$

The XY Hamiltonian in Eq. 4.45 becomes,

$$\begin{aligned} H_{\mathrm{XY}} &= \sum_j -J\left(\sigma_j^x\sigma_{j+1}^x + \sigma_j^y\sigma_{j+1}^y\right) \\ &= \sum_j -2J\left(\sigma_j^+\sigma_{j+1}^- + \sigma_j^-\sigma_{j+1}^+\right) \\ &= \sum_j -2J\left[\psi_j^\dagger \exp(i\pi n_j)\psi_{j+1} + h.c.\right] \\ &= \sum_j -2J\left[\psi_j^\dagger\left(1-2\psi_j^\dagger\psi_j\right)\psi_{j+1} + h.c.\right] \\ &= \sum_j -2J\left(\psi_j^\dagger\psi_{j+1} + \psi_{j+1}^\dagger\psi_j\right) \ . \end{aligned} \tag{4.51}$$

This can be diagonalized using the Fourier transformation,

$$\psi_j = \int_{-\pi}^{\pi}\frac{dk}{2\pi}\psi(k)e^{ijk} \ . \tag{4.52}$$

Performing the Fourier transformation we get,

$$H_{\mathrm{XY}} = \int_{-\pi}^{\pi}\frac{dk}{2\pi}\left(-4J\cos k\right)\psi^\dagger(k)\psi(k) \ . \tag{4.53}$$

This implies that all the states with momentum $-\pi/2 \le k \le \pi/2$ are occupied and the other states are empty. The model has a Fermi "surface" which actually consists of two Fermi points $K_F = \pm\pi/2$. At this point we make an approximation with which we can read the right and left movers. Since we are interested in the low energy physics of the model and the low energy excitations around the two Fermi points, we linearize the model around these two points with a cut-off Λ,

$$\begin{aligned} \psi_j &= \int_{-\pi}^{\pi}\frac{dk}{2\pi}\psi(k)e^{ijk} \\ &\simeq \int_{-\Lambda}^{\Lambda}\frac{dk}{2\pi}\psi(K_F+k)e^{iK_Fj}e^{ijk} + \int_{-\Lambda}^{\Lambda}\frac{dk}{2\pi}\psi(-K_F+k)e^{-iK_Fj}e^{ijk} \\ &= \sqrt{a}\left[e^{iK_Fj}\psi_+(x) + e^{-iK_Fj}\psi_-(x)\right] \ , \end{aligned} \tag{4.54}$$

where $x = ja$ is the continuum position, a is the lattice size and we defined the right and the left movers respectively,

$$\psi_\pm(ja) = \int_{-\Lambda}^{\Lambda}\frac{dk}{2\pi}\psi(\pm K_F+k)e^{ijk} \ . \tag{4.55}$$

The factor $\sqrt{a}$ in Eq. 4.54 is necessary for the correct dimension of the operators.

Therefore the first hopping term in Eq. 4.51 can be simplified as,

$$\begin{aligned}\sum_j \psi_j^\dagger \psi_{j+1} &\simeq \sum_j a \left[e^{-i\frac{\pi}{2}j}\psi_+^\dagger(x) + e^{+i\frac{\pi}{2}j}\psi_-^\dagger(x)\right] \\ &\quad \left[e^{i\frac{\pi}{2}(j+1)}\psi_+(x+a) + e^{-i\frac{\pi}{2}(j+1)}\psi_-(x+a)\right] \\ &= \sum_j a \left[\psi_+^\dagger(x)\ i\psi_+(x+a) + \psi_-^\dagger(x)\ (-i)\psi_-(x+a)\right] \\ &\quad + \sum_j a(-1)^j \left[(-i)\psi_+^\dagger(x)\psi_-(x+a) + i\psi_-^\dagger(x)\psi_+(x+a)\right].\end{aligned}$$

Since the last line is rapidly oscillating over a lattice size we can drop it in the continuum limit. We also use the fact that $\psi_\pm(x)$ are continuous fields and can be Taylor expanded,

$$\psi_\pm(x+a) = \psi_\pm(x) + a\partial_x\psi_\pm + \mathcal{O}(a^2)\ . \tag{4.56}$$

So the hopping term becomes,

$$\begin{aligned}\sum_j \psi_j^\dagger \psi_{j+1} &\simeq \sum_j a \left[\psi_+^\dagger(x)\ i\psi_+(x) + \psi_-^\dagger(x)\ (-i)\psi_-(x)\right] \\ &\quad + \sum_j a^2 \left[\psi_+^\dagger(x)\ i\partial_x\psi_+(x) + \psi_-^\dagger(x)\ (-i)\psi_-(x)\right] \\ &\quad + \mathcal{O}(a^3)\ .\end{aligned}$$

By adding the Hermitian conjugate to above, the first line will be cancelled and we arrive at [§],

$$H_{\rm XY} = -4J\sum_j a^2 \left[\psi_+^\dagger(x)\ i\partial_x\psi_+(x) + \psi_-^\dagger(x)\ (-i)\psi_-(x)\right] \tag{4.57}$$

$$\to (4Ja)\int dx \left[\psi_+^\dagger\left(-i\partial_x\right)\psi_+ + \psi_-^\dagger\left(i\partial_x\right)\psi_-\right]\ . \tag{4.58}$$

To get the Hamiltonian for a massless Dirac fermion as discussed earlier we rescale the Hamiltonian,

$$H_{0,c} = \frac{H_{\rm XY}}{4Ja} = \int dx \left[\psi_+^\dagger\left(-i\partial_x\right)\psi_+ + \psi_-^\dagger\left(i\partial_x\right)\psi_-\right] \tag{4.59}$$

$$= \frac{1}{2}\int \left(\Pi^2 + (\partial_x\phi)^2\right) dx\ . \tag{4.60}$$

[§] We also replace the sum over lattice sites with an integral, i.e. $\sum_j af_j \to \int dx f(x = ja)$.

The last equality can be shown using Eq. 4.36.

Having the free model at our hand, we can now study the other terms in the Hamiltonian, Eq. 4.45. We first study the term with the coupling δU,

$$\sum_j \sigma_j^x \sigma_{j+1}^x = \sum_j \sigma_j^+ \sigma_{j+1}^+ + \sigma_j^- \sigma_{j+1}^- + \sum_j \sigma_j^+ \sigma_{j+1}^- + \sigma_j^- \sigma_{j+1}^+ \ .$$

The last two terms are the XY Hamiltonian. Hence they only renormalize the free Hamiltonian and we neglect them. The first two terms, however, are more involved,

$$\begin{aligned} \delta U \sum_j \sigma_j^x \sigma_{j+1}^x &\to \delta U \sum_j \sigma_j^+ \sigma_{j+1}^+ + \sigma_j^- \sigma_{j+1}^- \\ &= \delta U \sum_j \left[\psi_j^\dagger \exp(i\pi n_j) \psi_{j+1}^\dagger + h.c. \right] \\ &= \delta U \sum_j \left[\psi_j^\dagger \psi_{j+1}^\dagger + h.c. \right] \ . \end{aligned}$$

Employing Eq. 4.54 we can further simplify the above equation. For simplicity we continue with the first term,

$$\begin{aligned} \psi_j^\dagger \psi_{j+1}^\dagger &\simeq a \left[e^{-i\frac{\pi}{2}j} \psi_+^\dagger(x) + e^{+i\frac{\pi}{2}j} \psi_-^\dagger(x) \right] \\ &\quad \left[e^{-i\frac{\pi}{2}(j+1)} \psi_+^\dagger(x+a) + e^{+i\frac{\pi}{2}(j+1)} \psi_-^\dagger(x+a) \right] \\ &\simeq 2 \ i \ a \psi_+^\dagger(x) \psi_-^\dagger(x) \ , \end{aligned}$$

where in the last term we dropped the fast oscillating and higher order terms in the Taylor expansion. As a result we have,

$$\begin{aligned} \delta U \sum_j \sigma_j^x \sigma_{j+1}^x &\to 2\delta U \sum_j a \left[i\psi_+^\dagger(x)\psi_-^\dagger(x) - i\psi_-(x)\psi_+(x) \right] \\ &= 2\delta U \int dx \left[i\psi_+^\dagger(x)\psi_-^\dagger(x) - i\psi_-(x)\psi_+(x) \right] \ . \end{aligned} \tag{4.61}$$

Using the Baker–Campbell–Hausdorff (BCH) formula and the bosnization dictionary we can rewrite the above equation in terms of bosonic fields,

$$\begin{aligned} \psi_-\psi_+ &= \frac{1}{2\pi\alpha} e^{-i\sqrt{4\pi}\phi_-} e^{+i\sqrt{4\pi}\phi_+} \\ &= \frac{1}{2\pi\alpha} e^{-i\sqrt{4\pi}(\phi_- - \phi_+)} e^{\frac{1}{2}\left[-i\sqrt{4\pi}\phi_-, i\sqrt{4\pi}\phi_+\right]} \\ &= \frac{1}{2\pi\alpha} e^{-i\sqrt{4\pi}\theta} e^{-i\frac{\pi}{2}} \ . \end{aligned} \tag{4.62}$$

Substituting Eq. 4.62 in Eq. 4.61 and rescaling the Hamiltonian we get,

$$\begin{aligned}\delta U \sum_j \sigma_j^x \sigma_{j+1}^x &\to -\frac{1}{4Ja}\int dx \frac{2\delta U}{2\pi\alpha}\left[e^{i\sqrt{4\pi}\theta} + e^{-i\sqrt{4\pi}\theta}\right] \\ &= -\frac{\delta U}{2Ja\pi\alpha}\int dx \cos\left(\sqrt{4\pi}\theta\right) \ . \end{aligned} \tag{4.63}$$

The last term in the Hamiltonian in Eq. 4.44 corresponds to the longitudinal field. We can find the bosonic continuum of it as follows,

$$\begin{aligned}\sigma_j^x &= \sigma_j^+ + \sigma_j^- \\ &= \left(e^{i\pi\sum_{k<j}\psi_j^\dagger\psi_j}\right)\left(\psi_j^\dagger + \psi_j\right) \ .\end{aligned}$$

To simplify we first calculate the exponent in the string operator,

$$\begin{aligned}i\pi\sum_{k<j}\psi_j^\dagger\psi_j &= i\pi\sum_{k<j}\left(:\psi_j^\dagger\psi_j: + \frac{1}{2}\right) \\ &= i\pi\int_0^x \frac{\partial_x\phi}{\sqrt{\pi}}dx + i\frac{\pi j}{2} \\ &= i\sqrt{\pi}\left[\phi(x) - \phi(0)\right] + i\frac{\pi j}{2} \ .\end{aligned}$$

Using this result we can continue to simplify, say, σ_j^-,

$$\begin{aligned}\sigma_j^- &= e^{i\sqrt{\pi}[\phi(x)-\phi(0)]}e^{i\frac{\pi j}{2}}\psi_j \\ &= e^{-i\sqrt{\pi}\phi(0)}e^{i\sqrt{\pi}\phi(x)}e^{i\frac{\pi j}{2}}\sqrt{a}\left[e^{i\frac{\pi j}{2}}\psi_+(x) + e^{-i\frac{\pi j}{2}}\psi_-(x)\right] \\ &= e^{-i\sqrt{\pi}\phi(0)}e^{i\sqrt{\pi}\phi(x)}\sqrt{a}\left[(-1)^j\psi_+(x) + \psi_-(x)\right] \\ &= e^{-i\sqrt{\pi}\phi(0)}e^{i\sqrt{\pi}[\phi_+(x)+\phi_-(x)]}\sqrt{\frac{a}{2\pi\alpha}}e^{-i\sqrt{4\pi}\phi_-} \\ &= e^{-i\sqrt{\pi}\phi(0)}e^{ic_0}e^{-i\sqrt{\pi}\theta(x)}\sqrt{\frac{a}{2\pi\alpha}} \ ,\end{aligned}$$

where we dropped the rapidly oscillating term and defined a phase c_0 coming from the commutation relations of the right and the left movers to get the θ field. As Giamarchi noted [51] we can choose $\phi(0)$ such that it cancels this phase. Since we are interested in the bulk properties in the continuum limit, this would not affect the final result. Hence after the rescaling we have,

$$\begin{aligned}-h\sum_j \sigma_j^x &\to -\frac{1}{4Ja}h\sqrt{\frac{a}{2\pi\alpha}}\sum_j 2\cos\left(\sqrt{\pi}\theta(ja)\right) \\ &\to -\frac{h}{2Ja}\frac{1}{\sqrt{2\pi a\alpha}}\int \cos(\sqrt{\pi}\theta)dx \ .\end{aligned} \tag{4.64}$$

By summing up all the contributions we get the final result,

$$H = \int dx \left[\frac{1}{2}\Pi^2 + \frac{1}{2} \left(\partial_x \phi\right)^2 - \frac{h}{2Ja} \frac{1}{\sqrt{2\pi a \alpha}} \cos(\sqrt{\pi}\theta) - \frac{\delta U}{2Ja\pi\alpha} \cos\left(\sqrt{4\pi}\theta\right) \right] . \tag{4.65}$$

We will use the bosonized Hamiltonian in above equation in chapter 6 to study the phase diagram of the KH model. This will help us to find the phase boundary between the trivial phase and the topological phase in the attractive regime. To do so we will also need to know the RG flow of the coupling which will be presented in the following sections. The predictions for the phase boundary between the trivial phase and the topological phase based on this low-energy effective field theory match very well with our numerical results. More details are presented in chapter 6 and paper III.

In principle we could have done the same for repulsive interactions, i.e. $U > 0$. However one needs to note that in the current approach we are implicitly assuming that the RG flow would not generate any new operator to the Hamiltonian or if new operators are generated they would have a negligible effect. This assumption breaks down for the repulsive interactions and the bosonization approach becomes much more involved [54, 55].

The spin-$\frac{1}{2}$ XXZ chain

Although the spin-$\frac{1}{2}$ XYZ chain is exactly solvable by means of Bethe ansatz [13], it is quite convenient to have a low-energy field theory description of it. This is practical in performing detailed calculations regarding the ground state properties of the model and in recognizing the connections between this model and the other ones where much less is known. The Hamiltonian of the spin-$\frac{1}{2}$ XXZ chain reads,

$$H_{\mathrm{XXZ}} = \sum_j -J \left(\sigma_j^x \sigma_{j+1}^x + \sigma_j^y \sigma_{j+1}^y\right) + J_z \sigma_j^z \sigma_{j+1}^z \, . \tag{4.66}$$

Without loss of generality we can assume that $J > 0$. Using the JW transformation and our previous result in Eq. 4.51 we get,

$$H_{\mathrm{XXZ}} = \sum_j -2J \left(\psi_j^\dagger \psi_{j+1} + \psi_{j+1}^\dagger \psi_j\right) + 4J_z \left(\psi_j^\dagger \psi_j - \frac{1}{2}\right)\left(\psi_{j+1}^\dagger \psi_{j+1} - \frac{1}{2}\right) . \tag{4.67}$$

First of all we note that the total number of particles is conserved. Moreover the free hopping Hamiltonian has a $\cos k$ band where all the modes with $-\pi/2 \leq k \leq \pi/2$ are filled. Therefore the ground state of the first two terms is at half-filling. Since the free hopping model gives us the massless Dirac Hamiltonian, we use the half-filled ground state to study the effect of the interaction on it

and simplify the last term in above equation,

$$\psi_j^\dagger \psi_j - \frac{1}{2} = :\psi_j^\dagger \psi_j: \ . \tag{4.68}$$

Now we use Eq. 4.54 to rewrite the interaction term,

$$\begin{aligned}
:\psi_j^\dagger \psi_j: \ &= a \ :\left[e^{-i\frac{\pi}{2}j}\psi_+^\dagger(x) + e^{+i\frac{\pi}{2}j}\psi_-^\dagger(x)\right] \\
&\quad \left[e^{i\frac{\pi}{2}j}\psi_+(x) + e^{-i\frac{\pi}{2}j}\psi_-(x)\right] \ : \\
&= a\left[:\psi_+^\dagger(x)\psi_+(x) + \psi_-^\dagger(x)\psi_-(x):\right] \\
&\quad + a(-1)^j\left[\psi_+^\dagger(x)\psi_-(x) + \psi_-^\dagger(x)\psi_+(x)\right] \\
&= a\frac{1}{\sqrt{\pi}}\frac{\partial\phi}{\partial x} + a(-1)^j\left[\psi_+^\dagger(x)\psi_-(x) + \psi_-^\dagger(x)\psi_+(x)\right] \ ,
\end{aligned}$$

where in the last line we also used Eq. 4.43. As a result we have,

$$\begin{aligned}
\left(\psi_j^\dagger\psi_j - \frac{1}{2}\right)\left(\psi_{j+1}^\dagger\psi_{j+1} - \frac{1}{2}\right) &= a^2\left(\frac{1}{\sqrt{\pi}}\frac{\partial\phi}{\partial x}\right)^2 \\
&\quad - a^2\left[\psi_+^\dagger(x)\psi_-(x) + \psi_-^\dagger(x)\psi_+(x)\right]^2 \ ,
\end{aligned} \tag{4.69}$$

in which we dropped the oscillatory terms with the factor $(-1)^j$ and neglected the terms of the order $\mathcal{O}(a^3)$. The first term is already in terms of bosonic fields. Utilizing Eq. 4.36 we carry on with second one,

$$\begin{aligned}
\psi_+^\dagger(x)\psi_-(x) + \psi_-^\dagger(x)\psi_+(x) &= \frac{1}{2\pi\alpha}e^{-i\sqrt{4\pi}\phi_+(x)}e^{-i\sqrt{4\pi}\phi_-(x)} + \text{h.c.} \\
&= \frac{1}{2\pi\alpha}e^{-i\sqrt{4\pi}\phi(x)}e^{-\frac{1}{2}4\pi\frac{i}{4}} + \text{h.c.} \\
&= -\frac{1}{\pi\alpha}\sin(\sqrt{4\pi}\phi) \ ,
\end{aligned}$$

where in the second line we used the BCH formula in accompany with Eq. 4.20. Now we use point splitting,

$$\begin{aligned}\left[\psi_+^\dagger(x)\psi_-(x)+\psi_-^\dagger(x)\psi_+(x)\right]^2 &= \left[\frac{1}{\pi\alpha}\sin\left(\sqrt{4\pi}\phi(x)\right)\right]^2 \\ &= \lim_{\ell\to 0}\frac{1}{\pi^2\alpha^2}\left(\frac{1}{2i}\right)^2 \\ &\left[e^{i\sqrt{4\pi}\phi(x+\ell)}-e^{-i\sqrt{4\pi}\phi(x+\ell)}\right] \\ &\left[e^{i\sqrt{4\pi}\phi(x)}-e^{-i\sqrt{4\pi}\phi(x)}\right] \\ &= \lim_{\ell\to 0}\frac{-1}{2\pi^2\alpha^2}\cos\left(\sqrt{4\pi}\phi(x+\ell)+\sqrt{4\pi}\phi(x)\right) \\ &+ \lim_{\ell\to 0}\frac{1}{2\pi^2\alpha^2}\cos\left(\sqrt{4\pi}\phi(x+\ell)-\sqrt{4\pi}\phi(x)\right) \\ &= \frac{-1}{2\pi^2\alpha^2}\cos\left(\sqrt{16\pi}\phi(x)\right) \\ &+ \lim_{\ell\to 0}\frac{1}{2\pi^2\alpha^2}\cos\left(\sqrt{4\pi}\phi(x+\ell)-\sqrt{4\pi}\phi(x)\right)\ .\end{aligned}$$

To simplify the second term we use Eqs. 4.30 and 4.32,

$$\begin{aligned}&\lim_{\ell\to 0}\frac{1}{2\pi^2\alpha^2}\cos\left(\sqrt{4\pi}\phi(x+\ell)-\sqrt{4\pi}\phi(x)\right) \\ &= \lim_{\ell\to 0}\frac{1}{4\pi^2\alpha^2}\left[e^{i\sqrt{4\pi}(\phi(x+\ell)-\phi(x))}+e^{-i\sqrt{4\pi}(\phi(x+\ell)-\phi(x))}\right] \\ &= \lim_{\ell\to 0}\frac{e^{4\pi G(\ell)}}{4\pi^2\alpha^2}\ :\left[e^{i\sqrt{4\pi}(\phi(x+\ell)-\phi(x))}+e^{-i\sqrt{4\pi}(\phi(x+\ell)-\phi(x))}\right]: \\ &= \lim_{\ell\to 0}\frac{1}{2\pi^2\left(\ell^2+\alpha^2\right)}\ :\cos\left(\sqrt{4\pi}\phi(x+\ell)-\sqrt{4\pi}\phi(x)\right): \\ &= \lim_{\ell\to 0}\frac{1}{2\pi^2\left(\ell^2+\alpha^2\right)}\ :1-\frac{1}{2}\left(\sqrt{4\pi}\ell\frac{\partial\phi}{\partial x}\right)^2+\mathcal{O}(\ell^4):\\ &= -\frac{1}{\pi}\left(\frac{\partial\phi}{\partial x}\right)^2\ .\end{aligned}$$

Putting it altogether we get,

$$\left[\psi_+^\dagger(x)\psi_-(x)+\psi_-^\dagger(x)\psi_+(x)\right]^2 = -\frac{1}{\pi}\left(\frac{\partial\phi}{\partial x}\right)^2-\frac{1}{2\pi^2\alpha^2}\cos\left(\sqrt{16\pi}\phi(x)\right)\ . \tag{4.70}$$

Using Eqs. 4.69 and 4.70 we conclude that,

$$\sum_j J_z\sigma_j^z\sigma_{j+1}^z = 4J_z a^2\sum_j\left[\frac{2}{\pi}\left(\frac{\partial\phi}{\partial x}\right)^2+\frac{1}{2\pi^2\alpha^2}\cos\left(\sqrt{16\pi}\phi(x)\right)\right]\ .$$

By changing the sum to integral and scaling it with $1/4Ja$ we get,

$$\sum_j J_z \sigma_j^z \sigma_{j+1}^z \to \frac{J_z}{J} \int dx \left[\frac{2}{\pi} \left(\frac{\partial \phi}{\partial x} \right)^2 + \frac{1}{2\pi^2 \alpha^2} \cos\left(\sqrt{16\pi} \phi(x) \right) \right] . \quad (4.71)$$

Having the low-energy field theory for the interaction term, we can write the full bosonized Hamiltonian,

$$H_{\mathrm{XXZ}} = \int dx \left[\frac{1}{2} \Pi^2 + \frac{1}{2} \left(1 + \frac{4J_z}{\pi J} \right) (\partial_x \phi)^2 + \frac{J_z}{2\pi^2 \alpha^2 J} \cos\left(\sqrt{16\pi} \phi(x) \right) \right] . \quad (4.72)$$

Defining the *Luttinger parameter* K, as,

$$K = \frac{1}{\sqrt{1 + \frac{4J_z}{\pi J}}} , \quad (4.73)$$

and multiplying the Hamiltonian with K, we get,

$$\begin{aligned} H_{\mathrm{eff}} &= K H_{\mathrm{XXZ}} \\ &= \int dx \left[\frac{K}{2} \Pi^2 + \frac{1}{2K} (\partial_x \phi)^2 + \frac{K J_z}{2\pi^2 \alpha^2 J} \cos\left(\sqrt{16\pi} \phi(x) \right) \right] . \end{aligned}$$

We can rescale the bosonic fields such that they still satisfy their commutation relation,

$$\phi' = \frac{1}{\sqrt{K}} \phi \quad (4.74)$$

$$\Pi' = \sqrt{K} \Pi . \quad (4.75)$$

By defining a new effective coupling Δ,

$$\Delta = \frac{K J_z}{2\pi^2 \alpha^2 J} , \quad (4.76)$$

we have the final result for the effective low-energy Hamiltonian,

$$H_{\mathrm{eff}} = \int dx \left[\frac{1}{2} \Pi^2 + \frac{1}{2} (\partial_x \phi)^2 + \Delta \cos\left(\sqrt{16\pi K} \phi(x) \right) \right] . \quad (4.77)$$

The important property of this effective Hamiltonian is that it still has the free part and the interaction is absorbed in the Luttinger parameter K and presented through the cos term. For some interactions, everything can be absorbed in the Luttinger parameter and hence in the end the bosonized Hamiltonian has only the free term [51, 53]. One should note that, however, in such cases two-point correlation functions in the fermionic model will be

affected by the Luttinger parameter, since we need to make the appropriate changes in the bosonization dictionary,

$$\psi_{\pm} = \frac{1}{\sqrt{2\pi\alpha}} e^{i\sqrt{\pi}\left(\pm\frac{\phi}{\sqrt{K}} - \sqrt{K}\theta\right)} \ . \tag{4.78}$$

This new bosonization dictionary and the Luttinger parameter will be used in chapter 7 to study effective low-energy properties of Fock parafermions hopping on a one dimensional lattice.

The renormalization group flow

We derived the effective low-energy model for the both Kitaev-Habbuard model and the spin-$\frac{1}{2}$ XXZ chain. In addition to the Hamiltonian they both have cos terms. Except studying the saddle points of the cos terms one can derive the RG flow for them which also helps to explore the phase diagram.

The essential idea of RG is that the phase diagram and the low-energy properties of a given system do not depend on the details. These "details" represent themselves through the high-energy/momentum modes. These high-energy modes in a free model are decoupled from the low-energy modes, and hence can be simply ignored. For an interacting model, however, all the modes are interacting with each other and hence should be taken into account. Therefore to consider the effect of the high-energy modes, one integrates them out which in turn gives rise to effective couplings for the low-energy modes. During this procedure the original coupling constants in the model get "renormalized" and new couplings could be also generated. This procedure can be done perturbatively using the standard path integral techniques [6, 8, 10].

For a free scalar field in two dimensions, or $1+1$ as it is the case here, the dominant term in the RG flow of a term like $\Delta\cos(\beta x)$ is,

$$\frac{d\log\Delta}{dl} = 2 - \frac{\beta^2}{4\pi} \ , \tag{4.79}$$

where we used l to parametrize the RG flow. This will help us in chapter 6 to find the phase boundary between the topological phase and the trivial phase of the KH model in the attractive regime. As we will show, the predictions from the field theory match very well with the numerics. Hence the first term in the RG flow captures the essential physics.

We can again comment on the bosonization for the KH model with repulsive interactions. In general one needs to treat Δ and K in Eq.4.77 independently and study their coupled flow equations. This procedure, although it can be done to some extend, is usually involved. For the attractive regime, as it turns out, we can ignore the RG flow of the Luttinger parameter and set $K = 1$, but this very assumption breaks down in the repulsive regime. Moreover the RG flow in the repulsive regime generates new operators which were not originally

in the model. This means that to study the model we need to start with a more general model from the very beginning to keep everything under the control. We do not go through this analysis in this thesis.

Chapter 5

A short introduction to matrix product states

Introduction

This chapter is devoted to the matrix product states (MPS) which is the building block of density matrix renormalization group (DMRG). This is the numerical method which was used in paper III (see chapter 6) and paper IV (see chapter 7). The basic idea is that to write down the ground state and the few low-lying excited states there is no need to use the full Hilbert space and one can restrict the numerical optimization to a subspace of it. This subspace has a special feature, namely the entanglement entropy of a subsystem scales with its area rather than its volume [56]. This is an important feature of the ground state wavefunction of one dimensional gapped systems [57], the systems of our interest in many cases. In addition the MPS ansatz can also capture one dimensional critical models where the entanglement entropy of a subsystem grows logarithmically with its size. Let us make this more concrete.

Consider a chain of size L. On each lattice site i, there exists a "spin" s_i which can take values $s_i = 0, 1, \cdots, q-1$. Therefore the full Hilbert space has the dimension $\mathcal{D} = q^L$. In principle any given state $|\psi\rangle$ can be written as a linear combination of all the states,

$$|\psi\rangle = \sum_{\{s_i\}} c_{s_1,\cdots,s_L} |s_1, \cdots, s_L\rangle \ . \tag{5.1}$$

This means that to specify a typical state we need to determine q^L complex numbers $c_{s_1,\cdots,s_L}$.

But what are we interested in? Are we interested in the full many-body spectrum or just the ground state and maybe the few low-lying ones?

If we are interested in the zero temperature behaviour of a system, we need to know the ground state [§]. Therefore, one would ask: Does the ground state of a quantum Hamiltonian with *local* interactions have a special feature with which one can simplify the general linear combination in Eq. 5.1 or put some constraint on it?

It turns out that *entanglement entropy* (EE) is the feature which distinguishes the ground state from a typical state at finite energy density in the

[§]For a gapped system with a gap Δ, this can be relaxed to the cases where $T \ll \Delta/k_B$ where k_B is the Boltzmann constant.

middle of the many-body spectrum [56]. To quantify EE consider a bipartition of a system described by a state $|\psi\rangle$, to two subsystems A and B with the Hilbert spaces $\mathcal{H}_A$ of dimension $\mathcal{D}_A$ and $\mathcal{H}_B$ of dimension $\mathcal{D}_B$ respectively. The state can be expanded as,

$$|\psi\rangle = \sum_{a,b} \psi_{ab} \, |e_a\rangle \, |\tilde{e}_b\rangle \ , \tag{5.2}$$

where the sets $\{e_a\}$ and $\{\tilde{e}_b\}$ form a complete orthonormal basis for the Hilbert spaces $\mathcal{H}_A$ and $\mathcal{H}_B$ respectively. Using the singular value decomposition and defining M as the Schmidt rank ($M \leq \min(\mathcal{D}_A, \mathcal{D}_B)$) we can get the *Schmidt decomposition* of the state,

$$|\psi\rangle = \sum_{i=1}^{M} \lambda_i \, |i\rangle_A \, |i\rangle_B \ , \tag{5.3}$$

where the sets $\{|i\rangle_A\}$ and $\{|i\rangle_B\}$ are orthonormal vectors in $\mathcal{H}_A$ and $\mathcal{H}_B$ and $\lambda_i \in \mathbb{R}^+$. Note that, unlike Eq. 5.2, there is a single sum in above equation.

To define the EE between the two subsystems we need to use the *reduced density matrix* for one of the subsystems, say A,

$$\begin{aligned} \rho_A &= \mathrm{Tr}_B |\psi\rangle\langle\psi| \\ &= \sum_{i=1}^{M} \lambda_i^2 \, |i\rangle_A \, {}_A\langle i| \ , \end{aligned} \tag{5.4}$$

where Tr_B is the trace over the B subsystem. It is also easy to calculate the reduced density matrix for B,

$$\begin{aligned} \rho_B &= \mathrm{Tr}_A |\psi\rangle\langle\psi| \\ &= \sum_{i=1}^{M} \lambda_i^2 \, |i\rangle_B \, {}_B\langle i| \ . \end{aligned} \tag{5.5}$$

Now we are in the position to define entanglement entropy (also known as von-Neumann entropy) between the two subsystems:

$$S_{A|B} = -\mathrm{Tr}\rho_A \ln \rho_A = -\mathrm{Tr}\rho_B \ln \rho_B \ . \tag{5.6}$$

This can be written in terms of the Schmidt eigenvalues $\{\lambda_i\}$ (which also proves the equality in above equation),

$$S_{A|B} = -\sum_{i=1}^{M} \lambda_i^2 \ln \lambda_i^2 \ . \tag{5.7}$$

Note that in literature one can also find the definition with $\log_2 \lambda_i^2$ which changes $S_{A|B}$ in Eq. 5.7 by a factor of $1/\ln 2$.

We may interpret the EE as follows. Intuitively EE captures the "deviation" from a "classical" state namely a product state. Consider a sate which can be written as a product state $|\psi\rangle = |f_A\rangle\,|\tilde{f}_B\rangle$ with $|f_A\rangle$ and $|\tilde{f}_B\rangle$ two unit vectors in $\mathcal{H}_A$ and $\mathcal{H}_B$. Such a state is already in the Schmidt form with $M = 1$ and $\lambda_1 = 1$. Therefore there is no EE between the two subsystems, i.e. $S_{A|B} = 0$. A simple example of this case for two spins is $|\uparrow\uparrow\rangle$, for which both reduce density matrices are $|\uparrow\rangle\langle\uparrow|$. However the state

$$\frac{1}{\sqrt{2}}\left(|\uparrow\uparrow\rangle + |\downarrow\downarrow\rangle\right) \ , \tag{5.8}$$

gives,

$$\rho_A = \frac{1}{2}\mathbf{1}_A \ , \qquad \rho_B = \frac{1}{2}\mathbf{1}_B \ , \tag{5.9}$$

for which the von-Neumann entropy is $S_{A|B} = \ln 2$. The state in Eq. 5.8 is a *maximally entangled* state. This was a simple example to show that non-zero EE of a given state shows that how much the state "deviates" from a simple product state.

To appreciate an important feature regarding the EE of the ground state of local Hamiltonians, we need to recall extensive quantities in thermodynamics. Studying thermodynamics and statistical mechanics of quantum systems in equilibrium at finite temperature T [§] can be done by replacing the von-Neumann entropy as the entropy of the system [58,59] (for dimensional reasons we need to multiply by k_B),

$$k_B S_{vN} = -k_B \mathrm{Tr}\rho \ln \rho \ . \tag{5.10}$$

By plugging the thermal density matrix,

$$\rho_{\mathrm{Th}} = \frac{e^{-\beta H}}{\mathcal{Z}} \ , \tag{5.11}$$

where $\beta = 1/k_B T$, H is the Hamiltonian and $\mathcal{Z}$ is the partition function in Eq. 5.10 we get,

$$k_B S_{vN} = \frac{U - F}{T} \ . \tag{5.12}$$

where U is the total energy and F is the free energy of the system and they are both extensive quantities in the system's volume. The entropy probes *all* the many-body spectrum and hence is extensive in the system's volume, a quite crucial feature for the thermodynamics.

Naively we may expect that the EE between the subsystems does also scale with the volume. This, however, turns out to be wrong. It has been shown that

[§] Just for the systems which thermalize.

for the ground state of a gapped local Hamiltonian, the EE between the two subsystems scales with the size of the boundary between them [56, 57, 60–62]. This is the so-called *are law* and has been proved for one dimensional gapped systems [57] for which the EE between two subsystems is simply *constant*.

Now we can rephrase our previous questions. How can we rewrite the wavefunction or "compress" our representation such that it captures the ground state of gapped one-dimensional systems?

Historically DMRG and MPS were not started in this way. In the beginning DMRG was proposed to overcome the failure of the block renormalization group [63–65]. Later the connection between the DMRG and an MPS representation of an infinite system was found [66]. It was also shown that based on the DMRG algorithm for a finite system size, the quantum state which is being variationally minimized has an MPS form [67].

In what follows we present the basics of an MPS representation, mainly following Ref. [65]. As an example we write down the exact ground state of the Affleck-Kennedy-Lieb-Tasaki (AKLT) Hamiltonian in the MPS form and calculate some two-point correlation functions of it [68, 69]. Implementation of MPS as an ansatz for the ground state wavefunction and discussing efficient numerical algorithms for variational optimization of it are beyond the scope of this thesis. For the numerical simulations in the following chapters we have used the ALPS libraries [70–72], one of the standard and very well optimized packages [§].

Canonical matrix product states

An essential tool to use MPS is the singular value decomposition (SVD) of a matrix. Given an arbitrary rectangular matrix C of size $N_r \times N_c$, matrices U, Λ and $V^\dagger$ exist such that,

$$C = U\Lambda V^\dagger \ , \tag{5.13}$$

in which U has the dimension $N_r \times \min(N_r, N_c)$ with orthonormal columns $U^\dagger U = \mathbf{1}$, Λ is a $\min(N_r, N_c) \times \min(N_r, N_c)$ diagonal matrix with real *non-negative* elements and $V^\dagger$ has the dimension $\min(N_r, N_c) \times N_c$ with orthonormal rows $V^\dagger V = \mathbf{1}$. In what follows we reduce the dimension of the matrix Λ from $\min(N_r, N_c)$ to $M \leq \min(N_r, N_c)$ which is defined as the (Schmidt) rank of the matrix C and denotes the number its *non-zero* Schmidt eigenvalues.

Using SVD we can actually prove the Schmidt decomposition and understand the role of the matrix Λ. We rewrite the matrix ψ_{ab} in Eq. 5.2 using

[§] The author of this thesis is mainly interested in analytical approaches. Simultaneously the author is completely aware of the importance of numerical simulations and appreciate their values. The main goal, however, is understanding the basic underlying ideas and concepts of numerical approaches and be able to use the tools developed in such fields.

SVD,

$$
\begin{aligned}
|\psi\rangle &= \sum_{a=1}^{N_A}\sum_{b=1}^{N_B} \psi_{ab}\,|e_a\rangle\,|\tilde{e}_b\rangle \\
&= \sum_{a=1}^{N_A}\sum_{b=1}^{N_B} \left(U\Lambda V^\dagger\right)_{ab}|e_a\rangle\,|\tilde{e}_b\rangle \\
&= \sum_{a=1}^{N_A}\sum_{b=1}^{N_B}\sum_{i=1}^{\min(N_A,N_B)} U_{ai}\lambda_i V^\dagger_{ib}\,|e_a\rangle\,|\tilde{e}_b\rangle \\
&= \sum_{i=1}^{M}\lambda_i\left(\sum_{a=1}^{N_A} U_{ai}\,|e_a\rangle\right)\left(\sum_{b=1}^{N_B} V^\dagger_{ib}\,|\tilde{e}_b\rangle\right)\ . \qquad (5.14)
\end{aligned}
$$

We applied SVD to the matrix ψ_{ab} which gives the second line. In the third line [§] we expanded the matrix multiplication in terms of the matrices' elements and group them appropriately to read the orthonormal set of vectors $\{|i\rangle_{A/B}\}$. Note that in the last line we only kept the M non-zero entries.

We need to show that the new set of vectors defined in the parenthesis in above equation are orthonormal,

$$
\begin{aligned}
\left(\sum_{a'=1}^{N_A} U^*_{a'j}\,\langle e_{a'}|\right)\left(\sum_{a=1}^{N_A} U_{ai}\,|e_a\rangle\right) &= \sum_{a=1}^{N_A}\sum_{a'=1}^{N_A} U^*_{a'j}U_{ai}\,\langle e_{a'}|e_a\rangle \\
&= \sum_{a=1}^{N_A}\sum_{a'=1}^{N_A} U^*_{a'j}U_{ai}\delta_{a'a} \\
&= \sum_{a=1}^{N_A} U^*_{aj}U_{ai} \\
&= \sum_{a=1}^{N_A}\left(U^\dagger\right)_{ja}U_{ai} \\
&= \left(U^\dagger U\right)_{ji} \\
&= \delta_{ji}\ .
\end{aligned}
$$

In the same way one can show that the new set of vectors in the B subspace

[§] $V^\dagger_{ib}$ is the ib entry of the matrix $V^\dagger$.

are also orthonormal. So by defining,

$$|i\rangle_A = \sum_{a=1}^{N_A} U_{ai} |e_a\rangle \ , \tag{5.15}$$

$$|i\rangle_B = \sum_{b=1}^{N_B} V_{ib}^\dagger |\tilde{e}_b\rangle \ , \tag{5.16}$$

Eq. 5.14 simplifies to the Schmidt decomposition as we had in Eq. 5.3. Therefore the eigenvalues of the matrix Λ determine the EE between the two subsystems.

Now we want to write down an arbitrary wavefunction in an MPS form. We first present the so-called left-canonical form which will be used in studying the AKLT model and then discuss the mixed-canonical form which is useful for understanding some of the concepts and the numerical implementations in DMRG.

Left-canonical MPS

Consider a one dimensional system of size L. On each site a "spin" variable lives which can take the values $s = 0, 1, \cdots, q-1$. In general the wavefunction is,

$$|\psi\rangle = \sum_{\{s_i\}} c_{s_1,\cdots,s_L} |s_1, \cdots, s_L\rangle \ . \tag{5.17}$$

We want to rewrite the coefficients in the MPS form. We need to use SVD for which we should reshape the coefficients $c_{s_1,\cdots,s_L}$ and make a matrix $C^{(1)}$,

$$C^{(1)}_{s_1 \underline{s}_2} = c_{s_1,\cdots,s_L} \ , \tag{5.18}$$

where we used the notation $\underline{s}_n = s_n, \cdots, s_L$. The matrix $C^{(1)}$ is of dimension $q \times q^{L-1}$. Applying SVD we get,

$$\begin{aligned} c_{s_1,\cdots,s_L} &= C^{(1)}_{s_1 \underline{s}_2} \\ &= \sum_{i_1=1}^{M_1} U^{(1)}_{s_1 i_1} \Lambda^{(1)}_{i_1} V^{(1)\dagger}_{i_1 \underline{s}_2} \ . \end{aligned}$$

Note that $M_1 \leq q$. We define a set of vectors $\{A^{s_1}\}$ with the elements,

$$A^{s_1}_i = U^{(1)}_{s_1 i} \ . \tag{5.19}$$

So we have,

$$c_{s_1,\cdots,s_L} = \sum_{i_1=1}^{M_1} A^{s_1}_{i_1} \left(\Lambda^{(1)} V^{(1)\dagger}\right)_{i_1 \underline{s}_2} \ . \tag{5.20}$$

We now reshape the matrix $\left(\Lambda^{(1)}V^{(1)\dagger}\right)$,

$$\left(\Lambda^{(1)}V^{(1)\dagger}\right)_{i_1\underline{s}_2} = \left(\Lambda^{(1)}V^{(1)\dagger}\right)_{(i_1s_2)\underline{s}_3} = C^{(2)}_{(i_1s_2)\underline{s}_3}$$

The matrix $C^{(2)}$ has the dimension $(M_1q)\times q^{L-2}$. Using SVD we get,

$$\begin{aligned} c_{s_1,\cdots,s_L} &= \sum_{i_1=1}^{M_1} A^{s_1}_{i_1} C^{(2)}_{(i_1s_2)\underline{s}_3} \\ &= \sum_{i_1=1}^{M_1} A^{s_1}_{i_1} \sum_{i_2=1}^{M_2} U^{(2)}_{(i_1s_2)i_2}\Lambda^{(2)}_{i_2}V^{(2)\dagger}_{i_2\underline{s}_3} \ . \end{aligned}$$

Note that $M_2 \leq M_1q$. We now define a set of matrices $\{A^{s_2}\}$ with the elements,

$$A^{s_2}_{i_1i_2} = U^{(2)}_{(i_1s_2)i_2} \ . \tag{5.21}$$

Therefore we have,

$$c_{s_1,\cdots,s_L} = \sum_{i_1=1}^{M_1}\sum_{i_2=1}^{M_2} A^{s_1}_{i_1}A^{s_2}_{i_1i_2}\left(\Lambda^{(2)}V^{(2)\dagger}\right)_{i_2\underline{s}_3} \ . \tag{5.22}$$

One can, of course, continue by defining the matrices $C^{(n)}$ using the matrix $\Lambda^{(n-1)}V^{(n-1)\dagger}$, applying SVD and reading the set of matrices $\{A^{s_n}\}$. Doing so we get the MPS form,

$$c_{s_1,\cdots,s_L} = \sum_{i_1,\cdots,i_{L-1}} A^{s_1}_{i_1}A^{s_2}_{i_1i_2}\cdots A^{s_{L-1}}_{i_{L-2}i_{L-1}}A^{s_L}_{i_{L-1}} \tag{5.23}$$

$$= A^{s_1}A^{s_2}\cdots A^{s_{L-1}}A^{s_L} \ . \tag{5.24}$$

We need to make a few comments.

1) In general the matrices are site dependent. For a model defined on a ring, as we will discuss for the AKLT Hamiltonian, or an infinite system we can assume that we only need to determine a set of q matrices $A^0,\cdots,A^{q-1}$.

2) For an open chain as we discussed above $\{A^{s_1}\}$ are row vectors and $\{A^{s_L}\}$ are column vectors. Therefore Eq. 5.23 does give a number indeed. Using the braket notation we may write it as

$$c_{s_1,\cdots,s_L} = \langle A^{s_1}|\, A^{s_2}\cdots A^{s_{L-1}}\,|A^{s_L}\rangle \ . \tag{5.25}$$

3) In principle we have $M_1 \leq \min(q, q^{L-1})$, which can be simplified to $M_1 \leq q$. The same simplification was done for M_2. Continuing this procedure, one can show that in the middle of the chain the rank M saturates to $q^{L/2}$ and then it decreases again. This can be shown either by the definition of M or simply by starting from the other end of the chain. For instance as we mentioned in 2) the matrices A^{s_L} are actually column vectors.

4) The fact that $U^\dagger U = \mathbf{1}$ in SVD implies that,

$$\sum_{s_i} A^{s_i\dagger} A^{s_i} = \mathbf{1} \ . \tag{5.26}$$

This is usually called *left-normalization*.

5) We can rewrite the wavefunction and decompose it at an arbitrary site l as follows,

$$\begin{aligned}
|\psi\rangle &= \sum_{\{s_i\}} c_{s_1,\cdots,s_L} |s_1,\cdots,s_L\rangle \\
&= \sum_{\{s_i\}} A^{s_1} A^{s_2} \cdots A^{s_{L-1}} A^{s_L} |s_1,\cdots,s_L\rangle \\
&= \sum_{i_l} \left[\sum_{\{s_1,\cdots,s_l\}} (A^{s_1} A^{s_2} \cdots A^{s_l})_{i_l} |s_1,\cdots,s_l\rangle \right] \\
&\left[\sum_{\{s_{l+1},\cdots,s_L\}} (A^{s_{l+1}} A^{s_{l+2}} \cdots A^{s_L})_{i_l} |s_{l+1},\cdots,s_L\rangle \right] \ .
\end{aligned}$$

One can check that the set $\{|i_l\rangle_A\}$,

$$|i_l\rangle_A = \sum_{\{s_1,\cdots,s_l\}} (A^{s_1} A^{s_2} \cdots A^{s_l})_{i_l} |s_1,\cdots,s_l\rangle \ , \tag{5.27}$$

consists of orthonormal vectors in the subsystem A, owing to the left-normalization of the A^s matrices (Eq. 5.26). The set $\{|\tilde{i_l}\rangle_B\}$

$$|\tilde{i_l}\rangle_B = \sum_{\{s_{l+1},\cdots,s_L\}} (A^{s_{l+1}} A^{s_{l+2}} \cdots A^{s_L})_{i_l} |s_{l+1},\cdots,s_L\rangle \ , \tag{5.28}$$

however, is not an orthonormal set.

Above we started from the left side of the chain, but one can also start from the right side of the chain. To connect this formalism with the Schmidt decomposition and the EE we look into the mixed-canonical form, in which we somehow discuss the the right-canonical one as well.

To have an MPS in its *left-canonical* form the set of matrices $\{A^s\}$ should satisfy Eq. 5.26 as well Eq. 5.43 which will be discussed in the next section.

Mixed-canonical MPS

Let us assume that we have found the A^{s_i} matrices upto site l,

$$c_{s_1,\cdots,s_L} = A^{s_1}_{i_1} A^{s_2}_{i_1 i_2} \cdots A^{s_l}_{i_{l-1} i_l} \Lambda^{(l)}_{i_l} V^{(l)\dagger}_{i_l \underline{s}_l} \ . \tag{5.29}$$

In above the sum over repeated indices is implicit. We now focus on $V^{(l)\dagger}$. One can reshape it as,

$$\tilde{C}^{(l)}_{(i_l,s_l,\cdots,s_{L-1})s_L} = V^{(l)\dagger}_{i_l \underline{s}_l} \ , \tag{5.30}$$

and perform SVD starting from site L,

$$\tilde{C}^{(l)}_{(i_l,s_l,\cdots,s_{L-1})s_L} = \tilde{U}^{(l)}_{(i_l,s_l,\cdots,s_{L-1})i_{L-1}} \Lambda^{(L-1)}_{i_L-1} \tilde{V}^{(L-1)\dagger}_{i_{L-1}s_L} \ , \tag{5.31}$$

with which we can define the set of column vectors $\{B^{s_L}\}$ with the elements

$$B^{s_L}_i = \tilde{V}^{(L-1)\dagger}_{i\ s_L} \ . \tag{5.32}$$

We can repeat this procedure as we did for the A matrices and define the B^{s_j} matrices upto the site $l+1$. Having done that Eq. 5.29 simplifies to,

$$c_{s_1,\cdots,s_L} = A^{s_1}_{i_1} A^{s_2}_{i_1 i_2} \cdots A^{s_l}_{i_{l-1} i_l} \Lambda^{(l)}_{i_l} B^{s_{l+1}}_{i_l i_{l+1}} B^{s_{l+2}}_{i_{l+1} i_{l+2}} \cdots B^{s_L}_{i_{L-1}} \ . \tag{5.33}$$

In matrix notation we can write it as,

$$c_{s_1,\cdots,s_L} = A^{s_1} A^{s_2} \cdots A^{s_l} \Lambda^{(l)} B^{s_{l+1}} \cdots B^{s_{L-1}} B^{s_L} \ . \tag{5.34}$$

We remind that the set $\{A^{s_1}\}$ are row vectors and the set $\{B^{s_L}\}$ are column vectors. So the right hand side of the above equation returns a number. As it was the case for the A matrices, the fact that $V^\dagger V = \mathbf{1}$ implies that,

$$\sum_{s_i} B^{s_i} B^{s_i \dagger} = \mathbf{1} \ . \tag{5.35}$$

Now consider the following set of vectors,

$$|i_l\rangle_A = \sum_{s_1,\cdots,s_l} \left(A^{s_1} A^{s_2} \cdots A^{s_l}\right)_{i_l} |s_1, \cdots, s_l\rangle \ , \tag{5.36}$$

$$|i_l\rangle_B = \sum_{s_{l+1},\cdots,s_L} \left(B^{s_{l+1}} \cdots B^{s_{L-1}} B^{s_L}\right)_{i_l} |s_{l+1}, \cdots, s_L\rangle \ , \tag{5.37}$$

where in the first equation we need the i_l-th component of the row vector $(A^{s_1} A^{s_2} \cdots A^{s_l})$ and in the second one we need the i_l-th component of the column vector $(B^{s_{l+1}} \cdots B^{s_{L-1}} B^{s_L})$. These are orthonormal sets. The proof is

as follows,

$$
\begin{aligned}
{}_A\langle j_l|i_l\rangle_A &= \sum_{s'_1,\cdots,s'_l}\sum_{s_1,\cdots,s_l} A^{s'_l *}_{\alpha'_{l-1}j_l}\cdots A^{s'_2 *}_{\alpha'_1\alpha'_2}A^{s'_1 *}_{\alpha'_1}A^{s_1}_{\alpha_1}A^{s_2}_{\alpha_1\alpha_2}\cdots A^{s_l}_{\alpha_{l-1}i_l} \\
&\quad\times\langle s'_1,\cdots,s'_l|s_1,\cdots,s_l\rangle \\
&= \sum_{s_1,\cdots,s_l} A^{s_l *}_{\alpha'_{l-1}j_l}\cdots A^{s_2 *}_{\alpha'_1\alpha'_2}A^{s_1 *}_{\alpha'_1}A^{s_1}_{\alpha_1}A^{s_2}_{\alpha_1\alpha_2}\cdots A^{s_l}_{\alpha_{l-1}i_l} \\
&= \sum_{s_2,\cdots,s_l} A^{s_l *}_{\alpha'_{l-1}j_l}\cdots A^{s_2 *}_{\alpha'_1\alpha'_2}\left(\sum_{s_1} A^{s_1\dagger}A^{s_1}\right)_{\alpha'_1\alpha_1} A^{s_2}_{\alpha_1\alpha_2}\cdots A^{s_l}_{\alpha_{l-1}i_l} \\
&= \sum_{s_2,\cdots,s_l} A^{s_l *}_{\alpha'_{l-1}j_l}\cdots A^{s_2 *}_{\alpha'_1\alpha'_2}\delta_{\alpha'_1\alpha_1}A^{s_2}_{\alpha_1\alpha_2}\cdots A^{s_l}_{\alpha_{l-1}i_l} \\
&= \sum_{s_3,\cdots,s_l} A^{s_l *}_{\alpha'_{l-1}j_l}\cdots\left(\sum_{s_2} A^{s_2 *}_{\alpha_1\alpha'_2}A^{s_2}_{\alpha_1\alpha_2}\right)\cdots A^{s_l}_{\alpha_{l-1}i_l} \\
&= \sum_{s_3,\cdots,s_l} A^{s_l *}_{\alpha'_{l-1}j_l}\cdots\left(\sum_{s_2} A^{s_2\dagger}_{\alpha'_2\alpha_1}A^{s_2}_{\alpha_1\alpha_2}\right)\cdots A^{s_l}_{\alpha_{l-1}i_l} \\
&= \sum_{s_3,\cdots,s_l} A^{s_l *}_{\alpha'_{l-1}j_l}\cdots\delta_{\alpha'_2\alpha_2}\cdots A^{s_l}_{\alpha_{l-1}i_l} \\
&= \delta_{j_l i_l}\ .
\end{aligned}
$$

In above derivation we just used the normalization property of the sets of $\{A^{s_i}\}$ matrices, Eq. 5.26, for $s_i \in \{s_1,\cdots,s_l\}$. In the same way, using the normalization of the sets of $\{B^{s_i}\}$ matrices, Eq. 5.35, for $s_i \in \{s_{l+1},\cdots,s_L\}$ one can show that,

$$
{}_B\langle j_l|i_l\rangle_B = \delta_{j_l i_l}\ . \tag{5.38}
$$

Therefore we conclude that the sets $\{|i\rangle_A\}$ and $\{|i\rangle_B\}$ consist of orthonormal vectors. We are now prepared to make the connection with the Schmidt decomposition,

$$
\begin{aligned}
|\psi\rangle &= \sum_{\{s_i\}} c_{s_1,\cdots,s_L}\,|s_1,\cdots,s_L\rangle \\
&= \sum_{\{s_i\}} A^{s_1}A^{s_2}\cdots A^{s_l}\Lambda^{(l)}B^{s_{l+1}}\cdots B^{s_{L-1}}B^{s_L}\,|s_1,\cdots,s_L\rangle \\
&= \sum_{i_l}\sum_{\{s_i\}}\left(A^{s_1}A^{s_2}\cdots A^{s_l}\right)_{i_l}\Lambda^{(l)}_{i_l}\left(B^{s_{l+1}}\cdots B^{s_{L-1}}B^{s_L}\right)_{i_l}|s_1,\cdots,s_L\rangle \\
&= \sum_{i_l}|i_l\rangle_A\,\lambda^{(l)}_{i_l}\,|i_l\rangle_B\ ,
\end{aligned} \tag{5.39}
$$

where in the last line we used $\lambda_{i_l}^{(l)}$ to denote the i_l-th diagonal element of the matrix $\Lambda^{(l)}$.

We can now derive [73] another requirement for the set of $\{A^s\}$ matrices to be in the canonical form. To do so consider the Schmidt decomposition of a state $|\psi\rangle$ for two cases. In one case the subsystem A consists of the sites $1, \cdots, l-1, l$ as we have in Eq. 5.39 and in the other it consists of of the sites $1, \cdots, l-1$,

$$|\psi\rangle = \sum_{i_{l-1}} |i_{l-1}\rangle_{A_{l-1}} \lambda_{i_{l-1}}^{(l-1)} |i_{l-1}\rangle_{B_{l-1}} \ . \tag{5.40}$$

To avoid confusion we changed the subscripts of the Schmidt eigenvectors to A_l and B_l. We can easily calculate the reduced density matrix for the subsystem A_{l-1},

$$\rho_{A_{l-1}} = \sum_{i_{l-1}} \left(\lambda_{i_{l-1}}^{(l-1)}\right)^2 |i_{l-1}\rangle_{A_{l-1}\ A_{l-1}}\langle i_{l-1}| \tag{5.41}$$

Using Eq. 5.36 we can rewrite Eq. 5.39,

$$\begin{aligned}
|\psi\rangle &= \sum_{i_l} |i_l\rangle_{A_l} \lambda_{i_l}^{(l)} |i_l\rangle_{B_l} \\
&= \sum_{i_l} \sum_{s_1,\cdots,s_l} \left(A^{s_1}A^{s_2}\cdots A^{s_l}\right)_{i_l} |s_1, \cdots, s_l\rangle \lambda_{i_l}^{(l)} |i_l\rangle_{B_l} \\
&= \sum_{i_l, i_{l-1}} \underbrace{\sum_{s_1,\cdots,s_{l-1}} \left(A^{s_1}A^{s_2}\cdots A^{s_{l-1}}\right)_{i_{l-1}} |s_1, \cdots, s_{l-1}\rangle}_{|i_{l-1}\rangle_{A_{l-1}}} \\
&\qquad \sum_{s_l} A^{s_l}_{i_{l-1}i_l} |s_l\rangle \lambda_{i_l}^{(l)} |i_l\rangle_{B_l} \\
&= \sum_{i_{l-1}} |i_{l-1}\rangle_{A_{l-1}} \sum_{i_l} \sum_{s_l} A^{s_l}_{i_{l-1}i_l} |s_l\rangle \lambda_{i_l}^{(l)} |i_l\rangle_{B_l} \ .
\end{aligned}$$

Employing the above equation we can calculate the reduced density matrix for the subsystem A_{l-1} in another way,

$$\rho_{A_{l-1}} = \sum_{i_{l-1}} \left[\sum_{s_l, i_l} A^{s_l}_{i_{l-1}i_l} \left(\lambda_{i_l}^{(l)}\right)^2 A^{s_l\dagger}_{i_l i_{l-1}} \right] |i_{l-1}\rangle_{A_{l-1}\ A_{l-1}}\langle i_{l-1}| \ . \tag{5.42}$$

The second requirement is based on Eqs. 5.41 and 5.42 and demands that,

$$\sum_{s_l} A^{s_l} \left(\lambda^{(l)}\right)^2 A^{s_l\dagger} = \left(\lambda^{(l-1)}\right)^2 \ . \tag{5.43}$$

The set of $\{A^s\}$ matrices which satisfy both Eqs. 5.26 and 5.43 are called *left-canonical* matrices. In above we showed that by our construction Eq. 5.43 is

already satisfied for the diagonal entries. One can prove that using the freedom in the matrices, namely $A^{s_i} \to A^{s_i} T_i$ and $A^{s_{i+1}} \to T_i^{-1} A^{s_{i+1}}$ for an invertible matrix T_i, the full matrix equation can be satisfied [74].

As it is clear using the mixed-canonical MPS we get the Schmidt decomposition. Now it became clear that the information on the entanglement is encoded in the matrices $\Lambda^{(l)}$. We mentioned that for one dimensional gapped local Hamiltonian the EE between two subsystems in the ground state, $S_{A|B}$, is constant. Moreover recall that for a maximally entangled state the von-Neumann entropy is $\ln \chi$ where χ is the Hilbert space dimension. We conclude that the subspace of the full many-body Hilbert space, of dimension q^L, in which the ground state lives has the dimension $\chi \sim e^{S_{A|B}}$. Since the EE, $S_{A|B}$, is a constant, the dimension of this subspace is finite. This means that in Eq. 5.39 it is sufficient to only consider a finite number of eigenvalues, independent of the system size.

We can further expand this and say that for all the Schmidt decomposition that we made through the procedure of finding the MPS form, it is actually sufficient to only keep a finite number of states. Therefore we do not need to keep growing the size of the matrices, i.e. M_n. One can simply consider a fixed *bond dimension* χ for all the matrices A and be sure that such an ansatz can encode the ground state information in itself. It has been shown that for a gapped system $S_{A|B} \sim \ln \xi$ where ξ is the correlation length and of the order of inverse of the gap, $1/\Delta$ [75]. This means that $\chi \sim \xi \sim 1/\Delta$. Variational optimization of such an ansatz is the main task of the density matrix renormalization group (DMRG).

Usually gapped systems in one dimension are separated by a second order phase transition which can be described by a conformal field theory (CFT) [7]. Approaching the critical point results in the divergence of the correlation length and hence one can wonder whether the MPS ansatz is useful. The EE of a one dimensinal system at criticality has been calculated [75–77]. For a system of size L the maximum EE is between the two halves of the system and it scales as $S(L/2) \sim (c/6) \ln L$ where c is the central charge. Therefore the bond dimension scales as $\chi \sim L^{c/6}$ with the system size. Although this is not a constant, it is not an exponential function either. It has a power law form and it is possible indeed to use an MPS ansatz at critical points or in critical phases with a rather small central charge. As we will show in the next chapters DMRG can capture the gapless phases with the central charge $c = 1$ and $c = 2$, though in such cases the numerics is usually more time consuming.

The AKLT chain

To illustrate the MPS formalism in this section we go through the Affleck-Kennedy-Lieb-Tasaki (AKLT) chain and present its ground state in an MPS form and calculate a few correlation functions of it. Consider a closed chain

(a ring) of size L with a $S = 1$ spin on each site. The AKLT Hamiltonian is [68, 69],

$$H = \sum_j \left[\frac{1}{6} \left(\mathbf{S}_j . \mathbf{S}_{j+1} \right)^2 + \frac{1}{2} \mathbf{S}_j . \mathbf{S}_{j+1} + \frac{1}{3} \right] \tag{5.44}$$

$$= \sum_j P^{(2)} \left(\mathbf{S}_j + \mathbf{S}_{j+1} \right) \ . \tag{5.45}$$

The Hamiltonian acts on all bonds between two neighbouring spins and project them to the $S = 2$ subspace. Since the Hamiltonian is a sum of projectors, the lowest possible energy is zero. Hence if we find a state which is annihilated by the projection operators, it is *a* ground state.

There is a nice trick to find the ground state [68]. Based on the SU(2) algebra we know that, fusing two spin$-\frac{1}{2}$ gives a spin-0 sector with a singlet state,

$$|0;0\rangle = |S = 0; S_z = 0\rangle = \frac{|\uparrow\downarrow\rangle - |\downarrow\uparrow\rangle}{\sqrt{2}} \ , \tag{5.46}$$

and a spin-1 sector,

$$|1;+1\rangle = |S = 1; S_z = +1\rangle = |\uparrow\uparrow\rangle \ , \tag{5.47}$$

$$|1;0\rangle = |S = 1; S_z = 0\rangle = \frac{|\uparrow\downarrow\rangle + |\downarrow\uparrow\rangle}{\sqrt{2}} \ , \tag{5.48}$$

$$|1;-1\rangle = |S = 1; S_z = -1\rangle = |\downarrow\downarrow\rangle \ . \tag{5.49}$$

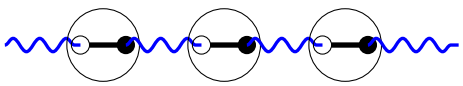

Figure 5.1: The ground state of the AKLT chain. Each small circle is a $S = 1/2$ spin. Two of them, a white and a black one, fuse to a $S = 1$ spin, indicated by a solid black line and a larger circle. Two $S = 1/2$ spins from neighbouring $S = 1$ spins form a singlet, shown by a wavy blue line.

As it is shown in Fig. 5.1 consider L pairs of $S = 1/2$ spins. A pair, consists of a white circle and a black circle, is shown by a big circle. By fusing a pair of $S = 1/2$ spins, we can choose the $S = 1$ sector and retrieve the original degrees of freedom. To have a state annihilated by the projection in Eq. 5.44, we make a singlet out of two $S = 1/2$ spins from neighbouring pairs. This is shown with a wavy blue line in Fig. 5.1. For example for the pairs j and $j + 1$ we perform

this as follows,

$$\begin{aligned}\underbrace{\left(\frac{1}{2}\otimes\frac{1}{2}\right)}_{j}\otimes\underbrace{\left(\frac{1}{2}\otimes\frac{1}{2}\right)}_{j+1} &= \frac{1}{2}\otimes\left(\frac{1}{2}\otimes\frac{1}{2}\right)\otimes\frac{1}{2}\\ &= \frac{1}{2}\otimes\underbrace{(0\oplus 1)}_{\text{Choose singlet}}\otimes\frac{1}{2}\\ &= \frac{1}{2}\otimes 0\otimes\frac{1}{2}\\ &= \frac{1}{2}\otimes\frac{1}{2}\\ &= 0\oplus 1\ ,\end{aligned}$$

which is of course annihilated by $P^{(2)}\left(\mathbf{S}_j+\mathbf{S}_{j+1}\right)$.

We now put this ground state into an MPS form. We first write the singlets' wavefunction. The j^{th} singlet consists of the black spin$-\frac{1}{2}$ from the pair j and the white spin$-\frac{1}{2}$ from the pair $j+1$. Such a singlet can be written as,

$$\frac{|\uparrow\downarrow\rangle-|\downarrow\uparrow\rangle}{\sqrt{2}}=\sum_{b_j=\uparrow,\downarrow}\sum_{w_{j+1}=\uparrow,\downarrow}S^{(0;0)}_{b_j w_{j+1}}\,|b_j w_{j+1}\rangle\ , \tag{5.50}$$

with,

$$S^{(0;0)}=\begin{pmatrix}0 & \frac{1}{\sqrt{2}}\\ -\frac{1}{\sqrt{2}} & 0\end{pmatrix}\ . \tag{5.51}$$

Therefore making all the singlets gives us,

$$|\text{All singlets}\ \rangle=\sum_{\{b\},\{w\}}S^{(0;0)}_{b_1w_2}S^{(0;0)}_{b_2w_3}\cdots S^{(0;0)}_{b_{L-1}w_L}S^{(0;0)}_{b_Lw_1}\,|w_1b_1\cdots w_Lb_L\rangle\ , \tag{5.52}$$

where we considered the model on a closed chain.

We now need to fuse the pair (w_j,b_j) and form a $S=1$ spin to retrieve the original degrees of freedom. Note that the fusion can give any of the triplet states in Eq. 5.47. Therefore a general fusion can be done by,

$$F=\prod_j\left(\sum_{S_{z,j},w_jb_j}S^{(1;S_{z,j})}_{w_jb_j}\,|S=1;S_{z,j}\rangle\,\langle w_jb_j|\right)\ , \tag{5.53}$$

where,

$$S^{(1;+1)}=\begin{pmatrix}1 & 0\\ 0 & 0\end{pmatrix}\ ,\quad S^{(1;0)}=\begin{pmatrix}0 & \frac{1}{\sqrt{2}}\\ \frac{1}{\sqrt{2}} & 0\end{pmatrix}\ ,\quad S^{(1;-1)}=\begin{pmatrix}0 & 0\\ 0 & 1\end{pmatrix}\ . \tag{5.54}$$

We can now write down the ground state in the S_z basis (not normalized),

$$\begin{aligned}|\tilde{G}\rangle &= F\,|\text{All singlets }\rangle \\ &= \sum_{\{S_i\},\{b\},\{w\}} S^{(1;S_1)}_{w_1 b_1} S^{(0;0)}_{b_1 w_2} S^{(1;S_2)}_{w_2 b_2} S^{(0;0)}_{b_2 w_3} \cdots S^{(0;0)}_{b_{L-1} w_L} S^{(1;S_L)}_{w_L b_L} S^{(0;0)}_{b_L w_1} \,|S_1 \cdots S_L\rangle \\ &= \sum_{\{S_i\}} \mathrm{Tr}\left[S^{(1;S_1)} S^{(0;0)} \cdots S^{(1;S_L)} S^{(0;0)}\right] |S_1 \cdots S_L\rangle \ .\end{aligned}$$

One can read the set of $A^{S_i} = \mathcal{N}(S_i) S^{(1;S_i)} S^{(0;0)}$ matrices upto the normalization $\mathcal{N}(S_i)$ which can be find using Eq. 5.26,

$$|G\rangle = \mathrm{Tr}\left(A^{S_1} \cdots A^{S_L}\right) |S_1 \cdots S_L\rangle \ , \tag{5.55}$$

with,

$$A^{+1} = \begin{pmatrix} 0 & \sqrt{\frac{2}{3}} \\ 0 & 0 \end{pmatrix} \ , \quad A^{0} = \begin{pmatrix} -\sqrt{\frac{2}{3}} & 0 \\ 0 & \sqrt{\frac{1}{3}} \end{pmatrix} \ , \quad A^{-1} = \begin{pmatrix} 0 & 0 \\ -\sqrt{\frac{2}{3}} & 0 \end{pmatrix} \ . \tag{5.56}$$

We now want to calculate a few observables and correlation functions. It would be quite handy to define the *transfer matrix*,

$$T = \sum_S A^{S*} \otimes A^S = \begin{pmatrix} \frac{1}{3} & 0 & 0 & \frac{2}{3} \\ 0 & -\frac{1}{3} & 0 & 0 \\ 0 & 0 & -\frac{1}{3} & 0 \\ \frac{2}{3} & 0 & 0 & \frac{1}{3} \end{pmatrix} \ . \tag{5.57}$$

The transfer matrix can be diagonalized, $D = RTR^{-1}$,

$$D = \begin{pmatrix} 1 & 0 & 0 & 0 \\ 0 & -\frac{1}{3} & 0 & 0 \\ 0 & 0 & -\frac{1}{3} & 0 \\ 0 & 0 & 0 & -\frac{1}{3} \end{pmatrix} \ ,$$

$$R = \begin{pmatrix} \frac{1}{\sqrt{2}} & 0 & 0 & \frac{1}{\sqrt{2}} \\ 0 & 1 & 0 & 0 \\ 0 & 0 & 1 & 0 \\ -\frac{1}{\sqrt{2}} & 0 & 0 & \frac{1}{\sqrt{2}} \end{pmatrix} \ .$$

To calculate the magnetization along the $z-$axis we can do as follows,

$$\begin{aligned}
\langle G|\hat{S}_1^z|G\rangle &= \mathrm{Tr}\left(A^{S_1 *}\cdots A^{S_L *}\right) S_1 \mathrm{Tr}\left(A^{S_1}\cdots A^{S_L}\right) \\
&= \mathrm{Tr}\left[\left(\sum_{S_1} S_1 A^{S_1 *}\otimes A^{S_1}\right)\left(\sum_{S} A^{S *}\otimes A^{S}\right)^{L-1}\right] \\
&= \mathrm{Tr}\left[\left(A^{+1}\otimes A^{+1} - A^{-1}\otimes A^{-1}\right) T^{L-1}\right] \\
&= \mathrm{Tr}\left[\begin{pmatrix} 0 & 0 & 0 & \frac{2}{3} \\ 0 & 0 & 0 & 0 \\ 0 & 0 & 0 & 0 \\ -\frac{2}{3} & 0 & 0 & 0 \end{pmatrix} R^{-1} D^{L-1} R\right] \\
&= \mathrm{Tr}\left[R\begin{pmatrix} 0 & 0 & 0 & \frac{2}{3} \\ 0 & 0 & 0 & 0 \\ 0 & 0 & 0 & 0 \\ -\frac{2}{3} & 0 & 0 & 0 \end{pmatrix} R^{-1} D^{L-1}\right] \\
&= \mathrm{Tr}\left[\begin{pmatrix} 0 & 0 & 0 & \frac{2}{3} \\ 0 & 0 & 0 & 0 \\ 0 & 0 & 0 & 0 \\ -\frac{2}{3} & 0 & 0 & 0 \end{pmatrix}\begin{pmatrix} 1 & 0 & 0 & 0 \\ 0 & \left(-\frac{1}{3}\right)^{L-1} & 0 & 0 \\ 0 & 0 & \left(-\frac{1}{3}\right)^{L-1} & 0 \\ 0 & 0 & 0 & \left(-\frac{1}{3}\right)^{L-1} \end{pmatrix}\right] \\
&= 0 \ .
\end{aligned}$$

Therefore there is no magnetization. Note that we used the fact that the state is normalized in the thermodynamic limit,

$$\begin{aligned}
\langle G|G\rangle &= \mathrm{Tr}\ T^L \\
&= 1 + 3\left(-\frac{1}{3}\right)^L \\
&\to 1 \ .
\end{aligned}$$

To proceed it is helpful to define $\tilde{S}_z$,

$$\tilde{S}_z = \sum_S S_1 A^{S_1 *}\otimes A^{S_1} = \begin{pmatrix} 0 & 0 & 0 & \frac{2}{3} \\ 0 & 0 & 0 & 0 \\ 0 & 0 & 0 & 0 \\ -\frac{2}{3} & 0 & 0 & 0 \end{pmatrix} \ , \tag{5.58}$$

and note that it has the following property,

$$R\tilde{S}_z R^{-1} = \tilde{S}_z \ . \tag{5.59}$$

We are now equipped to calculate the two-point correlation function for points separated by r lattice sites,

$$\begin{aligned}\langle G|\hat{S}_1^z\hat{S}_{r+1}^z|G\rangle &= \mathrm{Tr}\left[\tilde{S}_z T^{r-1}\tilde{S}_z T^{L-(r+1)}\right]\\ &= \mathrm{Tr}\left[\tilde{S}_z R^{-1}D^{r-1}R\tilde{S}_z R^{-1}D^{L-(r+1)}R\right]\\ &= \mathrm{Tr}\left[\left(R\tilde{S}_z R^{-1}\right)D^{r-1}\left(R\tilde{S}_z R^{-1}\right)D^{L-(r+1)}\right]\\ &= \mathrm{Tr}\left[\tilde{S}_z D^{r-1}\tilde{S}_z D^{L-(r+1)}\right]\\ &= -\frac{4}{9}\left(-\frac{1}{3}\right)^{r-1} - \frac{4}{9}\left(-\frac{1}{3}\right)^{L-(r+1)}\quad .\end{aligned}$$

Hence in the thermodynamic limit we have,

$$\langle G|\hat{S}_1^z\hat{S}_{r+1}^z|G\rangle = \frac{4}{3}\left(-\frac{1}{3}\right)^r \tag{5.60}$$

$$= (-1)^r\frac{4}{3}e^{-(\ln 3)r}\ . \tag{5.61}$$

It was proved that the model has a finite gap [69] which shows itself in an exponential decay of the two-point correlation function. The correlation length, $\xi = 1/\ln 3 \approx 0.91$, is of the order of a lattice spacing.

Although there is no local order parameter, one can calculate a string correlator which can serves as an "order parameter". Using the same type of calculations one can show that in the thermodynamic limit,

$$\langle G|\hat{S}_1^z\left(\prod_{k=2}^{r}e^{i\pi\hat{S}_k}\right)\hat{S}_{r+1}^z|G\rangle = -\frac{4}{9}\ . \tag{5.62}$$

One may think of this as an analogue of two-point correlation functions for fermions which using JW transformation transforms to a string correlation function of $S=\frac{1}{2}$ spins.

Therefore although the model does not have a local order parameter, the expectation value of a *string operator* is non-zero in the ground state. Moreover note that the model has a unique ground state on a ring, but has a fourfold degenerate ground state on an open chain [78]. This can be seen from Eq. 5.52 as well as Fig. 5.1 where in the case of an open chain there is no singlet pairing between the first white and the last black $S=1/2$ spins on the chain. Hence the state in Eq. 5.52 can be written for any configuration of these two edge spins [§]. This gives rise to the fourfold degenerate ground state.

[§]This means that one should *not* do the sum over w_1 and b_L. Instead for each configuration of these two *free* spins one would get one wavefunction as the starting point.

Actually the research on the AKLT chain was motivated by the earlier studies on the spin-S antiferromagnetic (AF) Heisenberg chain with a uniaxial anisotropy, $D > 0$, for which the Hamiltonian is,

$$H = \sum_j \mathbf{S}_j.\mathbf{S}_{j+1} + D\left(S_{j,z}\right)^2 \ . \tag{5.63}$$

Haldane predicted that the although the AF Heisenberg chain ($D \ll 1$) is gapless for half-integer spins which results in power law correlation functions, it has a finite gap for the integer ones with an exponentially decaying correlation functions [79]. In the limit of large anisotropy $D \gg 1$, however, the model has unique ground state of the *product state* form, namely $|S_z = 0\rangle^{\otimes L}$ where L is the system size. In this limit, the model is also gapped. The easiest excitation is changing one of the spins to be in $S_z = \pm 1$ which costs the energy D. But there is neither degeneracy in the ground state nor free spins on the edges. These two phases are *distinct* gapped phases, separated by a phase transition at $D \approx 1$, which can not be distinguished by a local order parameter or any type of symmetry breaking [80]. The high anisotropy phase is a trivial phase. The low anisotropy phase is a *symmetry protected topological* (SPT) phase and in this case is also called the *Haldane phase*.

For an *adiabatic* change (as we discussed in chapter 1) one needs to build a path in the space of Hamiltonians without any gap closing. If such a path exists between two Hamiltonians, the ground state of them belong to the same phase. An SPT phase is *protected* by *a symmetry* or *a set of symmetries* in the sense that the ground state in such a phase can not be *adiabatically* connected to a trivial product state if one respects the necessary *symmetries*. In the above case, as it is discussed in the Ref. [80], the Haldane phase is protected any of the following symmetries:(1) time-reversal symmetry, (2) π rotations around x, y and $z-$ axes, (3) reflection around middle of a bond [§]. The AKLT chain was proposed to show the ideas by Haldane in a solvable model (in the sense that the ground state is known exactly) and its ground state belongs to the Haldane phase [80].

As we described above an SPT phase is gapped, does not break any symmetry, can not be described by a local order parameter, usually has a non-local string order parameter and commonly has *edge modes*. Nevertheless a much more robust signature of an SPT phase is the degeneracy in the entanglement Hamiltonian $\mathcal{H}_{EE}$ of a subsystem which is defined as $\mathcal{H}_{EE} \sim -\ln \rho$ where ρ is the reduced density matrix of the subsystem [81].

Density matrix renormalization group

Previously we discussed the MPS ansatz and how it is useful for one dimensional systems. Using such an ansatz and variationally optimize it is the modern

[§]Ref. [80] also shows that only odd integer S case belongs to the SPT phase.

approach in DMRG. Here we briefly discuss how the ground state can be found.

To use an MPS ansatz one also needs to write the Hamiltonian in an appropriate form. This is called *Matrix product operators*. The natural generalization of an MPS such that it captures an operator acting on the Hilbert space is,

$$\hat{O} = \sum_{\{\underline{s}\},\{\underline{s}'\}} K^{s_1 s_1'} K^{s_2 s_2'} \cdots K^{s_{L-1} s_{L-1}'} K^{s_L s_L'} \left|\underline{s}\right\rangle \left\langle \underline{s}'\right| , \tag{5.64}$$

where $\{K^{ss'}\}$ is a set of matrices. This form is appropriate to act on an MPS and performing the numerical analysis. To continue and writing the local Hamiltonian in such a form it would be easier to rewrite the MPO as follows,

$$\hat{K}^{[j]} = \sum_{s_j s_j'} K^{s_j s_j'} \left|s_j\right\rangle \left\langle s_j'\right| \ , \tag{5.65}$$

$$\hat{O} = \hat{K}^{[1]} \hat{K}^{[2]} \cdots \hat{K}^{[L-1]} \hat{K}^{[L]} \ . \tag{5.66}$$

Let us show how these matrices may look like for an example of our interest. Consider the Kitaev-Hubbard chain,

$$H = \sum_{j=1}^{L-1} \left(\sigma_j^x \sigma_{j+1}^x + U \sigma_j^z \sigma_{j+1}^z\right) + h \sum_{j=1}^{L} \sigma_j^z \ , \tag{5.67}$$

where σ^α are Pauli matrices. In this case the $\hat{K}^{[j]}$ are,

$$\hat{K}^{[1]} = \begin{pmatrix} h\sigma^z & \sigma^x & U\sigma^z & \mathbf{1} \end{pmatrix} \ , \tag{5.68}$$

$$\hat{K}^{[j]} = \begin{pmatrix} \mathbf{1} & 0 & 0 & 0 \\ \sigma^x & 0 & 0 & 0 \\ \sigma^z & 0 & 0 & 0 \\ h\sigma^z & \sigma^x & U\sigma^z & \mathbf{1} \end{pmatrix} \ , \qquad 2 \leq j \leq L-1 \tag{5.69}$$

$$\hat{K}^{[L]} = \begin{pmatrix} \mathbf{1} \\ \sigma^x \\ \sigma^z \\ h\sigma^z \end{pmatrix} \ . \tag{5.70}$$

To show that this works, let us recall that how a term in the Hamiltonian looks like with the tensor product notation,

$$\sigma_j^x \sigma_{j+1}^x = \mathbf{1} \otimes \cdots \mathbf{1} \otimes \underbrace{\sigma^x}_{j} \otimes \underbrace{\sigma^x}_{j+1} \otimes \mathbf{1} \otimes \cdots \mathbf{1} \ . \tag{5.71}$$

It is now easy to check that our proposed MPO work for three sites[§],

[§]This makes it easier to show.

$$
\begin{aligned}
H &= \hat{K}^{[1]}\hat{K}^{[2]}\hat{K}^{[3]} \\
&= \begin{pmatrix} h\sigma^z & \sigma^x & U\sigma^z & \mathbf{1} \end{pmatrix}
\begin{pmatrix} \mathbf{1} & 0 & 0 & 0 \\ \sigma^x & 0 & 0 & 0 \\ \sigma^z & 0 & 0 & 0 \\ h\sigma^z & \sigma^x & U\sigma^z & \mathbf{1} \end{pmatrix}
\begin{pmatrix} \mathbf{1} \\ \sigma^x \\ \sigma^z \\ h\sigma^z \end{pmatrix} \\
&= \begin{pmatrix} h\sigma^z & \sigma^x & U\sigma^z & \mathbf{1} \end{pmatrix}
\begin{pmatrix} \mathbf{1}\otimes\mathbf{1} \\ \sigma^x\otimes\mathbf{1} \\ \sigma^z\otimes\mathbf{1} \\ h\sigma^z\otimes\mathbf{1} + \sigma^x\otimes\sigma^x + U\sigma^z\otimes\sigma^z + h\mathbf{1}\otimes\sigma^z \end{pmatrix} \\
&= \underbrace{h\sigma^z\otimes\mathbf{1}\otimes\mathbf{1}}_{h\sigma_1^z} \\
&+ \underbrace{\sigma^x\otimes\sigma^x\otimes\mathbf{1}}_{\sigma_1^x\sigma_2^x} \\
&+ \underbrace{U\sigma^z\otimes\sigma^z\otimes\mathbf{1}}_{U\sigma_1^z\sigma_2^z} \\
&+ \underbrace{h\mathbf{1}\otimes\sigma^z\otimes\mathbf{1}}_{h\sigma_2^z} + \underbrace{\mathbf{1}\otimes\sigma^x\otimes\sigma^x}_{\sigma_2^x\sigma_3^x} + \underbrace{U\mathbf{1}\otimes\sigma^z\otimes\sigma^z}_{U\sigma_2^z\sigma_3^z} + \underbrace{h\mathbf{1}\otimes\mathbf{1}\otimes\sigma^z}_{h\sigma_3^z} \ .
\end{aligned}
$$

Having an MPS ansatz and the MPO form of a Hamiltonian one can variationally minimize the energy. In fact in practice it is easier to use a Lagrange multiplier λ and minimize the following,

$$\langle\psi|H\psi\rangle - \lambda\left(\langle\psi|\psi\rangle - 1\right) \ . \tag{5.72}$$

Having done that $|\psi\rangle$ will be the ground state wavefunction and λ is its energy. To do this in practice one fixes all the matrices and minimizes the function with respect to the matrix on one site (or a bond, i.e. two sites), say A^{s_i}. Since the above function is quadratic in $A^s_{\alpha\beta}$, the minimization problem becomes a manageable problem of finding the lowest eigenvalue and eigenvector which can be symbolically written as $\mathcal{H}A^{s_i} = \lambda\mathcal{G}A^{s_i}$. To reach convergence, one starts from the first site and does the optimization and then moves to second and so on till the last site, the L^{th} one. Then one changes the direction and optimizes the site $L-1$, followed by the site $L-2$ till one reaches the first site. This procedure is usually called one *sweep*. Number of sweeps necessary to reach convergence does really depend on the system size and Hamiltonian. Therefore in practice we need to try different bond dimension χ and number of sweeps to be sure about the convergence of the results.

Chapter 6

The Kitaev-Hubbard chain

Introduction

In chapter 2 we discussed the Kitaev model for arbitrary real pairing and chemical potential and derived the MZMs' wavefunctions. We also studied the Kitaev chain with longer range hopping and pairing. In all these cases the model is exactly solvable due to the fact that the Hamiltonian was quadratic in the fermionic creation and annihilation operators. In addition the full classification of the possible gapped phases of free fermions, based on time-reversal symmetry, particle-hole symmetry, chiral symmetry and spatial dimension, is very well understood [30, 82–84]. For example the Kitaev chain with real couplings has all three symmetries and they square to one. This is known as the class **BDI**. In one dimension one can distinguish all the phases of it with the group $\mathbb{Z}$ which essentially reflects the number of MZMs on each edge.

The presence of interaction in physical systems and realistic situations is inevitable. Therefore we need to address the role of interactions and study how its presence affects the free fermionic classification. In comparison with free fermions much less is known and the full classification is lacking. In the special case of the class **BDI** in one dimension, however, Fidowski and Kitaev showed that in the presence of local interactions the gapped phases can be classified by the group $\mathbb{Z}_8$ [85, 86].

In this chapter we study the effect of a density-density interaction, i.e. a Hubbard-like term, on the Kitaev model. As a result we refer to it as the Kitaev-Hubbard (KH) chain. We consider both the repulsive and the attractive regimes. Although the attractive regime for spinless fermions, say polarized electrons, may sound unphysical, the connection between the KH model and the axial next-nearest neighbour Ising (ANNNI) model [87] encourages a thorough study.

We first describe the KH model and briefly mention its relation to the ANNNI model, namely the bosonic incarnation of the model. After presenting the phase diagram of the model we address the main properties of each phase. We briefly comment on the phase transitions between different phases. For more details we refer to paper III.

The Kitaev-Hubbard model

In chapter 2 we discussed the Ising/Kitaev chain with the Hamiltonian, Eq. 2.3,

$$H_{\mathrm{TFIM}} = -J_x \sum_{j=1}^{L-1} \sigma_j^x \sigma_{j+1}^x - h \sum_{j=1}^{L} \sigma_j^z \ .$$

To have a density-density interaction in the fermionic incarnation of the model, the JW transformation suggests the following Hamiltonian,

$$H_{\mathrm{KH-B}} = -J_x \sum_{j=1}^{L-1} \sigma_j^x \sigma_{j+1}^x - h \sum_{j=1}^{L} \sigma_j^z + U \sum_{j=1}^{L-1} \sigma_j^z \sigma_{j+1}^z \ . \tag{6.1}$$

The last term breaks the integrability [46] which in turn makes it challenging to study the model. This is exactly the same Hamiltonian that we studied in chapter 3 to discuss the PE line, a fine-tuned frustration free model for which the ground states are exactly known. In this chapter, however, we do not put any constraint on the couplings and we study the model in its general form.

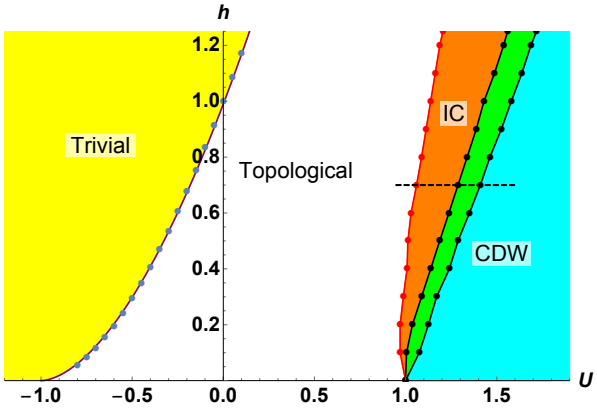

Figure 6.1: The phase diagram for the model in Eq. 6.2. The green region, between the IC and CDW phase, is the esCDW phase. Taken from paper III.

Using the JW transformation and setting $J_x = 1$ we get the KH model, i.e. the fermionic incarnation of the model,

$$\begin{aligned} H_{\mathrm{KH}} = &- \sum_{j=1}^{L-1} \left(c_j^\dagger - c_j\right)\left(c_{j+1}^\dagger + c_{j+1}\right) - h \sum_{j=1}^{L} \left(1 - 2c_j^\dagger c_j\right) \\ &+ U \sum_{j=1}^{L-1} \left(1 - 2c_j^\dagger c_j\right)\left(1 - 2c_{j+1}^\dagger c_{j+1}\right) \ . \end{aligned} \tag{6.2}$$

As it is evident the last term yields the density-density interaction as desired and a chemical potential term which was already present in the Ising/Kitaev chain.

The phase diagram of the KH model, our main result, is presented in Fig. 6.1. Note that the sign of J_x and h are immaterial and can always set to be positive using on-site rotations. The sign of the interaction has clearly far-reaching consequences. The model has five different phases, namely a trivial phase (the yellow region), a topological phase (the white region), an incommensurate (IC) phase (the orange region), an excited state charge-density wave (esCDW) phase (the green region) and a charge-density wave (CDW) phase (the cyan region). In what follows we present a summary of our results regarding each phase.

Before starting our tour through the phase diagram, we remind that the parity P,

$$P = \prod_{j=1}^{L} \sigma_j^z = \prod_{j=1}^{L} (1 - 2n_j) \ , \tag{6.3}$$

is a "good quantum number" since it is a conserved quantity. Since $P^2 = \mathbf{1}$ we will label the states with their parity eigenvalue. The states with $p = +1$ are called the even sector and those with $p = -1$ belong to the odd sector.

The attractive interaction case

In the attractive regime where $U < 0$, the model has the same two phases as in the case of the non-interacting model. Along the $h-$axis the model is the Ising/Kitaev chain and as we discussed in chapter 2 it has two phases, namely a trivial phase for $h > 1$ and a topological phase for $h < 1$. These two phases extend to the $U < 0$ regime.

To recall the properties of these two phases we study the limiting cases for $U = 0$. For $h \gg 1$ the ground state of the Hamiltonian in Eq. 6.2 is the vacuum. For negative h with $|h| \gg 1$ the ground state has each site filled with a particle. Both of these states are trivial product states. Hence there is no entanglement between different parts of the chain. For $|h| \ll 1$ the model has a doubly degenerate ground state with different parity. These states (the cat sates with definite parity as we discussed in chapter 3) are highly entangled and the EE, $S(l)$, as a function of subsystem size l saturates quite fast to a high value.

The topological phase in the non-interacting case ($U = 0$) supports MZMs localized on its edges, which was discussed in detail in chapter 2. In the topological phase in the presence of interaction, the model has still two highly entangled ground states, but the presence of *strong* MZMs all through this phase is not a likely scenario. We will comment on this issue, later in this

chapter. Nevertheless the *weak* MZMs exist, at least along the PE line [48] (see chapter 3 for more discussion on weak MZMs).

To determine the phase boundary between the trivial phase and the topological phase analytically, we performed an RG analysis on the bosonized Hamiltonian derived in Sec. 4.5.2, Eq. 4.65, and used DMRG to do finite size scaling (FSS). We start with the RG analysis.

As we pointed out in Sec. 4.5.2, we assume that in the attractive regime the RG flow of the Luttinger parameter K can be neglected and it set to be $K = 1$. Therefore we are left with the two operators in Eq. 4.65, the RG flow of which can be determined using Eq. 4.79,

$$h\cos(\sqrt{\pi}\theta): \qquad \frac{dh}{dl} = \frac{7}{4}h \ , \tag{6.4}$$

$$\delta U\cos\left(\sqrt{4\pi}\theta\right): \qquad \frac{d\delta U}{dl} = \delta U \ . \tag{6.5}$$

From these flow equations, starting from $h = 0$, $\delta U = 0$ we conclude that the boundary between the two phases can be described by

$$h \sim (U+1)^{7/4} \ . \tag{6.6}$$

We use DMRG and FSS to check this result and the assumption on the Luttinger parameter. For a given U we want to find the corresponding h where the transition between the two phases happens. Based on the FSS, close to a critical point the energy difference between the ground state and the first excited state, δ, has the following scaling [88],

$$\delta(L,h) = L^{-z}\mathcal{F}\left(L^{1/\nu}\left(h-h_c\right)\right) \ , \tag{6.7}$$

where L is the system size, z is the dynamical critical exponent, ν is the exponent for the diverging behaviour of the correlation length close to the transition, h_c is the critical magnetic field and $\mathcal{F}$ is a scaling function. In Fig. 6.2 we present the FSS procedure for $U = 0.4$. It is known that $z = \nu = 1$ for the TFIM, i.e. at $U = 0$. As we see the same exponents work perfectly fine in the interacting case as well. The upper plot shows that $L\delta$ for a set of system sizes cross at $h = 0.406$. From Eq. 6.7 we see that,

$$L\delta(L,h_c) = \mathcal{F}(0) \ , \tag{6.8}$$

which means that at the transition the quantity $L\delta$ is independent of system size. As a result we conclude that for $U = 0.4$, the transition occurs at $h_c = 0.406$. The lower plot in Fig. 6.2, which was plotted using this value of h_c, shows a perfect collapse of data for all system sizes close to the critical point,

$$L\delta(L,h) = \mathcal{F}\left(L\left(h-h_c\right)\right) \ . \tag{6.9}$$

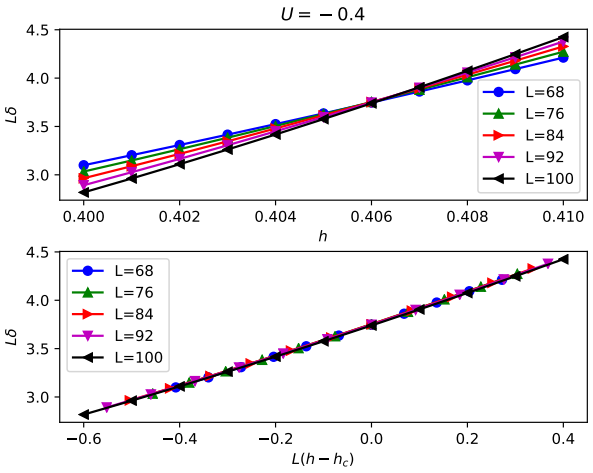

Figure 6.2: Finite size scaling for $U = -0.4$. The quantity $L\delta = L(E_1 - E_0)$ for different system sizes cross at $h = 0.406$. Taken from paper III.

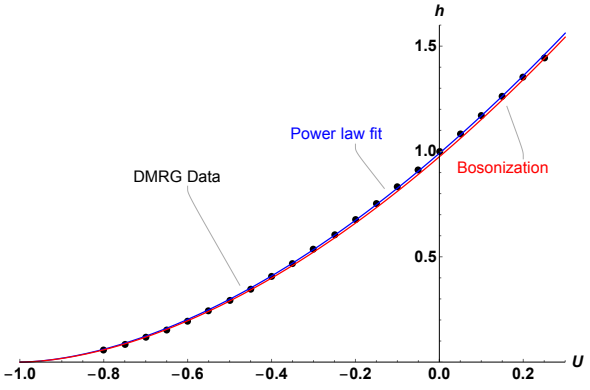

Figure 6.3: The phase boundary between the trivial band insulator and the topological phase. The blue line is $h_c(U) = 0.99(U+1)^{1.73}$. The red line is $h_c(U) = 0.97(U+1)^{\frac{7}{4}}$. Taken from paper III.

We employed FSS and found the critical magnetic field for a set of U. The result is given in Fig. 6.3. To compare with the bosonization prediction, we fitted a power law function,

$$h = a(U+1)^b \ , \tag{6.10}$$

to the DMRG data. Once we did this with free a and b coefficients which gives

$a \simeq 0.99$ and $b = 1.73$ and another time we did the fit with $b = 7/4$, which is the bosonization prediction. As it is evident the DMRG data confirms our bosonization prediction and more importantly the assumption that the RG flow of the Luttinger parameter K can be neglected.

The repulsive interaction case

In this section we present the model in the regime of repulsive interactions. As a first step, using DMRG, we present the energy of the ground state, denoted by $n = 0$, and the first excited state, denoted by $n = 1$, in each sector for a range of U for $h = 0.7$ in Fig. 6.4. We use E_n^P to refer to these energy levels. We see four different behaviours in Fig. 6.4, which is the signature of four different phases. We will explain each phase separately by presenting their EE as a function of subsystem size and the (site dependent) expectation value of the occupation number. For the DMRG we use a system of size $L = 240$ and the bond dimension $\chi = 500$.

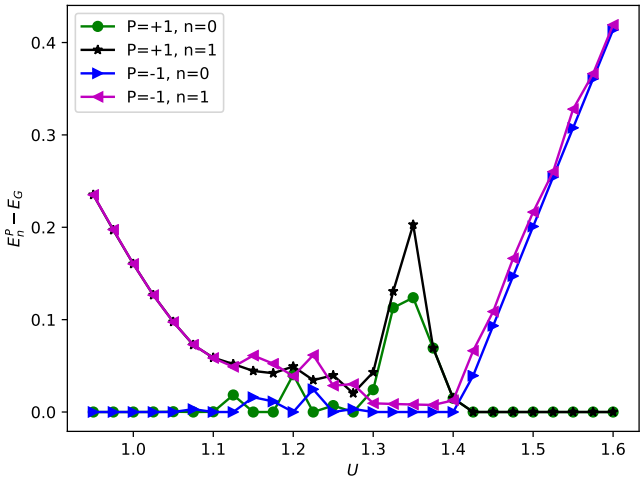

Figure 6.4: The energy levels with respect to *the ground state energy*, $E_n^P - E_G$ as a function of U for $h = 0.7$ along the dashed line in Fig. 6.1. Taken from paper III.

The topological phase

For $h = 0.7$ and $U \lesssim 1.05$ the model has a doubly degenerate ground state with opposite parity. There is a finite gap in both sectors to the first excited state (the levels with $n = 1$) and these two are also degenerate. In Fig. 6.5 we present the EE as a function subsystem size which saturates quite fast to a high value in both ground states. All of these observations lead us to conclude that this is the *topological phase* indeed.

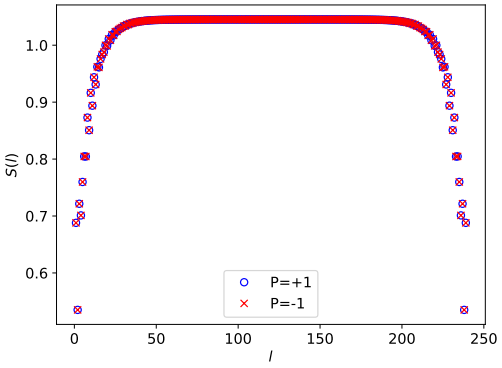

Figure 6.5: For a point in the topological phase, $h = 0.7$ and $U = 0.95$, EE as a function of subsystem size is plotted for both ground states. The system size is $L = 240$. Taken from paper III.

The incommensurate phase

By increasing the interaction strength U we enter the incommensurate (IC) phase which, for $h = 0.7$, is present for $1.05 \lesssim U \lesssim 1.29$. This phase has a unique ground state, the parity of which depends on the system size and the coupling constants. This behaviour shows itself in many level crossings between the ground states of the two parity sectors as is clear from Fig. 6.4.

The IC phase is a gapless phase. To verify this we looked at the energy difference between the first excited state and the ground state in each parity sector, i.e. $\delta^P(L) = E_1^P(L) - E_0^P(L)$ for $P = \pm 1$. The energy difference $\delta^P(L)$ vanishes as $1/L$ in each parity sector, as it is the case for one dimensional critical systems. Below we also see that the main growth of the EE can be captured by the Calabrese-Cardy (CC) formula which was derived for one dimensional critical systems [75–77].

To further investigate the properties of this phase we present the EE and the occupation number in Figs. 6.6a and 6.6b respectively. The IC phase of the

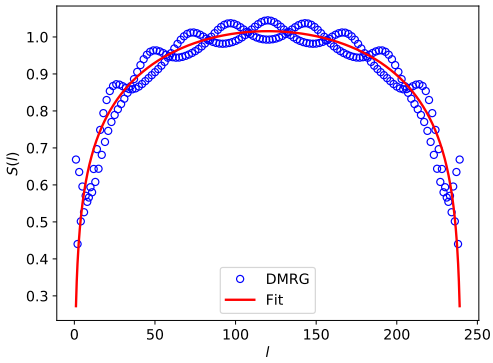

(a)

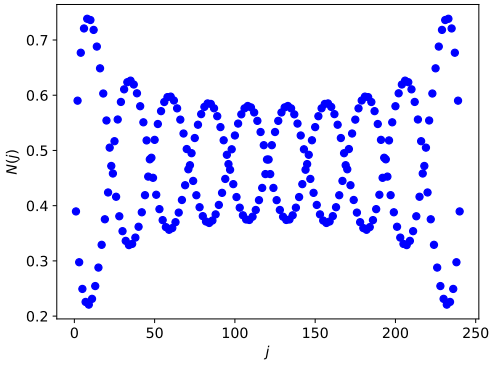

(b)

Figure 6.6: For a point in the IC phase, $h = 0.7$ and $U = 1.2$, EE as a function of subsystem size and the occupation number are plotted in (a) and (b) respectively. The system size is $L = 240$. Taken from paper III.

$\mathbb{Z}_3$ chiral clock model has been previously detected by fitting the CC formula with the central charge $c = 1$ to the EE [42]. The CC formula for an open chain reads [75–77],

$$S(l) = \frac{c}{6} \log \left[L \sin \left(\frac{\pi l}{L} \right) \right] + S_0 \ , \tag{6.11}$$

where $S(l)$ is the EE of a subsystem of size l, c is the central charge and S_0 is a constant. By fitting the CC formula to the DMRG data we get central charge $c = 1.03$ for the chosen sample point $(h = 0.7, U = 1.2)$ in Fig. 6.6a. The

red solid line in this figure shows the fitted curve. From our numerical data analysis we can conclude that the CC formula with the central charge $c = 1$ can capture the main behaviour of the EE in the IC phase.

Another characteristic feature of the IC phase is the presence of the oscillations. As it is evident there are oscillations in both EE and the occupation number. Note that the oscillations in the EE are not captured by the CC formula.

We studied the transition between the topological phase and the IC phase by calculating the ground state energy, $E_G = \min(E_0^{+1}, E_0^{-1})$, and its first, $\frac{\partial E_G}{\partial U}$, and second order, $-\frac{\partial^2 E_G}{\partial U^2}$ derivatives with respect to U for a cut along the $U-$axis. All of them were smooth and continuous. Hence these are compatible with the conjecture that the transition from the topological phase to the IC phase is of the Berezinskii-Kosterlitz-Thouless type [87, 89].

In Fig. 6.7 we present the the ground state energy, E_G, and its first, $\frac{\partial E_G}{\partial U}$, and second order, $-\frac{\partial^2 E_G}{\partial U^2}$, derivatives with respect to U for a cut along the $U-$axis at $h = 0.7$. The level crossings in Fig. 6.4 reveal themselves through the discontinuities (jumps) in the first order derivative and hence peaks in the second order derivative of the ground state energy. Although these peaks are also present in different system sizes, they occur at different points along the U-axis (though in the same interval). The precise positions of level crossings does vary depending on the couplings and the system size. These observations justify our (and the previous) conclusion that this is an IC phase.

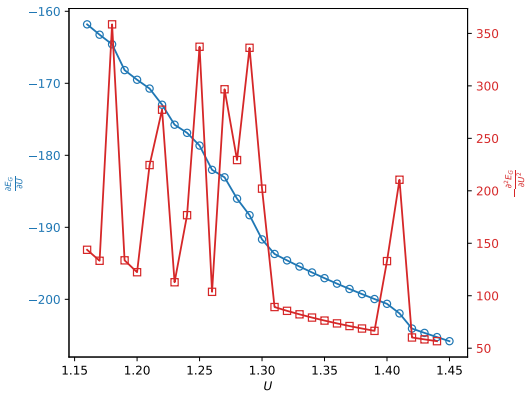

Figure 6.7: The derivatives of the ground state energy, $\frac{\partial E_G}{\partial U}$ (the blue circles) and $-\frac{\partial^2 E_G}{\partial U^2}$ (the red squares) are plotted as a function of U for $h = 0.7$. Taken from paper III.

There was an open question regarding the presence of the IC phase in the limit $h \to 0$. Having the essential features of the IC phase in our hand, we

looked at small magnetic fields. Specifically we performed DMRG for $h = 0.05$ and $h = 0.1$ and looked at the energy levels, oscillations in the EE and the derivatives of the ground state energy. They all show the signatures of the IC phase like $c = 1$ in a very small interval of U and a peak in the second order derivative of the ground state energy. As a result we concluded that the IC phase continues down to the XY critical point on the U-axis ($h = 0$, $U = +1$). This scenario is both intuitive and consistent with the fact that the XY critical point has central charge $c = 1$ [7] and the IC phase is also a gapless phase where the essential features of the EE can be captured by the CC formula with central charge $c = 1$.

The esCDW phase and the CDW phase

Before entering the charge-density wave (CDW) phase which is the phase for large interaction U, for the systems with an even number of sites the model has another phase, the exited state CDW (esCDW). Since this part of the phase diagram only appears for the even number of sites, one can argue that this part should not be considered as a phase. Moreover in this regime of parameters the energy per unit site (or per bond) for an odd number sites is slightly lower than the one for even number of sites. A system with odd number of sites has CDW ground state in this regime of parameters. As a result this is another reason to object calling this region a "phase". Nevertheless the very fact that the bulk properties of the model are sensitive to the number of sites motivates us to study this regime more thoroughly. In addition it is relevant for finite system sizes and hence one needs to be aware of it for finite-size numerical simulation.

In Fig. 6.4 we see that for large U the ground state is doubly degenerate and belongs to the even sector. These states are separated by a finite energy gap from the ground state in the odd sector. These states have no entanglement and $S(l)$ as a function of subsystem size saturates fast to a very low value. The occupation number in these two states, as it is presented in Fig. 6.8, also shows a density wave pattern as expected. In the bosonic incarnation of the model, Eq. 6.1, this phase is usually called the Néel phase.

By starting from large U and decreasing it, we see that the ground state's parity changes. For $1.28 \lesssim U \lesssim 1.41$ the two lowest states belong to the odd sector and are separated by a finite gap from the ground state in the even sector. In this regime there is no crossing between the energy levels and the parity of the ground state is determined by the system size. For $L = 4n$ with an integer n the ground state has an odd parity, as it is the case in Fig. 6.4, and for $L = 4n + 2$ it has an even parity. This is the esCDW phase.

In Figs. 6.9a and 6.9b we show the EE and the occupation number for a point in the esCDW phase. One would see the same patterns in the low lying excited states in the CDW phase. Hence we label this region with esCDW. From the EE in Fig. 6.9a we see that the EE grows as a function of subsystem

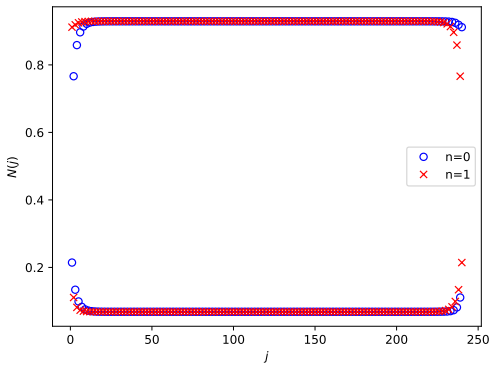

Figure 6.8: For a point in the CDW phase, $h = 0.7$ and $U = 1.5$, the occupation number of the two states $n = 0$ and $n = 1$, belonging to the even sector, are plotted for a system of size $L = 240$. At this point and with this system size, these two states are degenerate and have lower energy than the ground state in the odd sector (see Fig. 6.4). Taken from paper III.

size and the growth can not be captured by the CC formula. This is one of the characteristic features of the esCDW phase. Moreover the occupation number in this phase, as it is evident from Fig. 6.9b, is characterized with two oscillations. One has a long wavelength, roughly twice the system size, and one has a lattice constant wave length, i.e. a phase shift between neighbouring sites.

The esCDW phase is a gapless phase with an unusual dynamical critical exponent. In Figs. 6.10a and 6.10b we present the scaling of the energy differences in the odd sector, to which the ground state belongs, as well as the gap between the two sectors. The energy difference between the ground state and the first excited state in the odd sector, namely $E_1^{-1} - E_0^{-1}$, goes to zero as $L^{-1.8}$. The same scaling was observed for the second excited state as well, i.e. $E_2^{-1} - E_0^{-1} \sim L^{-1.8}$. These observations suggest that this is a gapless phase with the dynamical critical exponent $z = 1.8$. Since for a conformal field theory (CFT) the dynamical critical exponent should be $z = 1$, we conclude that this phase, although gapless, can not be described by a CFT. This is in agreement with our previous observation that the EE profile can not be captured by the CC formula. The ground state of the even sector, however, is separated by a finite gap from the ground state in the odd sector. For a point in the esCDW this is shown in Fig. 6.10b.

Finally we note that in the paper III we show that the width of the esCDW phase is sensitive to the boundary magnetic fields and one can control its width

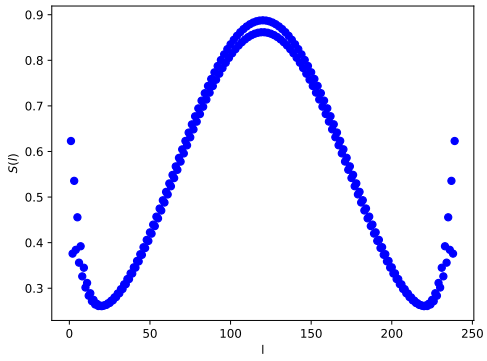

(a)

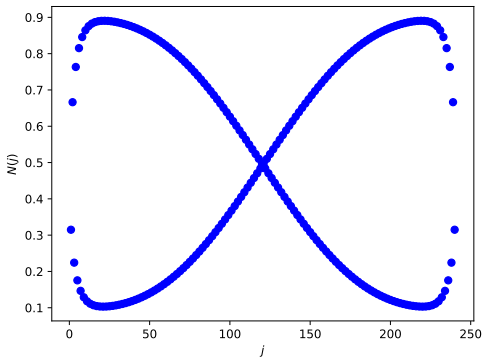

(b)

Figure 6.9: For a point in the esCDW phase, $h = 0.7$ and $U = 1.325$, EE as a function of subsystem size and the occupation number are plotted in (a) and (b) respectively. The system size is $L = 240$. Taken from paper III.

with the magnetic field on the very first and the very last spins. The model for odd system sizes, however, directly enters the CDW phase from the IC phase. For odd system sizes the ground state is unique in the CDW phase and there is a finite gap to the first excited state. In the limit of large U, however, this gap closes as one expects.

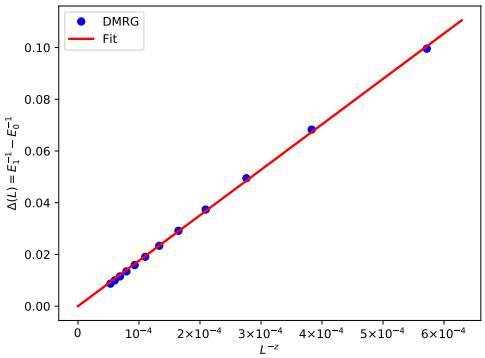

(a)

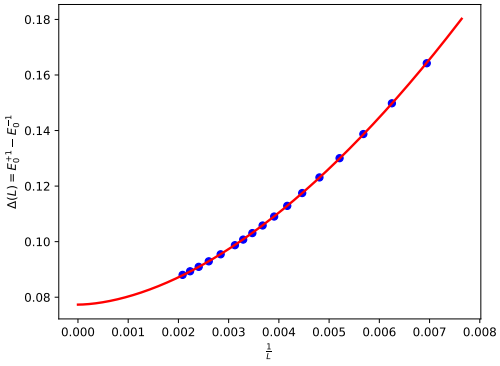

(b)

Figure 6.10: (a) Scaling of the gap in the odd sector, $E_1^{-1} - E_0^{-1}$, for systems of the size $L = 4n$ in the range of $L = 64 - 240$ as a function of L^{-z} with $z \simeq 1.8$. (b) Scaling of the gap between the two sectors, $E_0^{+1} - E_0^{-1}$, for systems of the size $L = 4n$ in the range of $L = 144 - 480$. In the thermodynamic limit the gap is $\Delta = 0.077$. These are for the point $h = 0.7$, $U = 1.325$. Taken from paper III.

On the degeneracy of the full many-body spectrum

The model in Eq. 6.1 is exactly solvable for $U = 0$ (TFIM) [36] and $h = 0$ (the XY model) [39]. Based on the solution for the TFIM we reviewed that the model hosts *strong* MZMs on the h-axis for $|h| < 1$ in chapter 2 and Sec 3.3. The situation is the same along the U-axis except on the two points

with $U = \pm 1$, namely the critical points [39, 41]. The presence of a strong zero mode guarantees that the model has a doubly degenerate spectrum upto an exponentially small correction in the system size. As a result asserting the presence of such a mode/operators, is a statement about the full many-body spectrum rather than only the ground state degeneracy which is typically the case of interest in studying the topological phases.

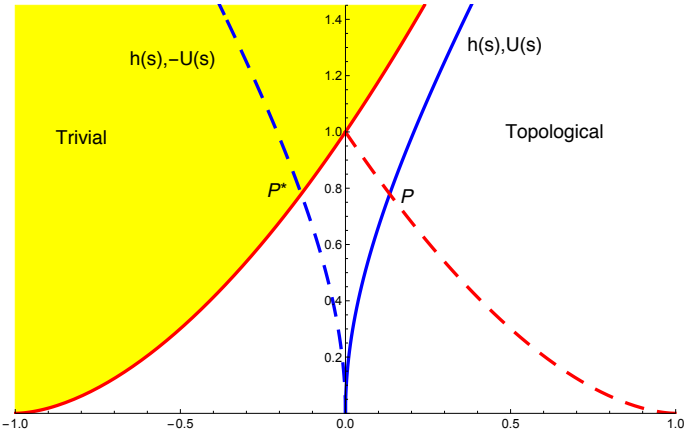

Figure 6.11: Selected part of the phase diagram. The solid blue line, an arbitrary line parametrized by s, lies in the topological phase. The dashed blue line is the mirrored blue line with respect to the $h-$axis. The dashed red line is the mirrored of a part of the solid red line with respect to the h-axis. Taken from paper III.

In this section we will ask whether such an operator is present in the topological phase of the KH model. Here we present an argument which rules out the possibility of the existence a strong zero mode for a large part of the topological phase. In the paper by studying the edge magnetization we further shrink the region where a strong zero can exist.

Consider the solid blue line, an arbitrary line parametrized by s, in Fig. 6.11. Since this line lies in the topological phase, it has a doubly degenerate ground state. Although we expect that the low lying states are also doubly degenerate, it is a nontrivial step to generalize this to the full many-body spectrum. We can, however, investigate the highest excited state. Note that the highest excited state of a Hmiltonian H, is the ground state of the Hamiltonian $-H$. Therefore we study the ground state of $-H$,

$$-H(h,U) = \sum_{j=1}^{L-1} \sigma_j^x \sigma_{j+1}^x + h \sum_{j=1}^{L} \sigma_j^z - U \sum_{j=1}^{L-1} \sigma_j^z \sigma_{j+1}^z \ . \tag{6.12}$$

We know that the sign of the first two terms does not affect the properties, and hence we absorb them by performing on-site rotations,

$$\sigma_j^x \to (-1)^j \sigma_j^x \ , \qquad \sigma_j^z \to -\sigma_j^z \ . \tag{6.13}$$

This transform the Hamiltonian as follows,

$$\begin{aligned} -H(h,U) &= -\sum_{j=1}^{L-1} \sigma_j^x \sigma_{j+1}^x - h \sum_{j=1}^{L} \sigma_j^z - U \sum_{j=1}^{L-1} \sigma_j^z \sigma_{j+1}^z \\ &= H(h,-U) \ . \end{aligned} \tag{6.14}$$

As a result the highest excited state of $H(h,U)$ along the solid blue line in Fig. 6.11 is the same as the ground state of the Hamitonian along the dashed blue line. By starting at the origin, $h = 0$ and $U = 0$, and going along the two lines, both Hamiltonians have a doubly degenerate ground state, since they both lie in the topological phase. By reaching the point P^* the dashed blue line enters the trivial phase. Hence from the point P onwards the highest excited state of the original Hamiltonian along the solid blue line is not doubly degenerate. We expect that the other states close to the highest one would not be degenerate as well. The very fact that the highest excited state is *not* doubly degenerate beyond the point P is sufficient to exclude the presence of the strong zero mode beyond the dashed red line. As a result the region which may support the strong zero mode is confined to the region between the U-axis, the solid red line and the dashed red line in Fig. 6.11. As we mentioned earlier by studying the time dependency of the edge magnetization for the finite system sizes, we can further shrink this region to a small region close to the origin. We refer to paper III for more detail on this.

Chapter 7

A tight-binding model of $\mathbb{Z}_3$ Fock parafermions

In chapter 2 we discussed Majorana fermions and their presence in the topological phase of the Kitaev chain. An important issue is that one *can not* talk about the occupancy of a single Majorana fermion. Filling and occupancy are only well-defined for Dirac fermions and one needs to fuse two Majorana fermions, form a Dirac fermion and then discuss the occupancy of such a state. This was the case in the topological phase of the Kitaev chain. Using the MZM on the left edge, say γ_L, and the MZM on the right edge, γ_R, we can construct $f_0 = (\gamma_L + i\gamma_R)/2$ and $f_0^\dagger = (\gamma_L - i\gamma_R)/2$ which are the annihilation and creation operators for the fermionic zero mode respectively. Having these operators, one would be able to calculate the number operator $n_0 = f_0^\dagger f_0$ with the eigenvalues 0 and 1.

In chapter 3 we talked about the parafermions and just like the Majoranas there is no notion of occupancy for them. One may, however, wonder about the possibility of making a *Fock* state out of $\mathbb{Z}_p$ parafermions in analogy with Dirac fermions. For such a state, as the name Fock suggests, the occupancy number would be a well-defined quantity.

This feat has been achieved by Cobanera and Ortiz [90]. Employing two $\mathbb{Z}_p$ parafermions with $p \geq 2$ they constructed a Fock state which can be filled with with at most $p-1$ particles. In the special case of $p = 2$, the constructed Fock state becomes a Dirac fermion. In general they show that by having $2L$ parafermions one can pair them and construct a many-body Hilbert space for L Fock parafermions (FPF) with the dimension p^L in one dimension. Considering a vacuum state $|0\rangle$ with no FPF, we can construct an arbitrary state in the Hilbert state using the creation FPF operators.

A natural step after having a well-defined and self-consistent local and many-body Hilbert space is studying model Hamiltonians. Along such a path the first model of interest would be a hopping model. The hopping model for fermions in one dimension (and in the higher dimensions), corresponding to $p = 2$, can be easily solved using the Fourier transformation. The crucial step in the solution is that the anti-commutation algebra of fermion operators in real space will be inherited by the fermionc operators in momentum space. This is not the case for FPFs with $p \geq 3$ and there is no well-defined and easy algebra in momentum space for FPFs. Therefore, as it will be shown in this chapter, even studying a hopping model for $p = 3$ is quite involved and required

numerics and other methods like bosonization.

In this chapter we will study a hopping model of $\mathbb{Z}_3$ FPFs with pairwise hopping. The hopping term for spinless fermions is fixed due to the Pauli principle. Since each fermionic state, say a given site on lattice, can host at most one spinless fermion, the only possible kinetic term consists of single-particle hopping. For $p \geq 3$, however, there are more possibilities since there can be $p-1$ particles per site. In the case of $p = 3$ one can imagine that a given site is occupied by two FPFs and these two can hop together to a neighbouring site. We call such a hopping a pairwise hopping.

In what follows a brief review of the FPF algebra will be followed by our model and its phase diagram. After that we summarize important features of each phase and in some cases we show how the bosonization can capture the physics of this inherently interacting model. More details can be found in paper IV.

Fock parafermions

Consider a set of $2L$ $\mathbb{Z}_p$ parafermions $\{\gamma_j\}$ with the algebra,

$$\gamma_j\gamma_k = \omega^{\mathrm{sgn}(k-j)}\gamma_k\gamma_j, \qquad \omega = \exp(2\pi i/p) \ , \tag{7.1}$$

$$\gamma_j^{p-1} = \gamma_j^\dagger \ , \qquad \gamma_j^p = \mathbf{1} \ , \tag{7.2}$$

in which $\mathbf{1}$ is the identity operator. We use the pair $\{\gamma_{2j-1}, \gamma_{2j}\}$ and define the annihilation FPF operator [90],

$$F_j = \frac{p-1}{p}\gamma_{2j-1} - \frac{1}{p}\sum_{m=1}^{p-1} \omega^{m(m+p)/2}\gamma_{2j-1}^{m+1}\gamma_{2j}^{\dagger m} \ . \tag{7.3}$$

For the FPF operators living on different sites we have,

$$F_jF_k = \omega^{\mathrm{sgn}(k-j)}F_kF_j \ , \qquad F_j^\dagger F_k = \omega^{-\mathrm{sgn}(k-j)}F_kF_j^\dagger \ . \tag{7.4}$$

The on-site algebra of FPFs is,

$$F_j^{\dagger p} = 0 \ , \tag{7.5}$$

$$F_j^{\dagger m}F_j^m + F_j^{p-m}F_j^{\dagger(p-m)} = \mathbf{1} \ , \qquad m \in \{1, \cdots, p-1\} \ . \tag{7.6}$$

The first equation is the generalization of Pauli principle and tells us that there can be at most $p-1$ particles per site while the second equation is the generalization of the on-site fermionic anticommutation relation.

We are looking for a number operator with the usual algebra with the creation and annihilation algebra. This can also be defined,

$$N_j = \sum_{m=1}^{p-1} F_j^{\dagger m} F_j^m \ , \tag{7.7}$$

$$\left[N_j, F_j^\dagger\right] = F_j^\dagger, \qquad [N_j, F_j] = -F_j \ . \tag{7.8}$$

The number operator has p different eigenvalues, $0, 1, \cdots$ and $p-1$.

The model and its phase diagram

In this section we present the model and its phase diagram. The model is,

$$H(g) = -t \sum_{j=1}^{L-1} \left[(1-g) F_j^\dagger F_{j+1} + g F_j^{\dagger 2} F_{j+1}^2 + \text{h.c.}\right] \ , \tag{7.9}$$

in which F_j is the FPF annihilation operator on site j, the unit of energy t will be set to one and g is a dimensionless coupling. The model is defined for an open chain of size L. The first term in above equation is the single-particle hopping of FPFs and the second term represents the pairwise hopping. The coupling g controls the relative hopping strength and will be assumed to be $0 \leq g \leq 1$. Using Eq. 7.8 one can show that the total number of particles $N = \sum_{j=1}^{L} N_j$ is a conserved quantity, i.e. $[H, N] = 0$. Moreover a useful quantity in the thermodynamic limit is the filling $n = N/L$. Hence we can study the model and present its phase diagram as a function of filling n and the coupling g. As we proved in the paper due to the "particle-hole" symmetry it is sufficient to restrict our study to the fillings $0 < n \leq 1$.

The Hamiltonian at $g = 0$, where the model has only the single-particle hopping, was studied by Rossini et al [91]. It was found the model for $n < 1$ is a gapless Luttinger liquid [92] with central charge $c = 1$. At unit filling $n = 1$, which can also be called "half-filling", the model is gapped with high entanglement entropy (EE).

The phase diagram of the model in Eq. 7.9 is presented in Fig. 7.1. The model has four phases. The L phase and the R phase are the gapless phases with central charge $c = 1$. The M phase is also a gapless phase, but with central charge $c = 2$. The G phase, however, is a gapped phase. Properties of these phases are summarized in Table 7.1. In addition to the gap [§] and the central charge one can find the functional form of the following two-point correlation

[§] Note that by *gap* we do not necessary mean the finite bulk gap in the thermodynamic limit. It could very well be the energy difference between the first excited state and the ground state.

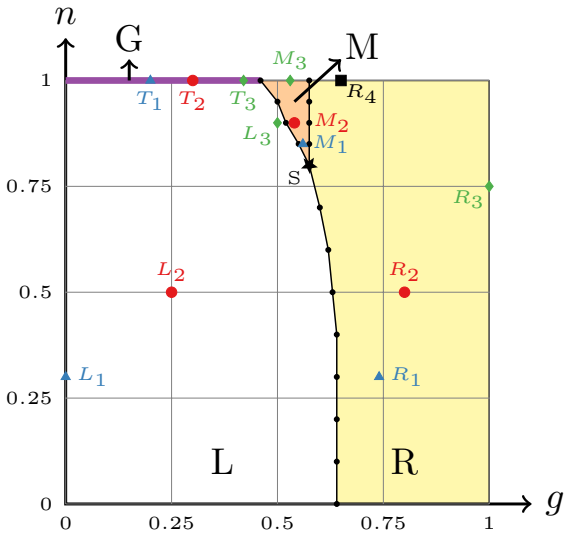

Figure 7.1: The phase diagram for the model in Eq. 7.9. The four phases are labeled by L, M, R and G. The gapped phase is only present at unit filling. Detailed properties of each phases are discussed in the main text by presenting the data for the points $L_{1,2,3}$ etc. Taken from paper IV.

functions,

$$G_1(r) = \left| \left\langle F^\dagger_{\frac{L}{2}-\frac{r}{2}} F_{\frac{L}{2}+\frac{r}{2}} \right\rangle \right|, \tag{7.10}$$

$$G_2(r) = \left| \left\langle F^{\dagger 2}_{\frac{L}{2}-\frac{r}{2}} F^2_{\frac{L}{2}+\frac{r}{2}} \right\rangle \right| . \tag{7.11}$$

Intuitively these two correlation functions probe the single-particle and the pairwise hopping terms. In the DMRG calculation, as it is evident in above equations, we measure the two-point correlation functions for two symmetric points around the middle of the chain separated by distance r. This is a strategy to measure these correlation functions in the "bulk" and minimize the finite size effects due to the edges.

In what follows we will describe the properties of the model in the L and the R phases in detail. We will present the numerical results from DMRG simulations and our analytical calculation using the bosonization technique. To perform DMRG and make the connections with the Luttinger liquid it would be handy to perform the Fradkin-Kadanoff transformation and write the model

Phase	**Gap**	c	$G_1(r)$	$G_2(r)$
L	gapless	1	$r^{-2/3}$	$r^{-\alpha_2(n,g)}$
R	gapless	1	0	$r^{-13/18}$
M	gapless	2	$r^{-\alpha_1'(n,g)}$	$r^{-\alpha_2'(n,g)}$
G	gapped	—	$\exp\left[-r/\xi_1(g)\right]$	$\exp\left[-r/\xi_2(g)\right]$

Table 7.1: Properties of the phases in Fig. 7.1. Taken from paper IV.

in a bosonic incarnation [43, 90, 91],

$$F_j = \left(\prod_{k=1}^{j-1} U_k\right) B_j \ , \tag{7.12}$$

where

$$U_k = \mathbf{1} \otimes \cdots \otimes \underbrace{U}_{k} \otimes \cdots \otimes \mathbf{1} \ , \qquad U = \begin{pmatrix} 1 & 0 & 0 \\ 0 & \omega & 0 \\ 0 & 0 & \omega^2 \end{pmatrix} \ , \tag{7.13}$$

$$B_j = \mathbf{1} \otimes \cdots \otimes \underbrace{B}_{j} \otimes \cdots \otimes \mathbf{1} \ , \qquad B = \begin{pmatrix} 0 & 1 & 0 \\ 0 & 0 & 1 \\ 0 & 0 & 0 \end{pmatrix} \ . \tag{7.14}$$

Note that the Hilbert space on the right hand side of the transformation belongs to the Z_3 clock variables and the B_j operator can be written in terms of Σ^0 as we defined in chapter 3,

$$\begin{aligned} B_j &= X_j - \Sigma_j^0 \\ &= \frac{X_j}{3}(\mathbf{2} - Z_j - Z_j^\dagger) \ , \end{aligned}$$

where $\mathbf{2}$ is twice the identity operator. One can check that the on-site algebra is,

$$B_j U_j = \omega U_j B_j \ , \tag{7.15}$$

and the Hamiltonian in Eq. 7.9 in the bosonic incarnation reads,

$$H(g) = -t \sum_{j=1}^{L-1} \left[(1-g) B_j^\dagger U_j B_{j+1} + g B_j^{\dagger 2} B_{j+1}^2 + \text{h.c.}\right] \ . \tag{7.16}$$

The results

We start with the L phase. In Figs. 7.2a and 7.2b we present the EE and the two-point correlation function $G_1(r)$ for the three points $L_{1,2,3}$ in the L phase. This phase is also present at $g = 0$ and is, in fact, the extension of the phase which was found in Ref. [91] for $n < 1$ to finite g.

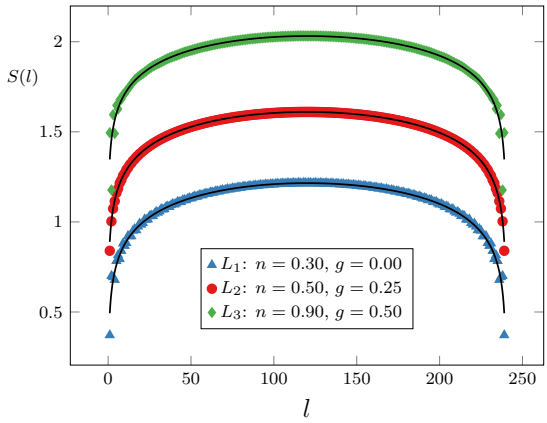

(a)

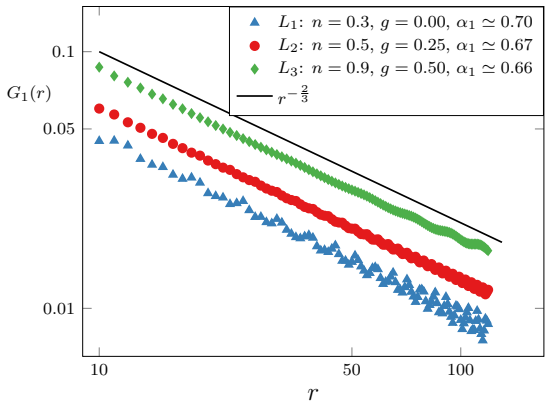

(b)

Figure 7.2: (a) Entanglement entropy, $S(l)$, as a function of subsystem size l and (b) the two-point correlation function $G_1(r)$ for the three selected points in the L phase. The point are marked in Fig. 7.1. Taken from paper IV.

In Fig. 7.2a we have the data for the subsystem's EE, $S(l)$, as a function of its size l from the DMRG simulation. We also plot the fitted CC formula, Eq. 6.11, to the data with solid black lines. Employing the CC formula gives

the central charge $c = 1$ all through the L phase. We have also checked the energy difference between the ground state and the first excited state in this phase for various system sizes L and verified that it goes to zero as $1/L$. Hence the L phase has the dynamical critical exponent $z = 1$ as it is predicted by CFT. Our results are consistent with those in Ref. [91] for $g = 0$.

In Fig. 7.2b we present the two-point correlation function $G_1(r)$. There is a clear power law decay, $G_1(r) \sim r^{-\alpha_1}$, as it should be for a two-point correlation function in a CFT. An intriguing feature is that the exponent $\alpha_1 = 2/3$ does neither depend on the filling n nor on the coupling g. The same exponent was also observed in Ref. [91]. This exponent can be derived using the bosonization technique. Recall that the free massless bosonic CFT has the central charge $c = 1$ [7] which is the same as what we have in the L phase.

An essential observation to use bosonization is that deep in the L phase for a typical point the probability of having two particles per site, $P(2)$, is quite small, say $P(2) \approx 0.05$. Therefore we project the model on to the local Hilbert space spanned by $|0\rangle$ and $|1\rangle$ states,

$$B_j \to \sigma_j^+ = \begin{pmatrix} 0 & 1 \\ 0 & 0 \end{pmatrix} , \tag{7.17}$$

and

$$U_k^{(p)} = \mathbf{1} \otimes \cdots \otimes \underbrace{U^{(p)}}_{k} \otimes \cdots \otimes \mathbf{1} , \qquad U^{(p)} = \begin{pmatrix} 1 & 0 \\ 0 & \omega \end{pmatrix} . \tag{7.18}$$

Using these we can simplify the two-point correlation function $G_1(r)$,

$$G_1(r) \sim \left| \left\langle \sigma_0^- U_0^{(p)} U_1^{(p)} \cdots U_{r-1}^{(p)} \sigma_r^+ \right\rangle \right| . \tag{7.19}$$

In this case for the JW transformation we use the following convention (different from Eq. 2.5) to relate the model to the fermions,

$$\sigma_j^z = 2n_j - 1 , \qquad \sigma_j^+ = e^{i\pi \sum_{k<j} n_k} \psi_j^\dagger , \tag{7.20}$$

with spinless fermions $\{\psi_j\}$. Hence the two-point correlation function $G_1(r)$ can be written in terms of fermions,

$$G_1(r) \sim \left| \left\langle \psi_0 e^{\sum_{k=0}^{r-1} i \frac{\pi}{3} n_k} \psi_r^\dagger \right\rangle \right| . \tag{7.21}$$

To use the bosonization dictionary we use Eq. 4.54 to go to the continuum limit. Moreover we consider the Luttinger liquid parameter K as a free parameter and use Eq. 4.78 to incorporate it and relate the fermions to the bosons. In summary we use,

$$\psi_j = \sqrt{\frac{a}{2\pi\alpha}} \left[e^{iK_F r} e^{i\sqrt{\pi}\left(\sqrt{K}\phi(r) - \frac{\theta(r)}{\sqrt{K}}\right)} + e^{-iK_F r} e^{-i\sqrt{\pi}\left(\sqrt{K}\phi(r) + \frac{\theta(r)}{\sqrt{K}}\right)} \right] . \tag{7.22}$$

By plugging the above form in Eq. 7.21 and using Wick's theorem, we can show that for $K > 0$ the dominant term in the two point correlation function is,

$$G_1(r) \sim r^{-\frac{1}{2K} - \frac{2}{9}K} \ . \tag{7.23}$$

It was previously predicted that the Luttinger parameter for $\mathbb{Z}_p$ anyonic gas is $K = p/2$ [92]. Therefore in the case of our interest the Luttinger parameter is $K = 3/2$. This prediction was checked for the case of $g = 0$ in Ref. [91]. Plugging the Luttinger parameter $K = 3/2$ in Eq. 7.23 we get,

$$G_1(r) \sim r^{-2/3} \ , \tag{7.24}$$

which is really close to what we get from the numerics (see Fig. 7.2b). We emphasize that although the previous phenomenological approaches predict the same power law decay for the two-point correlation function $G_1(r)$ as we have in Eq. 7.23, *we derived it from the microscopic model.*

Although the correlation function $G_2(r)$ does also decay as a power law, $G_2(r) \sim r^{-\alpha_2}$, it does not have a universal exponent all through the L phase (details can be found in the paper IV). As it is mentioned in Table. 7.1 its exponent varies with the filling n and the coupling g. The phenomenological model, however, predicts $\alpha_2 = 4\alpha_1 = 8/3$ which is not consistent with the numerical data [91, 92].

In Figs. 7.3a and 7.3b we present the EE and the two-point correlation function $G_2(r)$ for the three points $R_{1,2,3}$ (marked in the Fig. 7.1). As we see, this phase is also a gapless phase with central charge $c = 1$. The CC formula with central charge $c = 1$ captures the growth of subsystem's EE very well. We have also checked that the energy of the first excited state in this phase vanishes as $1/L$ by increasing the system size L.

We numerically found that the two-point correlation function $G_1(r)$ decays exponentially fast with a correlation length of the order of one site deep in the R phase. Therefore one can effectively assume that $G_1(r) = 0$ in the R phase. In the numerics we have also seen that the probability of having one particle per site in the R phase is quite negligible in comparison with the probability of having an empty site or a site with two particles. Therefore the low-lying states are spanned by the local Hilbert space spanned by $|0\rangle$ and $|2\rangle$. Projecting the model to this local Hilbert space gives the XX-Hamiltonian. It is known that the XX model has central charge $c = 1$ [7]. This is in agreement with the obtained value from the numerical data.

To obtain the two-point correlation function $G_2(r)$ using bosonization we used the replacement,

$$B_j^2 \to \sigma_j^+ \ . \tag{7.25}$$

We showed that this yields the same expression as we had in Eq. 7.23 but now for $G_2(r)$. Using the fact that the model reduces to the XX model after the projection one expects no interaction among fermions. This justifies using

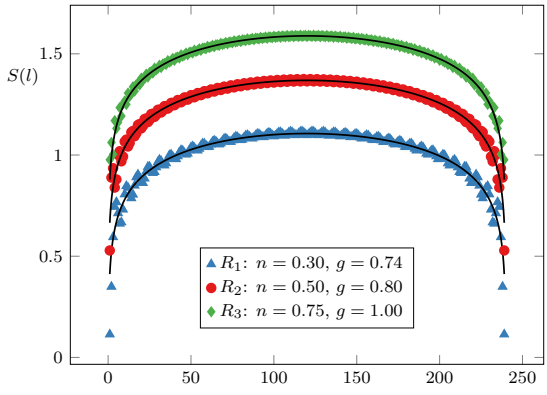

(a)

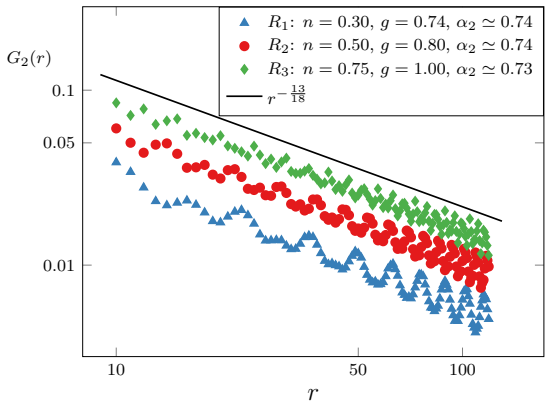

(b)

Figure 7.3: (a) Entanglement entropy, $S(l)$, as a function of subsystem size l and (b) the two-point correlation function $G_2(r)$ for the three selected points in the R phase. The point are marked in Fig. 7.1. Taken from paper IV.

the Luttinger parameter $K = 1$ in the R phase. As a result the bosonization predicts,

$$G_2(r) \sim r^{-13/18} \ . \tag{7.26}$$

As we see in Fig. 7.3b, the theoretical prediction matches very well with the numerical data obtained from DMRG.

In paper IV we also present the our numerical results for the M and the G phases. We show that the M phase is also gapless since the CC formula with central charge $c = 2$ is in a very good agreement with the numerical data for the

EE [§]. Hence intuitively one can imagine that the M phase has two copies of the CFT with central charge $c = 1$ and by going to the L phase the pair excitations gap out, whilst at the transition to the R phase the single particle excitations gap out. Both two-point correlation functions $G_1(r)$ and $G_2(r)$ show a power law decay, consistent with a CFT description.

The G phase for finite coupling g is the continuation of what has been found at $g = 0$ in Ref. [91] and is a gapped phase. We calculated the energy of the first excited state and showed that it converges to a finite value in the thermodynamic limit. Both two-point correlation functions $G_1(r)$ and $G_2(r)$ decay exponentially with a finite correlation length. The EE as a function of subsystem size saturates to a high value quite fast, which is a signature of a finite correlation length in this phase. These observations are all consistent with interpreting the G phase as a *gapped topological phase*.

[§]This could also be $c = 1 + 1$ as well, which means that it consists of two CFT with different velocities.

Chapter 8

Summary and Outlook

We studied $\mathbb{Z}_p$ symmetric "spin" chains. We showed how one can analytically solve the non-interacting $\mathbb{Z}_2$ symmetric models on an open chain, where the Fourier transformation can not be applied and momentum is not a good quantum number, using the Lieb-Schultz-Mattis method. The LSM method is also quite useful to derive the Majorana zero mode wavefunctions. We have also examined the effect of density-density interaction on the Kitaev chain by studying the Kitaev-Hubbard chain. As we saw the model has a rich phase diagram which consists of a trivial phase, a topological phase, an incommensurate phase, a charge-density wave phase and an excited state CDW "phase". Exploring the esCDW phase that we discovered and applying bosonization to understand different phases and phase transitions of the KH chain close to the XY critical point where the four phases meet, are the natural future directions of research.

In the case of $\mathbb{Z}_3$ symmetric chains we found a one parameter family of frustration free models for which the model is gapped and the ground state has an exact threefold degeneracy. After that we studied a hopping model of $\mathbb{Z}_3$ Fock parafermions, the generalization of Dirac fermions which could host at most two particles per site. We investigated the phase diagram of the model in detail and showed how bosonization can be applied to the gapless phases.

There are also interesting problems on Fock parafermions to continue with. To name a few I can mention exploring the nature of the gapped phase in Fig. 7.1 that has a high entanglement entropy, about which we do not have a good understanding. This is a rather peculiar case since for any other p the hopping model at of Fock parafermions is gapless at "half-filling", i.e. $n = (p-1)/2$. For fermions, $p = 2$, this can be easily seen from the *cosine* band which is the solution to the fermion hopping problem. For $p > 3$ there is no analytical solution, but the numerics show that the model is gapless at half-filling. In addition one can also add pairing terms and break the U(1) symmetry down to a $\mathbb{Z}_3$ symmetry. Such terms correspond to superconductivity terms for the FPFs which can also relate the model to well-known models like the three-state quantum Potts model.

Bibliography

[1] P. Böckh, T. Wetzel, *Heat transfer: basics and practice*, Springer (2012).

[2] N.W. Ashcroft, N.D. Mermin, *Solid State Physics*, Saunders College publishing, Harcourt college publishers (1976).

[3] I. Bloch, *Ultracold quantum gases in optical lattices*, Nt. Phys. **1**, 23 (2005).

[4] I. Bloch, J. Dalibard, W. Zwerger, *Many-body physics with ultracold gases*, Rev. Mod. Phys. **80**, 885 (2008).

[5] I. Bloch, J. Dalibard, S. Nascimbène *Quantum simulations with ultracold quantum gases* Nat. Phys. **8**,267 (2012).

[6] R. Shankar, *Quantum field theory and condensed matter - An introduction*, Cambridge University press, 2017.

[7] P. Francesco, P. Mathieu, D. Sénéchal, *Conformal field theory*, Springer (2012).

[8] N. Goldenfeld, *Lectures On Phase Transitions And The Renormalization Group*, Addison-Wesley (1992).

[9] S. Sachdev, *Quantum phase transitions*, Cambridge University Press (2011).

[10] M. Kardar, *Statistical physics of fields*, Cambridge University Press (2007).

[11] M. Henkel, *Conformal Invariance and Critical Phenomena*, Springer (1999).

[12] M. Maggiore, *A Modern Introduction to Quantum Field Theory*, Oxfor University Press (2005).

[13] R.J. Baxter, *Exactly solved models in statistical mechanics*, Academic Press (1982).

[14] N.D. Mermin,H. Wagner, *Absence of Ferromagnetism or Antiferromagnetism in One- or Two-Dimensional Isotropic Heisenberg Models*, Phys. Rev. Lett. **17**, 1133(1966).

[15] H.E. Stanley,T.A. Kaplan, *Possibility of a Phase Transition for the Two-Dimensional Heisenberg Model*, Phys. Rev. Lett. **17**, 913 (1966).

[16] V.L. Berezinskii, *Destruction of long-range order in one-dimensional and two-dimensional systems having a continuous symmetry group I. Classical systems*, Sov. Phys. JETP, **32** 493 (1971).

[17] J.M. Kosterlitz, D.J. Thouless, *Ordering, metastability and phase transitions in two-dimensional systems*, [J. Phys. C **6**, 1181 (1973).

[18] K. von Klitzing, G. Dorda, M. Pepper, *New Method for High-Accuracy Determination of the Fine-Structure Constant Based on Quantized Hall Resistance*, Phys. Rev. Lett. textbf45, 494 (1980).

[19] D.C. Tsui, H.L. Stormer, A.C. Gossard, *Two-Dimensional Magnetotransport in the Extreme Quantum Limit*, Phys. Rev. Lett. **48**, 1559 (1982).

[20] C.L. Kane, E.J. Mele, *Quantum Spin Hall Effect in Graphene*, Phys. Rev. Lett. **95**, 226801 (2005).

[21] C.L. Kane, E.J. Mele, $\mathbb{Z}_2$ *Topological Order and the Quantum Spin Hall Effect*, Phys. Rev. Lett. **95**, 146802 (2005).

[22] L. Fu, C.L. Kane, E.J. Mele, *Topological Insulators in Three Dimensions*, Phys. Rev. Lett. **98**, 106803 (2007).

[23] B.A. Bernevig, T.L. Hughes,S.-C. Zhang, *Quantum Spin Hall Effect and Topological Phase Transition in HgTe Quantum Wells*, Science **314**, 1757 (2006).

[24] N. Read, D. Green, *Paired states of fermions in two dimensions with breaking of parity and time-reversal symmetries and the fractional quantum Hall effect*, Phys. Rev. B **61**, 10267 (2000).

[25] A.Y. Kitaev, *Unpaired Majorana fermions in quantum wires*, Phys. Usp. **44**, 131 (2001).

[26] A.Y. Kitaev, *Fault-tolerant quantum computation by anyons*, Ann. Phys. **303**, 2 (2003).

[27] C. Nayak, S.H. Simon, A. Stern, M. Freedman, S. Das Sarma *Non-Abelian anyons and topological quantum computation*, Rev. Mod. Phys. **80**, 1083 (2008).

[28] A. Altland, M.R. Zirnbauer, *Nonstandard symmetry classes in mesoscopic normal-superconducting hybrid structures*, Phys. Rev. B **55**, 1142 (1997).

[29] A.W.W. Ludwig, *Topological phases: classification of topological insulators and superconductors of non-interacting fermions, and beyond*, Phys. Scr. **T168** (2016) 014001.

[30] A.P. Schnyder, S. Ryu, A. Furusaki, A.W.W. Ludwig, *Classification of topological insulators and superconductors in three spatial dimensions*, Phys. Rev. B. **78**, 195125 (2008).

[31] S. Ryu, A.P. Schnyder, A. Furusaki, A.W.W. Ludwig, *Topological insulators and superconductors: tenfold way and dimensional hierarchy*, New J. Phys. **12**, 065010 (2010).

[32] C.-K. Chiu, J.C.Y. Teo, A.P. Schnyder,S. Ryu, *Classification of topological quantum matter with symmetries*, Rev. Mod. Phys. **88**, 035005 (2016).

[33] D.J. Thouless, M. Kohmoto, M.P. Nightingale, M. den Nijs, *Quantized Hall Conductance in a Two-Dimensional Periodic Potential*, Phys. Rev. Lett. **49**, 405 (1982)

[34] R.M.F. Houtappel, *Order-disorder in hexagonal lattices*, Physica **16**, 425 (1950).

[35] E. Fradkin, L. Susskind, *Order and disorder in gauge systems and magnets*, Phys. Rev. D **17**, 2637 (1978).

[36] P. Pfeuty, *The one-dimensional Ising model with a transverse field*, Ann. Phys. **57**, 79 (1970).

[37] P. Jordan, E. Wigner, *Über das Paulische Äquivalenzverbot*, Z. Physik **47**, 631 (1928).

[38] J. Alicea, *New directions in the pursuit of Majorana fermions in solid state systems*, Rep. Prog. Phys. **75**, 076501 (2012).

[39] E. Lieb, T. Schultz, D. Mattis, *Two soluble models of an antiferromagnetic chain*, Ann. Phys. **16**, 407 (1961).

[40] D. Sticlet, C. Bena, P. Simon, *Josephson effect in superconducting wires supporting multiple Majorana edge states*, Phys. Rev. B **87**, 104509 (2013).

[41] P. Fendley, *Parafermionic edge zero modes in Zn-invariant spin chains*, J. Stat. Mech.:Theory Exp. P11020 (2012).

[42] Y. Zhuang, H.J. Changlani, N.M. Tubman,T.L. Hughes, *Phase diagram of the Z3 parafermionic chain with chiral interactions*, Phys. Rev. B. **92**, 035154(2015).

[43] E. Fradkin, L.P. Kadanoff, *Disorder variables and para-fermions in two-dimensional statistical mechanics*, Nucl. Phys. B **170** 1 (1980).

[44] A.S. Jermyn, R.S.K. Mong, J. Alicea, P. Fendley, *Stability of zero modes in parafermion chains* Phys. Rev. B **90**, 165106 (2014).

[45] N. Moran, D. Pellegrino, J.K. Slingerland, G. Kells, *Parafermionic clock models and quantum resonance*, Phys. Rev. B **95**, 235127 (2017).

[46] J. Kemp, N.Y. Yao, C.R. Laumann, P. Fendley, *Long coherence times for edge spins*, J. Stat. Mech. 063105 (2017).

[47] I. Peschel, V.J. Emery, *Calculation of spin correlations in two-dimensional Ising systems from one-dimensional kinetic models*, Z. Phys. B **43**, 241 (1981).

[48] H. Katsura, D. Schuricht, M. Takahashi, *Exact ground states and topological order in interacting Kitaev/Majorana chains*, Phys. Rev. B **92**, 115137 (2015).

[49] P. Fendley, *Strong zero modes and eigenstate phase transitions in the XYZ/interacting Majorana chain*, J. Phys. A: Math. Theor. **49**, 30LT01 (2016).

[50] F. Iemini, C. Mora, L. Mazza, *Topological Phases of Parafermions: A Model with Exactly Solvable Ground States*, Phys. Rev. Lett. **118**, 170402 (2017).

[51] T. Giamarchi, *Quantum physics in one dimension*, Clarendon Press, 2003.

[52] J. von Delft, H. Schoeller, *Bosonization for beginners – refermionization for experts*, Annalen Phys. **7**, 225 (1998).

[53] D. Sénéchal, *An introduction to Bosonization*, arXiv:cond-mat/9908262.

[54] D. Allen, P. Azaria, P. Lecheminant, *A two-leg quantum Ising ladder: a bosonization study of the ANNNI model*, J. Phys. A **34**, L305 (2001).

[55] A. Dutta, D. sen, *Gapless line for the anisotropic Heisenberg spin-$\frac{1}{2}$ chain in a magnetic field and the quantum axial next-nearest-neighbor Ising chain* Phys. Rev. B **67**, 094435 (2003).

[56] J. Eisert, M. Cramer, M.B. Plenio, *Colloquium: Area laws for the entanglement entropy*, Rev. Mod. Phys. **82**, 277 (2010).

[57] M.B. Hastings, *An area law for one-dimensional quantum systems*, J. Stat. Mech.:Theory Exp. P08024 (2007).

[58] K. Huang, *Statistical Mechanics*, John Wiley & Sons (1987).

[59] M. Kardar, *Statistical Physics of Particles*, Cambridge University Press (2007).

[60] M.B. Plenio, J. Eisert, J. Dreißig, M. Cramer, *Entropy, Entanglement, and Area: Analytical Results for Harmonic Lattice Systems*, Phys. Rev. Lett. **94**, 060503 (2005).

[61] M. Srednicki, *Entropy and area*, Phys. Rev. Lett. **71**, 666 (1993).

[62] C.G. Callan, F. Wilczek, *On geometric entropy*, Phys. Lett B **333**, 55 (1994).

[63] S.R. White, *Density matrix formulation for quantum renormalization groups*, Phys. Rev. Lett. **69**, 2863 (1992).

[64] U. Schollwöck, *The density-matrix renormalization group*, Rev. Mod. Phys. **77**, 259 (2005).

[65] U. Schollwöck, *The density-matrix renormalization group in the age of matrix product states*, Ann. Phys. **326**, 96 (2011).

[66] S. Östlund, S. Rommer, *Thermodynamic Limit of Density Matrix Renormalization*, Phys. Rev. Lett. **75**, 3537 (1995).

[67] J. Dukelsky, M.A. Martin-Delgado, T. Nishino, G. Sierra, *Equivalence of the Variational Matrix Product Method and the Density Matrix Renormalization Group applied to Spin Chains*, Euro. Phys. Lett. **43**, 457 (1998).

[68] I. Affleck, T. Kennedy, E.H. Lieb, H. Tasaki, *Rigorous results on valence-bond ground states in antiferromagnets*, Phys. Rev. Lett. **59**, 799 (1987).

[69] I. Affleck, T. Kennedy, E.H. Lieb, H. Tasaki, *Valence bond ground states in isotropic quantum antiferromagnets*, Comm. Math. Phys. **115**, 477 (1988).

[70] F. Albuquerque, F. Alet, P. Corboz, P. Dayal, A. Feiguin, S. Fuchs, L. Gamper, E. Gull, S. Gürtler, A. Honecker, R. Igarashi, M. Körner, A. Kozhevnikov, A. Läuchli, S.R. Manmana, M. Matsumoto, I.P. McCulloch, F. Michel, R.M. Noack, G. Pawlowski, L. Pollet, T. Pruschke, U. Schollwöck, S. Todo, S. Trebst, M. Troyer, P. Werner, S. Wessel, and for the ALPS collaboration, *The ALPS project release 1.3: Open-source software for strongly correlated systems*, J. Magn. Magn. Mater. **310**, 1187 (2007).

[71] B. Bauer, L.D. Carr, H.G. Evertz, A. Feiguin, J. Freire, S. Fuchs, L. Gamper, J. Gukelberger, E. Gull, S. Güertler, A. Hehn, R. Igarashi, S.V. Isakov, D. Koop, P.N. Ma, P. Mates, H. Matsuo, O. Parcollet, G. Pawlowski, J.D. Picon, L. Pollet, E. Santos, V.W. Scarola, U. Schollwöck, C. Silva, B. Surer, S. Todo, S. Trebst, M. Troyer, M.L. Wall, P. Werner, S. Wessel, *The ALPS project release 2.0: open source software for strongly correlated systems*, J. Stat. Mech (2011) P05001.

[72] M. Dolfi, B. Bauer, S. Keller, A. Kosenkov, T. Ewart, A. Kantian, T. Giamarchi, M. Troyer, *Matrix product state applications for the ALPS project*, Comput. Phys. Commun. **185**, 3430 (2014).

[73] P. Silvi, *Tensor Networks: a quantum-information perspective on numerical renormalization groups*, The International School for Advanced Studies (SISSA/ISAS) - Trieste(2011).

[74] D. Perez-Garcia, F. Verstraete, M.M. Wolf, J.I. Cirac, *Matrix Product State Representations*, Quantum Inf. Comput. **7**, 401 (2007).

[75] P. Calabrese, J. Cardy, *Entanglement entropy and quantum field theory*, J. Stat. Mech.(2004) P06002.

[76] C. Holzhey, F. Larsen, F. Wilczek, *Geometric and renormalized entropy in conformal field theory*, Nuc. Phys. B **424**, 443 (1994).

[77] P. Calabrese, J. Cardy, *Entanglement entropy and conformal field theory*, J. Phys. A: Math. Theor. **42**, 504005 (2009).

[78] T. Kennedy, *Exact diagonalisations of open spin-1 chains*, J. Phys. Condens. Matter **2**, 5737 (1990).

[79] F.D.M. Haldane, *Nonlinear Field Theory of Large-Spin Heisenberg Antiferromagnets: Semiclassically Quantized Solitons of the One-Dimensional Easy-Axis Néel State*, Phys. Rev. Lett **50**, 1153 (1983).

[80] F. Pollmann, E. Berg, A.M. Turner, M. Oshikawa, *Symmetry protection of topological phases in one-dimensional quantum spin systems*, Phys. Rev. B **85**, 075125 (2012).

[81] F. Pollmann, A.M. Turner, E. Berg, M. Oshikawa *Entanglement spectrum of a topological phase in one dimension*, Phys. Rev. B **81**, 064439 (2010).

[82] C.-K. Chiu, J.C.Y. Teo, A.P. Schnyder, S. Ryu, *Classification of topological quantum matter with symmetries*, Rev. Mod. Phys. **88**, 035005 (2016).

[83] S. Ryu, A.P. Schnyder, A. Furusaki, A.W.W. Ludwig, *Topological insulators and superconductors: tenfold way and dimensional hierarchy*, New J. Phys. **12**, 065010 (2010).

[84] A.Y. Kitaev, *Periodic table for topological insulators and superconductors*, AIP Conf. Proc. **1134** 22 (2009).

[85] L. Fidkowski, A. Kitaev, *Effects of interactions on the topological classification of free fermion systems*, Phys. Rev. B. **81**, 134509 (2010).

[86] L. Fidkowski, A. Kitaev, *Topological phases of fermions in one dimension*, Phys. Rev. B. **83**, 075103 (2011).

[87] W. Selke, *The ANNNI model – Theoretical analysis and experimental application*, Phys. Rep. **170**, 213 (1988).

[88] M.E. Fisher, M.N. Barber, *Scaling Theory for Finite-Size Effects in the Critical Region*, Phys. Rev. Lett. **28**, 1516(1972).

[89] M. Beccaria, M. Campostrini, A. Feo, *Evidence for a floating phase of the transverse ANNNI model at high frustration*, Phys. Rev. B. **76**, 094410 (2007).

[90] E. Cobanera, G. Ortiz, *Fock parafermions and self-dual representations of the braid group*, Phys. Rev. A **89**, 012328 (2014).

[91] D. Rossini, M. Carrega, M.C. Strinati, L. Mazza, *Anyonic tight-binding models of parafermions and of fractionalized fermions*, Phys. Rev. B **99** ,085113 (2019).

[92] P. Calabrese, M. Mintchev, *Correlation functions of one-dimensional anyonic fluids*, Phys. Rev. B **75** , 233104 (2007).

Accompanied Papers